NTNU

Norwegian University of
Science and Technology

Design optimization of offshore construction vessels

Endre Sandvik

Marine Technology
Submission date: August 2016
Supervisor: Sverre Steen, IMT
Co-supervisor: Stein Ove Erikstad, IMT

Norwegian University of Science and Technology
Department of Marine Technology

NTNU Trondheim
Norwegian University of Science and Technology
Department of Marine Technology

MASTER THESIS IN MARINE TECHNOLOGY

SPRING 2016

FOR

Endre Sandvik

Design optimization of offshore construction vessels

Offshore construction vessels shall fulfill many requirements, many of them conflicting, like large beam being good for lifting capacity but not for resistance and general sea-keeping. The purpose of this master thesis is to explore methods to optimize the design of offshore construction vessels by balancing the performance with respect to the many different performance criteria. This shall be done through case studies of (tentatively) three different offshore construction vessels. The three vessels should be designed according to significantly different requirements, for instance three different classes of lifting capacity. Preferably, the same optimization method shall be applied to all cases, so that one can see the effect of different criteria on the final design.

The thesis work will have to start with clarifying the performance criteria and by defining the (tentatively) three different design cases. Then, a system for balancing the (possibly conflicting) performance criteria will have to be established – Key Performance Indicators or Balanced Score Card or some other established methodology might be applied. Furthermore, tools for evaluating the performance must be chosen.

In the thesis the candidate shall present his personal contribution to the resolution of problem within the scope of the thesis work.

Theories and conclusions shall be based on mathematical derivations and/or logic reasoning identifying the various steps in the deduction.

The thesis work shall be based on the current state of knowledge in the field of study. The current state of knowledge shall be established through a thorough literature study, the results of this study shall be written into the thesis. The candidate should utilize the existing possibilities for obtaining relevant literature.

The thesis should be organized in a rational manner to give a clear exposition of results, assessments, and conclusions. The text should be brief and to the point, with a clear language. Telegraphic language should be avoided.

The thesis shall contain the following elements: A text defining the scope, preface, list of contents, summary, main body of thesis, conclusions with recommendations for further work, list of symbols and acronyms, reference and (optional) appendices. All figures, tables and equations shall be numerated.

The supervisor may require that the candidate, in an early stage of the work, present a written plan for the completion of the work. The plan should include a budget for the use of computer and laboratory resources that will be charged to the department. Overruns shall be reported to the supervisor.

NTNU Trondheim
Norwegian University of Science and Technology
Department of Marine Technology

The original contribution of the candidate and material taken from other sources shall be clearly defined. Work from other sources shall be properly referenced using an acknowledged referencing system.

The thesis shall be submitted electronically (pdf) in DAIM:

- Signed by the candidate
- The text defining the scope (signed by the supervisor) included
- Computer code, input files, videos and other electronic appendages can be uploaded in a zip-file in DAIM. Any electronic appendages shall be listed in the main thesis.

The candidate will receive a printed copy of the thesis.

Supervisor : Professor Sverre Steen
Co-supervisor : Professor Stein Ove Erikstad
Start : 18.01.2016
Deadline : 10.06.2016

Trondheim, 24.02.2016

Sverre Steen
Supervisor

Preface

This thesis is the final delivery of a master's degree in marine hydrodynamics at the Norwegian University of Science and Technology, department of Marine Technology in Trondheim. With its approval comes the title Master of Science in Marine Technology.

The theme of this thesis is ship design of Offshore Subsea Construction Vessels. The objective is to improve methods for designing ships with high levels of operational performance. It is written in cooperation with VARD Design AS, one of Norway's leading suppliers of OSCV designs.

I would like to thank my supervisors Professor Sverre Steen and Professor Stein Ove Erikstad for their guidance and support during work on this thesis. I would also like to thank Henning Borgen, Ivar Knutsen and Bjarte Holene at VARD for their expert advice, guidance and opportunity to work with vessels at the frontline of technological advancement. Last, but not least, I would like to thank PhD student and researcher at MARINTEK, Martin Gutsch, for his cooperation, help and many discussions throughout the work on this thesis.

Endre Sandvik

Trondheim, August 2016

Summary

The topic of this thesis is optimization of ship design with regards to operational performance. 4 VARD Offshore Subsea Construction Vessels are analysed to find the optimum compromise of operability versus required power, building costs and machinery costs.

Operability is assessed with regards to subsea lifting operations using the ShipX plug-in VERES. Criteria is established for lifting phases in air, splash-zone and lowering through the water column. Parametric variations of beam, draught, GM and radius of gyration for roll motion is done to find their effect on operability. Required power at transit speed for beam and draught variations is found using experimental results from MARINTEK and the empirical method Holtrop 84. Building and machinery costs are assessed using empirical methods.

Statistics from the North Sea and Norwegian Sea is applied to determine operability. Results from these areas is found to differ significantly. The only parameter resulting in consistent change in operability is the vessel length. The remaining parameters vary in terms of their effect on operability depending on vessel and operational area. The length is found to have the largest impact on costs, and the beam is found to be a more cost effective parameter for increasing operability compared to draught.

It is shown that variation of beam is more difficult compared to draught if a constant GM is required without large modifications of general arrangement. The applied methodology of assessing operability differs from the procedure of planning and executing lifting operations since weather windows and α-factors are neglected. This lead to an overestimate of operability represented as the expected percentage of time the vessel is capable of performing operations.

Sammendrag

Temaet for denne masteroppgaven er design av skip med tanke på operasjonell ytelse. 4 VARD offshore subsea konstruksjonsfartøy er analysert for å finne det optimale kompromisset mellom operabilitet og nødvendig effekt, bygge- og maskinerikostnader.

Operabilitet blir vurdert for en subsea løfteoperasjon ved å bruke modulen VERES i ShipX. Kriterier etableres for løftefasene i luft, bølgesone og nedsenkning gjennom vannet. Parameterendringer for bredde, dypgang, GM og gyrasjonsradius for rullebevegelse gjøres for å kartlegge deres effekt på operabilitet. Nødvendig effekt ved transitthastighet for bredde- og dypgangsvariasjoner gjøres ved bruk av eksperimentelle data fra MARINTEK samt empirisk metode Holtrop 84. Bygge- og maskinerikostnader vurderes ved bruk av empiriske metoder.

Bølgestatistikk fra Nordsjøen og Norskehavet anvendes for å vurdere operabilitet. Resultatene fra disse områdene er funnet å gi betydningsfulle avvik. Den eneste parameteren som gir konsistent endring med tanke på operabilitet er lengden av fartøyet. De resterende parameterene varierer i måten de påvirker operabilitet avhengig av fartøy og operasjonsområde. Lengden er funnet til å være parameteren med størst inflytelse på kostnader, og bredde er funnet å være mer kostnadseffektiv enn dypgang for å øke operabilitet.

Det kommer frem at bredde er vanskeligere å endre sammenlignet med dypgang dersom konstant GM kreves uten store endringer i skipets arrangement. Den anvendte metoden for å undersøke operabilitet er ulik prosedyren for planlegging og gjennomføring av løfteoperasjoner fordi værvinduer og α-faktor neglisjeres. Dette fører til en overestimering av operabilitet tatt som den forventede prosenten av tid skipet er i stand til å utføre operasjoner.

Contents

List of Tables

List of Figures

Nomenclature

OSCV	=	Offshore Subsea Construction Vessel
RAO	=	Response Amplitude Operator
DOF	=	Degree Of Freedom
CFD	=	Computational Fluid Dynamics
DNV	=	Det Norske Veritas AS (now DNV GL)
HAZID	=	Hazard identification analysis
HAZOP	=	Hazard and operability study
POR	=	Point of no return
ULS	=	Ultimate limit state
ALS	=	Accidental limit state
DP	=	Dynamic positioning
RMS	=	Root mean square
PDF	=	Probability density function
VCG	=	Vertical Centre of Gravity
COB	=	Centre of buoyancy
COG	=	Centre of gravity
CONREP	=	Connected replenishment at sea
VERTREP	=	Vertical replenishment at sea
FAS	=	Fuelling at sea
g	=	Gravitational acceleration
ρ	=	Density
A_{ii}	=	Uncoupled added mass coefficient for DOF i
B_{ii}	=	Uncoupled damping coefficient for DOF i
B_{ii}	=	Uncoupled damping coefficient for DOF i
B_{44}^{V1}	=	Added linear damping coefficient in roll
B_{44}^{V2}	=	Added non-linear damping coefficient in roll
B_l^i	=	Linearized damping iteration i
C_{ii}	=	Uncoupled restoring coefficient for DOF i
F_i	=	Excitation force for DOF i

ω_n	=	Natural frequency for
ω_e	=	Frequency of encounter
k	=	Wave number
T_{0i}	=	Natural period for DOF i
ξ	=	critical damping ratio
$\|H(\omega)\|$	=	RAO
ϵ	=	Phase angle
Φ	=	Complete potential
ϕ	=	Potential component
ζ	=	Wave amplitude
F_n	=	Froude number
η_A	=	Response amplitude
$S_{\zeta\zeta}(\omega)$	=	Wave spectrum
$S_{\eta\eta}(\omega)$	=	Response spectrum
m_{n_η}	=	n-th response spectral moment
σ_η^2	=	Response spectral variance
η_{a,m_0}	=	Significant response amplitude
H_s	=	Significant wave height
T_z	=	Zero-crossing period
T_z^{mf}	=	Most frequent zero-crossing period
γ	=	JONSWAP peakedness parameter
D	=	Draught of vessel
D_{DWL}	=	Design draught of vessel
B	=	Vessel beam
L_{pp}	=	Length between perpendiculars
∇	=	Vessel volume displacement
S	=	Wet surface area of ship
S_{BD}	=	Wet surface area of transom stern
R_{ii}	=	Radius of gyration for DOF i
GM	=	Transverse metacentric height
C_R	=	Residual resistance coefficient
C_W	=	Wave resistance coefficient in Holtrop 84

C_F	=	Frictional resistance coefficient
ΔC_F	=	Added resistance coefficient
C_{AA}	=	Air resistance coefficient
$\bar{C}$	=	Non-Froude scaling resistance coefficient
h_t	=	Height of transom stern
k_{st}	=	Specific hull steel costs
θ	=	Line angle pendulum motion
L	=	Extended line length from crane tip
F_{mi}	=	Characteristic mass force
F_D	=	Characteristic drag force
F_{hyd}	=	Characteristic mass and drag force
F_s	=	Characteristic slam force
C_s	=	Slam coefficient
C_D	=	Drag coefficient
C_m	=	Added mass coefficient
M_i	=	Dry weight of compressor
m_i	=	Dry weight of cable per meter
EA	=	Cable stiffness
T_{POP}	=	Planned operation period
T_C	=	Contingency period
T_R	=	Operation reference period

Chapter 1

Problem description

This chapter is dedicated to give a description of the problem examined in this master thesis. The motivation for choosing this topic is presented in order to show how the results of this work can be applied, and a concrete problem description is presented.

1.1 Motivation

Since the end of the 1960s Norway has enjoyed welfare and growth much due to oil and gas reserves in the North Sea. Both Norwegian and foreign oil companies have since then been pumping, processing and selling oil from the Norwegian Continental Shelf, often with large profits compared to similar-scale projects in other industries.

Traditional exploration, drilling and production were performed by drill ships and oil rigs from the surface. Supply ships provided equipment and supplies needed to maintain operation and crew. Oil tankers would transport crude oil from the field to plants along the coast for refinement. All these activities led to the largest industrial growth in Norway's history, providing jobs and income for both Norwegian and foreign companies. Continuous work towards improving marine and petroleum technology has since then been done in order to make the industry as efficient and profitable as possible. Development of subsea technology and support systems have made huge leaps forward in recent years due to the extensive work of scientists and engineers.

1.1.1 Subsea field development

In 1961 Shell developed and produced oil from the first subsea well in the Gulf of Mexico. This was achieved at a water depth of approximately 15 meters. The first subsea well in the North Sea was at the Ekofisk field in 1970 at a depth of approximately 65 meters. Today's subsea technology allow operators to produce oil and gas at depths close to 3 kilometres (Shell at Tobago field in the Gulf of Mexico 2935 meters).

Ormen Lange subsea gas field

Ormen Lange is a gas field located in the Norwegian Sea approximately 120 kilometres north west of Kristiansund (Shell Global). It was developed by Hydro (merged with Statoil in October 2007) and handed over to Shell in December of 2007. It currently supplies approximately 20 % of United Kingdom's natural gas.

Figure 1.1: Ormen Lange gas field pipeline to Nyhamna and the UK (Norsk Oljemuseum 2016)

Figure 1.1 show the location of the Ormen Lange field and the pipeline to Nyhamna and Easington. Ormen Lange is located at water depths between 850-1100 meters. Installing the necessary equipment on the ocean floor presents a challenge due to the ultra-deep lifting operations that is required.

1.1.2 Offshore Subsea Construction Vessels

The most commonly used vessels for subsea lifting operations are the offshore subsea construction vessels (OSCV). Figure 1.2 show an example of an OSCV design VARD 3 07. These vessels are recognized by their large deck area that allow storage of equipment during transit and large crane. Many also have helidecks to allow easy access at site by helicopter.

Figure 1.2: VARD 3 07 OSCV (Vard Group AS)

OSCVs are usually limited to light lift operations (sec. 2.1.1). Important features of such vessels are sufficient stability that allow lifting of heavy objects over the side of the vessel and good seakeeping performance that provides a safe platform for crew and cargo during operation. Many OSCVs are also built with one or more moonpools for launching and retrieval of remotely operated vehicles (ROVs) and diving support capabilities.

1.2 Problem Description

Subsea technology represents a leap in the way oil and gas companies operates compared to traditional manned oil rigs and drill ships. Ormen Lange is a good example of the scale and complexity associated with subsea fields. The drawback of choosing subsea solutions is increased complexity during installation, maintenance and decommissioning. OSCVs are restricted by weather when performing these operations, which often lead to increased costs for the operator due to waiting on weather (WoW). Vessel design with respect to operability is therefore important in order to make weather windows as long as possible. Much work is required before production at a subsea field can commence. Preparing the sea floor (excavating, drenching etc.), installing equipment (pumps, compressors etc.) and pipe-laying are some of the major tasks. The focus in this thesis is lifting operations performed during installation of subsea equipment.

Vessel motion is often the limiting factor for safe and efficient operations. Motion characteristics is governed by the hydrodynamic properties of the hull, and mass distribution inside the vessel. Hull and general arrangement are therefore important factors for ship designers to consider to ensure good operational properties.

Ship design is a complex process, and is always subject to compromise. Varying dimensions to improve operability affects other key characteristics of the vessel such as resistance and building costs. Good ship design is therefore dependent on the designers knowledge, experience and ability to view the vessel as a system in order to make the optimal compromise. A study of vessel design with respect to operability is therefore not complete without considering other aspects of the ship's performance. This thesis aims to bring clarity to these issues by answering the following questions on the next page.

1. Which vessel parameters are important for ship designers to consider when considering operability of OSCVs?

2. How do these parameters affect other key performances of the vessel?

    - Required power at transit/fuel costs
    - Building costs

3. Which change of parameters are the optimal choice for increasing operability while maintaining other key characteristics?

Chapter 2

Marine lifting operations

This chapter presents different types of lifting operations performed offshore and the challenges that face engineers during of planning such operations. The aim is to show the background for the analysis and limiting criteria that is used later in the report to evaluate vessel operational performance.

2.1 Types of marine lifting operations

It is common to sort offshore lifting operations into two groups (Nielsen 2007):

- **Light lifts:** Mass of lifted object does not influence motion characteristics of vessel. Less than 2 % of vessel displacement.
  - Small subsea modules and spool pieces
  - Anchors, foundations, pipelines and risers
  - ROV launching and retrieval
- **Heavy lifts:** Mass of lifted object influences motion characteristics of vessel. More than 2 % of vessel displacement.
  - Large modules, typically more than 1000 tonnes
  - Involves heavy lift crane vessel and/or barge
  - Dynamic and hydrodynamic interaction between object and crane vessel
  - Heave compensation not possible

2.1.1 Light lifts

Light lifting operations are typically performed by smaller vessels that have a maximum lifting capacity of 150-500 tons. Since the weight of the lifted object is small compared to vessel displacement, it is assumed that the inertia of the dynamic system that give vessel response is unchanged. In practice, this implies that the response amplitude operators (RAO) calculated for the vessel without the object on board are valid for use in analysis of lifting operation.

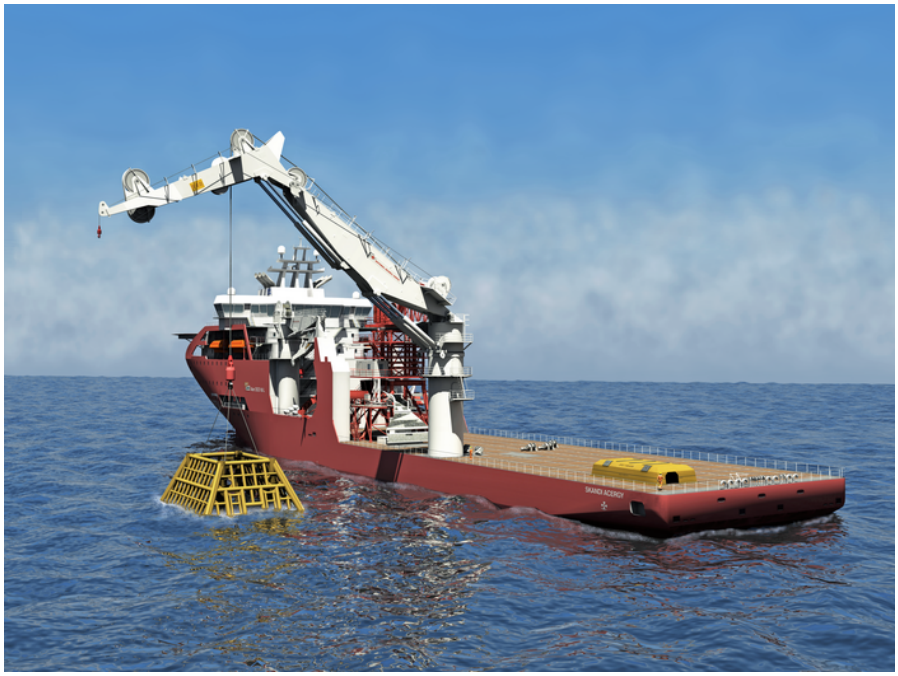

Figure 2.1: Lift of subsea module (SMSC 2009)

Figure 2.1 shows a typical example of a subsea light lift operation. The subsea module shown in the picture has been hoisted from deck and over the side, and is currently in the splash-zone while preparing for lowering through the water column. Since the mass of the lifted object is relatively low, it is possible to apply heave compensation in order to keep the object stable vertically. Heave compensation are useful for critical phases of the lift where vertical motions must be limited or there is a risk of resonance in the object-lifting cable mass-spring system.

2.1.2 Heavy lifts

Heavy lift operations are typically performed by specially designed heavy-lift vessels. Such vessels are designed with lifting capacity in mind, with one or more large cranes and high ballast water capacity. Planning heavy lift operations requires detailed analysis of the influence hoisting and moving the heavy object has on the vessel stability and motion response. Hence, RAOs needs to be recalculated to account for changes in inertia and stiffness from lifted object and ballast water.

Figure 2.2: Lift of topside Saipem 7000 (Boyd 2015)

Figure 2.2 shows a typical heavy lift operation. Compared to figure 2.1, it is clear that heavy and light lift operations represent two different classes of lifts. Both classes of operation present challenges towards the capacity of the crane and lifting gear, motions induced from the environment and vessel stability. However, analysing the operations with respect to planning and risk management require different approaches and different levels of limiting criteria.

2.2 Planning lifting operations

Marine operations, like subsea lifting operations, are in general non-routine activities. This means that each operation require a high level of planning. DNV GL states in its offshore standard OS-H101 *Marine Operations, General* the philosophy behind the planning of such operations (DNV 2011a).

"Marine operations shall be planned according to safe and sound practice, and according to defined codes and standards. A marine operation shall be designed to bring an object from one defined safe condition to another."

The term *safe condition* is defined as a condition where the object is considered exposed to the same level of risk as during in-place condition for damage or loss. In order to document compliance with this philosophy, the operation is split into different phases, where hazards and risks are identified and shown to be within acceptable limits. Contingency planning and emergency procedures are also to be included.

2.2.1 Planning and design sequence

DNV recommends adopting the following procedure (DNV 2011a):

1. Identify relevant and applicable regulations, rules, company specifications, codes and standards, both statutory and self-elected.

2. Identify physical limitations. This may involve pre-surveys of structures, local conditions and soil parameters.

3. Overall planning of operation i.e. evaluate operational concepts, available equipment, limitations, economical consequences, etc.

4. Develop a design basis describing environmental conditions and physical limitations applicable for the operation.

5. Develop design briefs describing activities planned in order to verify the operation, i.e. available tools, planned analysis including method and particulars, applicable codes, acceptance criteria, etc.

6. Carry out engineering and design analyses.

7. Develop operation procedures.

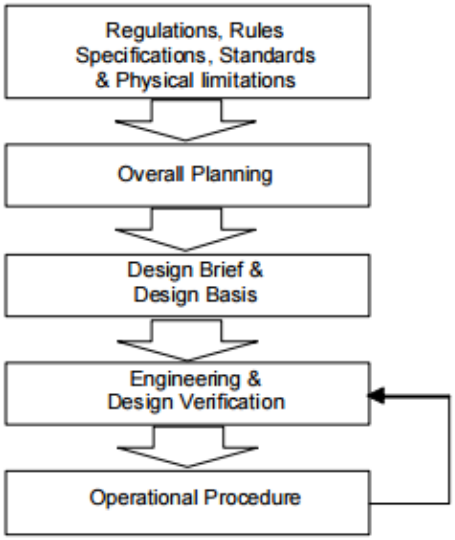

Figure 2.3: Sequence of marine operations planning (DNV 2011a)

Figure 2.3 shows that planning and design of an operation is an iterative process. This thesis aims to investigate the operability for different vessels towards carrying out a lifting operation. Operability is evaluated from a set of concrete criteria that represent the limit of operation. Developing such criteria is done in step 4 and 5 in the previous list.

2.2.2 Risk management

Risk is defined as probability multiplied by consequence. The main objective of a risk analysis is therefore to identify potential hazardous scenarios that may occur during the operation, and then estimate the probability of occurrence. DNV recommends that risk within marine operations are assessed against criteria for (DNV 2003):

- Personnel safety
- Environment
- Assets and/or lost production
- Reputation

Assessment Parameter	*Keywords for assessment*
Personnel exposure	– Qualification and experience of personnel – Organisation – Required presence – Shift arrangements – Deputy and backup arrangements
Overall project particulars	– Delay – Replacement time/cost – Repair possibilities – No. of interfaces and contractors or subcontractors – Project development period
Existing field infrastructure	– Infrastructure – surface – Infrastructure – subsea
Handled object	– Value – Structural Strength/Robustness
Marine operation method	– Novelty and feasibility – Robustness – Type of operations – Previous experience – Installability
Equipment used	– Margins/robustness – Condition/Maintenance – Previous experience – Suitability – Experience with operators or contractors (track record)
Operational aspects	– Cost of mobilised equipment and spread – Language barriers/hindrance – Season/Environmental conditions – Local marine traffic – Proximity to shore

Figure 2.4: Risk analysis assessment parameters (DNV 2003)

From figure 2.4 it is clear that the risk assessment should involve more than strictly technical or physical concerns. Parameters like qualification and experience of personnel, shift arrangements, language barriers and operator organisation should also be included. This shows that assessing operation feasibility and risk level is a highly complex and intricate procedure.

This thesis will not show details regarding risk analysis, but rather mention it as an important step towards ensuring safe and well organized operations. There are however some key terms often met when discussing marine operations that are related to finding limiting criteria and assessing operability.

HAZID

HAZID is short for hazard identification analysis. The purpose is to evaluate hazards early in a project at the conceptual and front-end engineering stages or at later stages if suitable (DNV 2003). This procedure aims to assist choosing the most advantageous procedures and design of operation. Critical stages of the operation along with potential hazards for that stage is produced as an end result.

HAZOP

HAZOP is short for hazard and operability study. HAZOP is not only focused on possible hazards, but also on issues related to the operability of an activity or operation, including possible improvements (DNV 2003). It is an interdisciplinary activity used during the development of operation procedures. A well executed HAZOP involves key personnel in the design and operation along with experienced personnel within similar projects, relevant systems and safety issues.

2.2.3 Phases of operation

As mentioned above, risk analysis involves identifying critical stages of the operation. The phases differ according to the work being done, risks and configuration (i.e. ballasting, free deck space etc.). Each phase has requirements for start-up with regards to necessary personnel, equipment and environmental conditions.

Some phases result in a point of no return (POR) at start-up. Some typical examples of POR are removing sea fastening after transport given certain environmental conditions or filling the lifted object with water before lowering through the water column. Deciding to proceed beyond such points involves a commitment towards being able to get the object to the next safe condition. These phases are planned with particular care and detail. Below follows an overview over the phases in a lifting operation. This overview is meant to show the background for the choice of limiting criteria which is defined in chapter 5.

Transport of object to field

Subsea equipment are typically transported on deck from shore to the field for installation. To avoid sliding, which can cause damage to surrounding structure, loss of stability and loss of template, the template is welded or bolted to the deck. This is called seafastening, and is designed to carry inertia loads due to vessel motion, wind and green water. The weight of the transported object must also be distributed over a sufficient number of load-carrying elements in the hull girder (DNV 2015).

Figure 2.5: Subsea template during transport (Aker Solutions ASA 2012)

Figure 2.5 show a subsea template during transport fastened to the deck of an OSCV. Adequate fastening, placement of the object on deck and ballasting are the most important factors for planning this phase. Start-up of this phase is normally weather restricted, and limits with regard to seastate and wind must be defined.

Lift-off

The lift-off phase starts with cutting the seafastening in order to avoid vertical restraints. Once the object is lifted off deck, it's behaviour turns from static to dynamic. The horizontal motion resembles a pendulum swinging at the end of a rope. Vertically, the template moves as a mass-spring system with the weight of the object and rigging and the stiffness in the cables being the mass and spring respectively. These dynamic systems are excited by the movement of the crane tip, wind loads and hoisting of cable.

The main challenge during this phase is to control the motion of the lifted object. Fixed limits of horizontal motion is important due to surrounding structures and cargo on deck. Controlling the tension of the lifting wire is also important to check against crane capacity.

Figure 2.6: Subsea template lifted off deck (Subsea 7 2015)

Moving object over the side of the vessel

Once the object is lifted clear of the deck, the next phase is to move it horizontally over the side and into its lowering position. This presents challenges with regards to stability and extended crane capacity. Access to the stability manual for the vessel and crane curves are therefore critical for planning. Uncontrolled horizontal motion may occur either through excitation by wind loads or motions at the crane tip.

Figure 2.7: Subsea compressor moved into lowering position (Statoil ASA 2015)

Splash-zone

As the object is lowered into the water it is entering what is known as the splash-zone. Here there are hydrodynamic loading affecting the object directly. The main loads are:

- Mean buoyancy (static component)
- Time dependent buoyancy (dynamic component)
- Time dependent mass (water filling)
- Added mass forces due to acceleration of object
- Slamming forces due to water entry
- Impulse forces due to water exit
- Wave excitation forces (inertia and drag)
- Current forces (often applied as static in analysis)

Figure 2.8: Subsea template in splash zone being filled (Statoil ASA 2012)

Controlling object behaviour in this phase involves a detailed understanding of the physics that occur around a structure at the free surface. Avoiding slack in the lifting cable is important since snap-loads that occur when tension is reapplied can exceed cable capacity. Contact between object and lifting vessel must also be avoided to avoid damage to object or vessel.

Figure 2.8 shows a subsea template being lowered through the splash zone. The template is being filled with water as it is being submerged. Filling the object with water creates a POR in some cases. This happens if the crane does not have capacity to lift the object with the additional weight of water.

Vertical motion is important to control for execution of this phase. Relative velocity between object and free surface governs the amplitude of the slamming loads, submergence governs the time dependent buoyancy and wave excitation loads and relative acceleration governs the added mass forces. Establishing hydrodynamic coefficients for the object is therefore necessary to be able to predict its behaviour in this phase. Filling and lowering through the splash-zone is always limited by weather.

Lowering through the water column

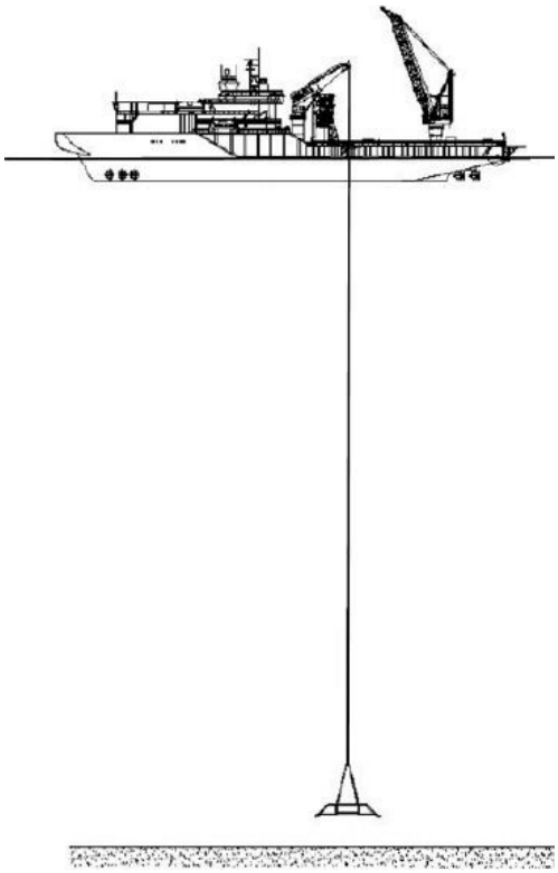

Figure 2.9: Object lowered through water column (Kjell Larsen 2015)

Lowering through the water column takes the object out of the wave-zone. This phase is mainly governed by current forces in the horizontal plane, and added mass, drag and crane tip forces in the vertical plane. An important effect to consider is that the natural period of the mass-spring system changes for varying depth. Pay-out of the lifting cable means that the length of elongated cable increases, affecting the stiffness of the system. The mass of the additional cable increases the inertia. For operations where there is a significant chance of resonant excitation, active heave compensation is often used to control this phase of the lift. The crane tip is usually moved closer to the vessel and towards midship once the object is clear below the vessel. This is done to reduce roll and pitch contributions on the vertical crane tip motion.

Touch down

The final step is to place the object in the correct position and retrieving the lifting cable and gear. For large water depths, placing the object correctly can be difficult due to current loads on the object and cable as seen in figure 2.10. Ability to control the position of the lifting vessel is therefore crucial for this phase, and the capacity of the dynamic positioning system (DP) is governing for determining operational seastates.

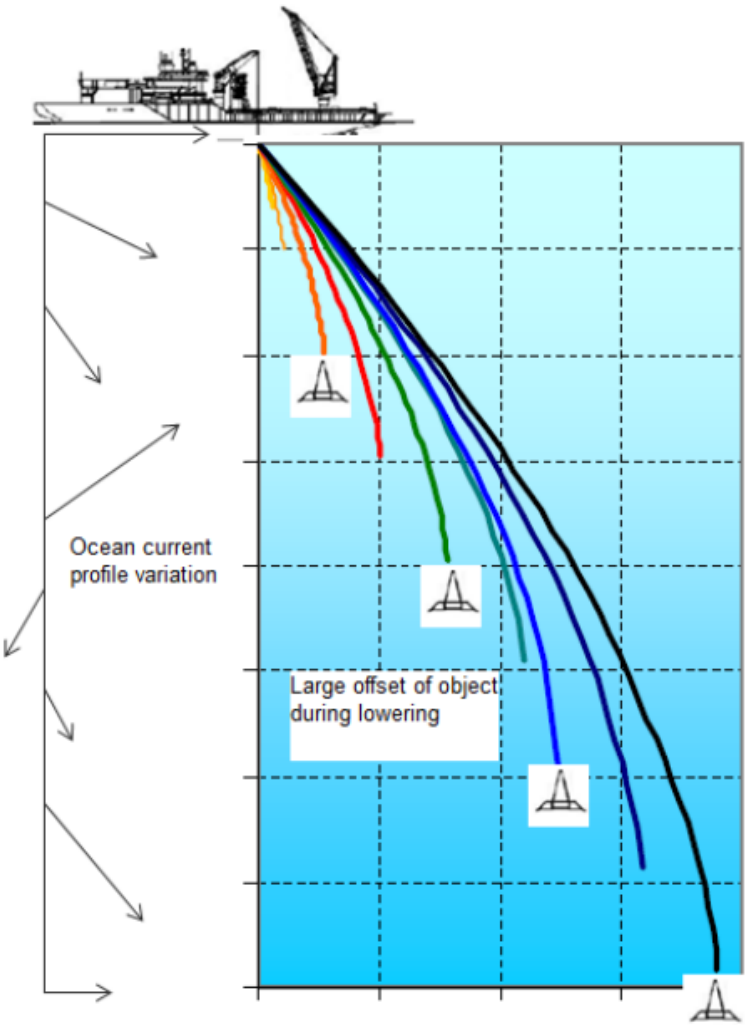

Figure 2.10: Offset due to current (Kjell Larsen 2015)

2.3 Operational requirements

DNV GL has defined a set of requirements for performance of marine operations (DNV 2011a). The purpose of these requirements is to ensure that:

- The environmental criteria are not exceeded
- The operation is properly manned and organised
- Adequate surveys are performed before and during operation
- Proper documentation of operation

2.3.1 Weather restricted- and unrestricted operations

Marine operations are either classified as weather restricted or unrestricted. The main difference between these two types of the operation is the basis of which the environmental loads are selected.

Weather unrestricted operations

If a marine operation has a planned operation period (T_{POP}) of more than 72 hours and a reference period (T_R) more than 96 hours, it has to be defined as a weather unrestricted operation. This involves design using statistical extremes for the operational area as a basis, ultimate limit state (ULS) and accidental limit state (ALS). An example of a weather unrestricted operation is a drilling campaign. Such operations typically involve semi-submersible platforms that drill at several location is search for oil and gas deposits. Depending on soil conditions and depth of drilling, a platform may stay at a location for several weeks, meaning that ULS and ALS is the design basis for the mooring and DP-system used for stationkeeping.

Weather restricted operations

Operations with T_{POP} less than 72 hours and T_R less than 96 hours is usually defined as weather restricted. Such operations may use design criteria less than statistical extremes, but must then use weather forecasts at start-up of the operation. T_{POP} is normally based

on a detailed schedule of the operation. The estimated contingency time, T_C, takes uncertainty during planning and possible contingency situations into account.

$$T_R = T_{POP} + T_C \tag{2.1}$$

T_C less than 6 hours is normally not applicable. The use of weather forecasts is shown in figure 2.11. Starting point of T_{POP} is at the issuance of the latest weather forecast. The decision is then made whether to go forward with the operation or wait for a better weather window. If the operational team and all responsible partners agree to proceed, the operation starts.

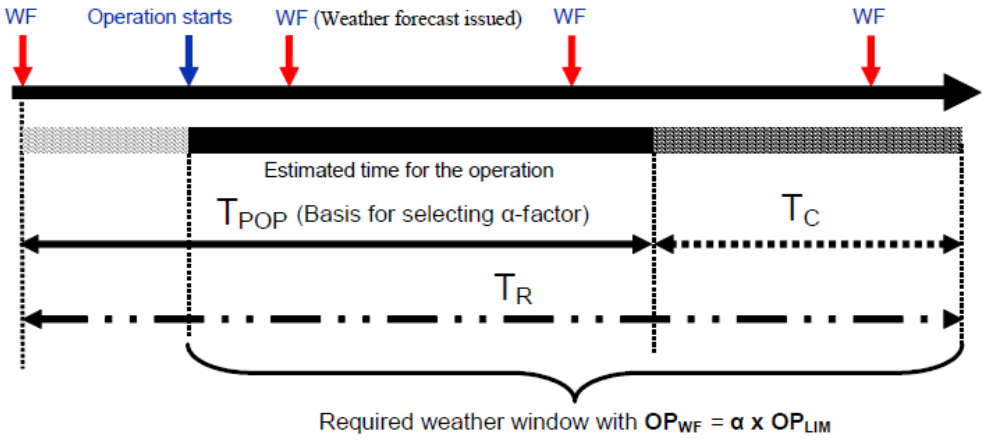

Figure 2.11: Operational periods (DNV 2011a)

α-factor

There is always uncertainty related to weather forecasts and monitoring. In marine operations, one of the main concerns is the forecast significant wave height (H_S). Asle Natskår, Torgeir Moan and Per O. Alvær tried to quantify this uncertainty. The difference between forecast and experienced levels for a lead time of 7 days over one year in the Norwegian Sea is shown in figure 2.12.

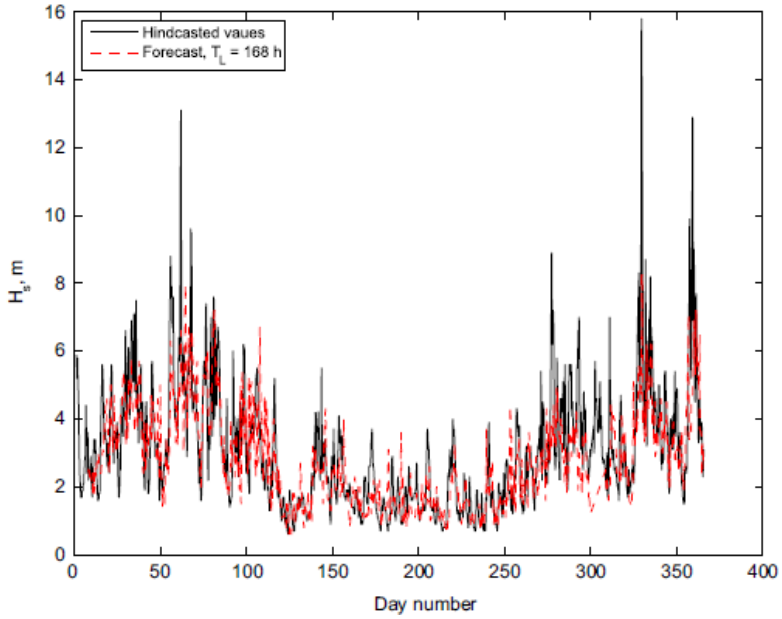

Figure 2.12: Experienced and forecast levels of H_S. Lead time 7 days (Natskår, Moan, and Alvær 2015)

Based on statistical analysis of forecast and hindcast data from the Norwegian Sea, they estimated the probability of exceeding $H_S = 6m$ as a function of the forecast H_S ($H_{S,fc}$) and T_R.

Figure 2.13 show a significant probability of exceeding $H_S = 6m$ for $H_{S,fc} < 6m$ values. This uncertainty is handled by use of what is known as the α-factor.

$$OP_{WF} = \alpha \cdot OP_{LIM} \tag{2.2}$$

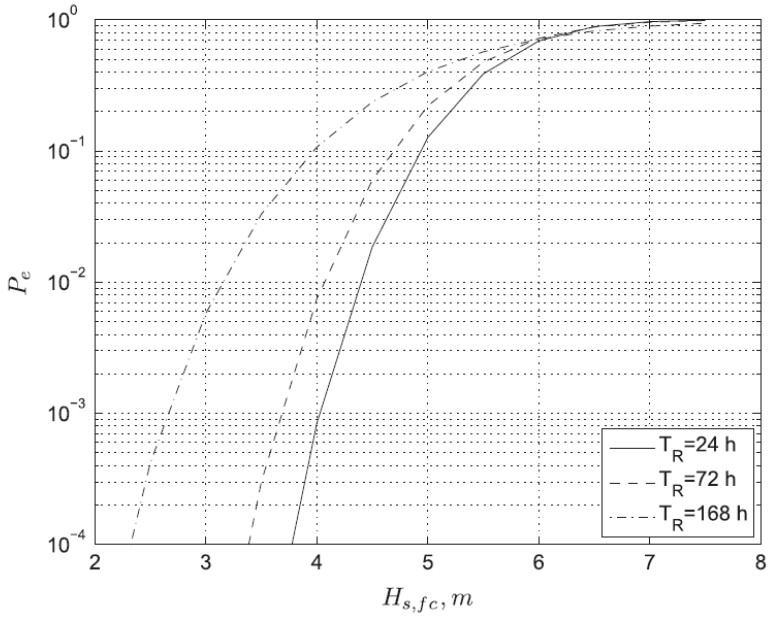

Figure 2.13: Probability of exceeding $H_S = 6m$ as a function of forecast H_S (Natskår, Moan, and Alvær 2015)

Limiting operational environmental criteria (OP_{LIM}) shall not be taken greater than the minimum of (DNV 2011a):

- The environmental design criteria
- Maximum wind and waves for safe work for personnel
- Equipment specified weather restrictions
- Limiting weather conditions for diving system (if part of operation)
- Limiting conditions for stationkeeping systems
- Limitations identified in HAZID/HAZOP
- Conditions that limits the possibility of executing contingency plans

Based on the planned operation period, the α-factor scales the operational criteria down for comparison with weather forecasts. The α-factor is calibrated such that probability of exceeding OP_{LIM} with more than 50% is less than 10^{-4}. DNV-OS-H101 section B700 includes tables for choosing the α-factor based on H_S, T_{POP} and weather forecast level. The forecast levels have different requirements and are intended for different

types of operations. Offshore lifting and subsea installation operations often use level B forecasts.

Weather Forecast Level	*Meteorologist required on site?*	*Independent WF sources*	*Maximum WF interval*
A	Yes[1)]	2[2)]	12 hours[3)]
B	No[4)]	2[5)]	12 hours
C	No	1	12 hours

1) There should be a dedicated meteorologist, but it may be acceptable that he/she is not physically present at site. The meteorologist opinion regarding his preferable location should be duly considered. It is anyhow mandatory that the dedicated meteorologist has continuous access to weather information from the site and that he/she is familiar with any local phenomena that may influence the weather conditions. Note also that the meteorologist shall be on site in order to use alpha factors from Table 4-3 and Table 4-5.

2) It is assumed that the dedicated meteorologist (and other involved key personnel) will consider weather information/forecasts from several (all available) sources.

3) Based on sensitivity with regards to weather conditions smaller intervals may be required. However, see 305.

4) Meteorologist shall be conferred if the weather situation is unstable and/or close to the defined limit.

5) The most severe weather forecast to be used.

Figure 2.14: Requirements for forecast levels (DNV 2011a)

Chapter 3

Methodology of operability study

This chapter presents the methodology applied for operability analysis. First an overview of the methodology is given to show how the analysis is performed and required inputs. Then the method of calculating vessel response is presented in detail. The last part of the chapter show the statistical method of assessing characteristic motions in a seastate and the calculation of the corresponding operability.

3.1 Overview of method

The chosen methodology for assessing operability is shown in figure 3.1. First step is to calculate the vessel motion characteristics, defined in linear analysis through RAOs. Combining the RAOs with wave spectra produces response spectra, from which short term statistics for the response process can be calculated. Using a set of operational limits (limiting criteria), the limiting sea states corresponding to the exceedance of these limits are calculated. Finally, comparing these limiting sea states against scatter diagrams results in the percentage operability.

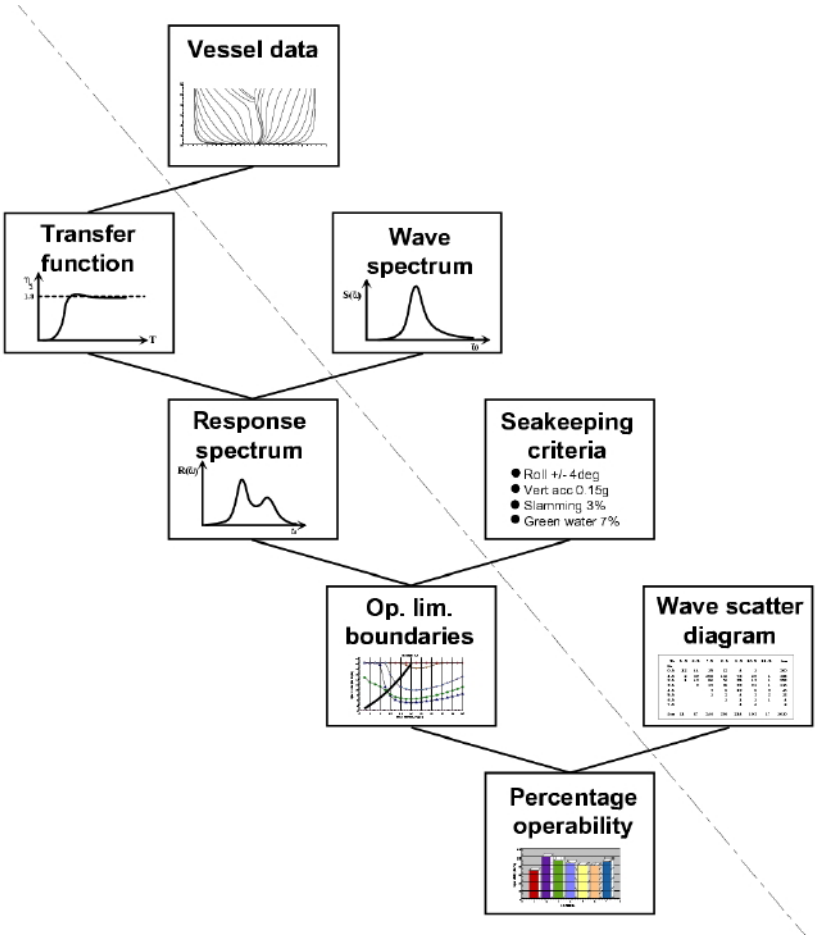

Figure 3.1: Operability analysis procedure (Fathi and Hoff 2014)

3.2 Vessel response

The vessel motion characteristics are calculated using the VERES plugin in ShipX. 2D strip theory is applied. This method allows calculation of sway, heave, roll, pitch and yaw motions for a ship advancing at constant speed in regular waves (Salvesen, Tuck, and Faltinsen 1970). It applies potential theory for calculating hydrodynamic coefficients for coupled and uncoupled added mass and damping.

Strip theory divides the hull into separate and independent strips, for which the hydrodynamic coefficients are calculated using 2D theory. The 3D coefficients is found by integrating along the length of the hull for each coefficient. This assumption is good for vessels where the variation of flow is dominating in the cross-sectional plane (Faltinsen 1990). This is true for long and uniformly shaped vessels.

3.2.1 Formulation of the velocity potential

VERES applies linear potential theory for calculating hydrodynamic coefficients. This implies that viscous effects are neglected and that fluid motion is assumed to be irrotational. The total velocity potential, $\Phi(x, y, z)$, must satisfy the Laplace equation in the fluid domain.

$$\nabla^2\Phi = 0 \tag{3.1}$$

Solving this partial differential equation requires boundary conditions at the hull, the free surface and the sea bottom. These boundary conditions replicate the physical properties associated for each location. At the hull, the requirement is no fluid transport through the hull surface.

$$\frac{DF}{Dt} = 0 \tag{3.2}$$

Where $F(x', y', z') = 0$ is the hull surface in a ship fixed coordinate system (x', y', z'). Replicating the physics of the free surface is more complicated. This surface is free, meaning that it changes location with time. The location of the surface is physically governed by the requirement of equal pressure at the surface and surrounding air. This is expressed mathematically through the following expression for the boundary condition on the unknown free surface (Fathi and Hoff 2014):

$$\frac{Dp}{Dt} = -\rho\left(\frac{\partial\Phi}{\partial t} + \frac{1}{2}|\nabla\Phi|^2 + gz\right) = 0 \tag{3.3}$$

Where g is the acceleration due to gravity and ρ is the mass density of the fluid. Suitable conditions at infinity for radiated waves must also be satisfied. For forward speed problems, VERES separates the total velocity potential into two parts. One is steady (time-independent) due to forward speed effects, and the other is due to the incident wave field and unsteady vessel motions. These are named perturbation potential, ϕ_S, and unsteady potential , ϕ_T, respectively.

$$\Phi(x, y, z, t) = [Ux + \phi_S(x, y, z)] + \phi_T(x, y, z)e^{i\omega t} \tag{3.4}$$

Here $Ux + \phi_S(x, y, z)$ is the steady contribution where U is the forward speed of the vessel. ϕ_T is the complex amplitude of the unsteady potential. Only the real part of ϕ_T has physical meaning.

Linearisation of boundary conditions 3.2 and 3.3 involves making assumptions about the geometry of the hull and response amplitudes. The geometry of the hull is assumed to be shaped such that the perturbation potential and its derivatives are small. Oscillatory motions of the vessel are assumed small such that unsteady potential and its derivatives are small. These assumptions allow linearisation of the problem by neglecting non-linear terms in both ϕ_S and ϕ_T as well as cross products of ϕ_S and ϕ_T. This linearisation allow for linear decomposition of the unsteady potential.

$$\phi_T = \phi_I + \phi_D + \sum_{j=1}^{6} \phi_j \eta_j \tag{3.5}$$

ϕ_D is the diffraction potential due to the presence of the vessel. ϕ_j is the contribution to the potential from the jth mode of motion. ϕ_I is the incident wave potential, which replicate the effect of incoming waves on the response process.

$$\phi_I = \frac{g\zeta_a}{\omega_0} e^{kz} e^{-ik(x\cos\beta + y\sin\beta)} \tag{3.6}$$

ζ_a is the incident wave amplitude, k is the wave number, β is the wave heading angle and $\omega_0 = \sqrt{kg}$ is the wave frequency according to deep water dispersion relation. VERES has the capability of calculating vessel responses for forward speed problems. The exciting frequency is then the frequency of encounter, defined as:

$$\omega_e = \omega_0 + kU\cos\beta \tag{3.7}$$

Linear theory calculates the resulting forces on the mean position of the hull only. Furthermore, the free surface condition is applied at the undisturbed free surface, $z = 0$. These simplifications allow the following linear expression of boundary conditions 3.2 and 3.3:

1. The perturbation potential must satisfy the body condition on the mean position of the hull

$$\frac{\partial}{\partial n}[Ux + \phi_S] = 0 \tag{3.8}$$

At the undisturbed free surface it must satisfy

$$U^2\frac{\partial^2\phi_S}{\partial x^2} + g\frac{\partial\phi_S}{\partial z} = 0 \tag{3.9}$$

2. The incident wave potential and diffraction potential must satisfy

$$\frac{\partial\phi_I}{\partial n} + \frac{\partial\phi_D}{\partial n} = 0 \tag{3.10}$$

on the mean position of the hull and

$$\left[\left(i\omega + U\frac{\partial}{\partial x}\right)^2 + g\frac{\partial}{\partial z}\right](\phi_I, \phi_D) = 0 \tag{3.11}$$

on the undisturbed free surface $z = 0$.

3. Potential components due to oscillatory motion must satisfy

$$\frac{\partial\phi_j}{\partial n} = i\omega n_j - Um_j \tag{3.12}$$

on the mean position of the hull and

$$\left(i\omega + U\frac{\partial}{\partial x}\right)^2\phi_j + g\frac{\partial\phi_j}{\partial z} = 0 \tag{3.13}$$

on the free surface $z = 0$.

The generalized normal, n_j, is defined by

$$(n_1, n_2, n_3) = \vec{n}$$
$$(n_4, n_5, n_6) = \vec{r} \times \vec{n}$$

Where $\vec{r} = (x, y, z)$ is the position vector with respect to the coordinate system and $\vec{n}$ is

the unit normal vector pointing into the fluid.

$$
\begin{aligned}
(m_1, m_2, m_3) &= \vec{m} = (\vec{n} \cdot \nabla)\nabla(x + \frac{\phi_S}{U}) \\
(m_4, m_5, m_6) &= \vec{r} \times \vec{m} - \nabla(x + \frac{\phi_S}{U}) \\
m_j &= 0, j = 1, 2, 3, 4 \\
m_5 &= n_3 \\
m_6 &= -n_2
\end{aligned}
$$

In addition to these boundary conditions, the potentials must each satisfy the Laplace equation (equation 3.1) and conditions for radiation conditions at infinity.

3.2.2 Calculating hydrodynamic forces and coefficients

A vessel floating on the surface will be subject to hydrodynamic forces due to the static (time-independent) and dynamic (time-dependent) pressure in the surrounding fluid. The hydrostatic pressure is the origin of restoring forces, and can be determined by analysing the submerged vessel geometry in calm water. Added mass, damping and excitation forces arise from the dynamic pressure field that occur due to vessel motions and incoming waves.

The pressure in the fluid is determined using the velocity potential and Bernoulli's equation.

$$
p = -\rho \left(\frac{\partial \Phi}{\partial t} + \frac{1}{2} |\nabla \Phi|^2 + gz \right) \tag{3.14}
$$

This expression contains both linear, non-linear and static terms. As mentioned above, VERES neglects non-linear terms in all expressions when calculating hydrodynamic forces and vessel response. The dynamic pressure, p_d, is therefore expressed as follows:

$$
p_d = -\rho \frac{\partial \Phi}{\partial t} = -\rho \left(i\omega + U \frac{\partial}{\partial x} \right) \phi_T e^{i\omega t} \tag{3.15}
$$

Hydrodynamic forces and moments are obtained by integrating the pressure over the surface of the hull.

$$H_j = -\iint_S p_d n_j dS, j = 1, 2, 3, .., 6 \tag{3.16}$$

Since this is linear theory, S is here the surface over the mean position of the hull. H_1, H_2 and H_3 are force components in the x, y and z directions, and H_4, H_5 and H_6 are moments around the x, y and z axis. H_j can be split into two independent parts, F_j and G_j, where F_j is the exciting forces and moments and G_j is the forces and moments due to vessel motions.

$$\begin{aligned}
H_j &= F_j + G_j \\
F_j &= \rho \iint_S n_j \left(i\omega + U\frac{\partial}{\partial x} \right) (\phi_I + \phi_D) dS \\
G_j &= \rho \iint_S n_j \left(i\omega + U\frac{\partial}{\partial x} \right) \sum_{k=1}^{6} \phi_k \eta_k dS = \sum_{k=1}^{6} T_{jk}\eta_k
\end{aligned}$$

T_{jk} represents the hydrodynamic force and moment in the jth direction due to unit displacement in the kth mode. It may be separated into a real and a imaginary part as:

$$T_{jk} = \omega^2 A_{jk} - i\omega B_{jk} \tag{3.17}$$

A_{jk} and b_{jk} here represents frequency dependent added mass and damping respectively.

3.2.3 Strip Theory - local analysis of each strip

VERES applies strip theory for obtaining hydrodynamic coefficients and loads. The vessel is divided into strips along the length, and 2D analysis is applied locally for each strip. Analysis is done independent of other strips. This implies that diffraction of the incoming wave field is neglected.

The diffraction and radiation problems are solved by matching the near-field and far-

field solutions (Fathi and Hoff 2014). A boundary-element formulation is applied for finding the near-field solution, and the far-field solution is obtained by asymptotic analysis. Green's second identity (3.18) is used for analysis in the cross-sectional plane. Fundamental 2D sources and dipoles are used to represent the flow.

$$-2\pi\phi = \int_S \left(\phi \frac{\partial \log r}{\partial n} - \log r \frac{\partial \phi}{\partial n} \right) dS \tag{3.18}$$

The hull is represented by straight line segments. Each segment is assumed to have a constant value for the velocity potential and its normal derivative.

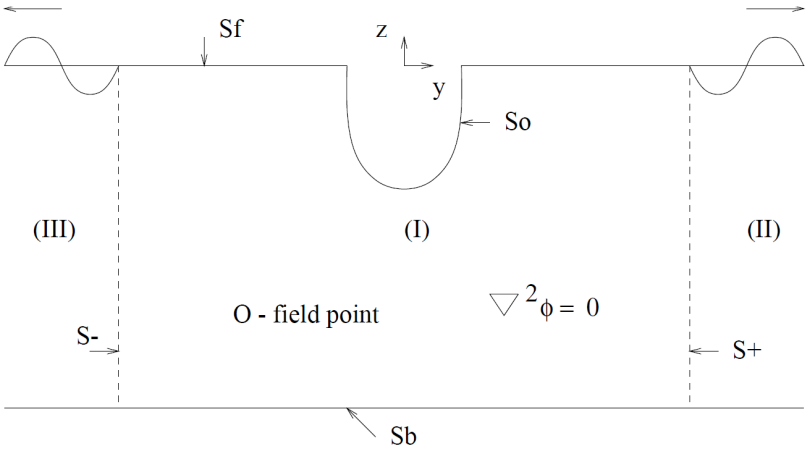

Figure 3.2: 2D analysis in VERES (Fathi and Hoff 2014)

Figure 3.2 illustrate the analysis set-up and domain for 2D analysis in VERES. Calculating the strength of each potential component is done by creating a $N \times N$ linear equation system where N is the number of unknowns. Obtaining this equation system is done by moving the field point O towards the center of each boundary element. At the hull surface, S_0, the velocity potential strength ϕ_i is the unknown. At the free surface, S_f, the normal derivative of the velocity potential $\frac{\partial \phi}{\partial n}$ is unknown. The velocity potential strength is known at the free surface through the free surface condition (equation 3.3).

VERES can apply different theories for calculating the hydrodynamic coefficients. The choice of method depends on the shape and configuration of the hull and the relevant vessel speeds. This thesis concerns monohull vessels at low speeds, which makes the Low Speed Strip Theory a suitable choice for determining vessel response characteris-

tics. This formulation was first presented by Salvesen, Tuck, and Faltinsen in 1970.

3.2.4 Viscous roll damping

Roll motion is important to model accurately when doing an operability study for lifting operations. The crane tip is, depending on operational phase, located high and far out on the vessel. This means that roll influences both sway and heave motion of the crane tip, which could limit the operation. The roll amplitude near resonance is highly dependent on the damping level. The natural period for roll is typically higher than other modes, and the roll mode of motion is not efficient for generating waves for long and slender monohull vessels. Potential damping is therefore typically low, resulting in high roll amplitudes near resonance. Models for viscous roll damping is therefore included in order to obtain more accurate roll motion characteristics.

Frictional roll damping

Skin friction is a force component acting tangentially to the hull surface. It is dependent on the relative velocity of the hull and the surrounding fluid squared, which means that it is a non-linear damping contribution. For turbulent flow, which is to expect for the flow conditions around a ship, Kato applies Hughes formula for the frictional coefficient (Kato 1958). Linearisation by demanding equal energy over one period results in the following contributions to the roll damping:

$$B_{44}^{V1} = \frac{8}{3\pi} \cdot 0.09275 \cdot \rho \cdot S \cdot r_S^2 \cdot \omega^{0.5} \cdot \nu^{0.5} \tag{3.19}$$

$$B_{44}^{V2} = 0.00755 \cdot \rho \cdot S \cdot r_S^{2.772} \cdot \omega^{-0.114} \cdot \nu^{0.114} \cdot \eta_{4a}^{-0.228} \tag{3.20}$$

An important note is that B_{44}^{V2} is dependent on the roll amplitude. VERES applies the same addition to roll damping for all seastates analysed, meaning that the wave amplitude given as input to calculate the frictional damping must be chosen carefully. Use of the resulting RAO must also be done with this simplification in mind. The effect of this parameter on operability is discussed in section 7.3.3.

Eddy damping

Eddy damping occurs as a result of energy dissipation due to the work of creating eddies. Eddies are created from flow separation at the cross section bilges when the vessel rolls. Using forced roll tests, Ikeda proposed a prediction method for roll damping from eddies (Ikeda 1978a).

$$B_{44}^{V1} = 0 \tag{3.21}$$

$$B_{44}^{V2} = \frac{1}{2}\rho r_{max}^2 \int_S c_p(s) l(s) dS \tag{3.22}$$

Here r_{max} is the maximum distance from the roll axis to the hull surface, $c_p(s)$ is the pressure coefficient and $l(s)$ is the roll moment lever.

Damping due to lift effects

A ship moving forward with sway motion will create lift forces on the hull. The same type of lift occurs for a ship during roll motion (Himeno 1981). Himeno presents the following coefficients for roll damping due to lift:

$$B_{44}^{V1} = \frac{1}{2} \cdot \rho \cdot U \cdot L \cdot d \cdot k_N \cdot l_0 \cdot l_R \left[1 - 1.4\frac{z_G}{l_R} + 0.7\frac{z_G^2}{l_0 l_R}\right] \tag{3.23}$$

$$B_{44}^{V2} = 0 \tag{3.24}$$

Here d is the draught, $l_0 = 0.3d$ and $l_R = 0.5d$. k_N is the derivative of the lift coefficient of the hull when towed obliquely. Below B is the beam of the vessel and C_M is the subsectional area coefficient of the midsubsection.

$$k_N = 2\pi\frac{d}{L} + \kappa\left(4.1\frac{B}{L} - 0.045\right) \tag{3.25}$$

$$\kappa = \begin{cases} 0, & C_M \leq 0.92 \\ 0.1, & 0.92 < C_M \leq 0.97 \\ 0.3, & 0.97 < C_M \leq 0.99 \end{cases} \tag{3.26}$$

Bilge keel damping

Bilge keels are found on nearly all modern monohull vessels. The bilge keels are approximately 30cm wide plates mounted along the bilges of the vessel for about $1/3L_{PP}$ of the length of vessel. Figure 3.3 show the velocity field surrounding a bilge keel on a FPSO during roll motion. Two effects cause damping due to bilge keels; normal forces on the bilge keel and pressure variation on the hull surface. Methods for calculating coefficients for these effects were proposed by Ikeda.

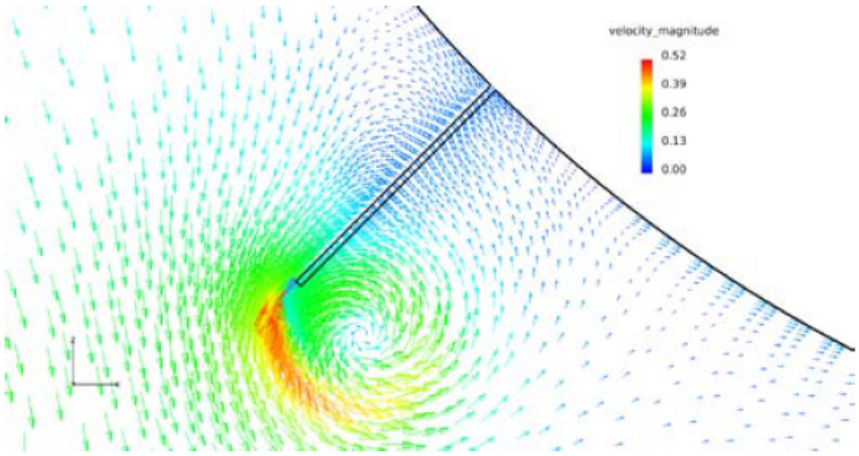

Figure 3.3: Bilge keel on FPSO simulated at KC=2 using CFD (Yan et al. 2013)

1. Damping due to normal forces at bilge keels. The method for calculating the coefficients is given in (Ikeda 1978b).

$$B_{44}^{V1} = \frac{8}{3\pi^2} \cdot 22.5 \cdot b_{bk}^2 \cdot r_{bk}^2 \cdot f \cdot \omega \tag{3.27}$$

$$B_{44}^{V2} = 2.4 \cdot b_{bk} \cdot f^2 \cdot r_{bk}^2 \tag{3.28}$$

Here b_{bk} is the width of the bilge keel, r_{bk} is the distance from the roll axis to the bilge keel and f is a correction factor for the velocity increment at the bilge keel

given as:

$$f = 1 + 0.3 \cdot e^{-160(1-\sigma)} \tag{3.29}$$

σ is the area coefficient of the cross-subsection.

2. Damping due to pressure induced at the hull. The method for calculating the coefficients is given in (Ikeda 1979).

   - Damping due to increase of pressure on the hull

$$B_{1H}^{+} = 0 \tag{3.30}$$

$$B_{2H}^{+} = \frac{1}{2} \cdot f \cdot r_{bk}^{2} \cdot 1.2 \cdot (I_2 + I_4) \tag{3.31}$$

   I_2 and I_4 are given as

$$I_2 = \int_{s_2}^{s_3} l(s) dS \tag{3.32}$$

$$I_4 = \int_{s_5}^{s_6} l(s) dS \tag{3.33}$$

   - Damping due to decrease of pressure at the hull

$$B_{1H}^{-} = \frac{4}{2\pi^2} \cdot f \cdot r_{bk} \cdot b_{bk} \cdot \omega \cdot 22.5(I_1 + I_3) \tag{3.34}$$

$$B_{2H}^{-} = \frac{1}{2} \cdot f^2 \cdot r_{bk}^{2} \cdot 1.2 \cdot (I_1 + I_3) \tag{3.35}$$

   I_2 and I_4 are given as

$$I_1 = \int_{s_1}^{s_2} l(s) dS \tag{3.36}$$

$$I_3 = \int_{s_4}^{s_5} l(s) dS \tag{3.37}$$

- Total damping coefficient due to pressure induced by bilge keels on the hull

$$B_{44}^{V1} = B_{1H}^{+} + B_{1H}^{-} \tag{3.38}$$

$$B_{44}^{V2} = B_{2H}^{+} + B_{2H}^{-} \tag{3.39}$$

Roll equation of motion

The roll equation of motion may be expressed as (Fathi 2014):

$$\begin{aligned}
&(M_{42} + A_{42})\ddot{\eta}_2 + B_{42}\dot{\eta}_2 \\
&+ (I_{44} + A_{44})\ddot{\eta}_4 + (B_{44} + B_{44}^{V1})\dot{\eta}_4 + B_{44}^{V2}|\dot{\eta}_4|\dot{\eta}_4 + C_{44}\eta_4 \\
&+ (I_{46} + A_{46})\ddot{\eta}_6 + B_{46}\dot{\eta}_6 = F_4
\end{aligned} \tag{3.40}$$

Equation 3.40 show that roll motion is coupled with sway (line 1) and yaw (line 3). Line 2 shows an additional linear and non-linear term for roll damping, B_{44}^{V1} and B_{44}^{V2} respectively. These terms are included to represent the viscous roll damping terms discussed in the previous sections.

3.2.5 Calculating vessel response characteristics

Once the hydrodynamic coefficients and exciting forces have been found, calculation of vessel response characteristics can be performed. The governing equation for the vessel response process is Newton's second law of motion. The uncoupled, linear formulation of this equation is shown in equation 3.41.

$$m\ddot{y} + c\dot{y} + ky = F(t) \tag{3.41}$$

Here m is the inertia (mass), c is the linear damping and k is the restoring coefficient. $F(t)$ is the time dependent exciting force for the system. If the response process is assumed linear and $F(t)$ is an harmonically oscillating force, the system response $y(t)$ may be calculated using the frequency response method (Newland 1993). Vessel response is a coupled 6 degree of freedom (DOF) system subjected to wave loads that are often assumed harmonic. Uncoupled, linear equations for the response process for a floating structure is formulated as:

$$(m_i + A_{ii})\ddot{\eta}_i + B_{ii}\dot{\eta}_i + C_{ii}\eta_i = F_i(t) \tag{3.42}$$

Where A_{ii} is added mass due to increased inertia from acceleration of surrounding fluid, B_{ii} is linear damping representing energy dissipation from the system, C_{ii} is the restoring due to offset from equilibrium position and F_i is excitation force from waves. $\eta_i(t)$ is the system response as a function of time for DOF i. A detailed description of the solutions to this equation was given in the project work prior to this thesis. It is assumed known to the reader that the frequency response method is a method for calculating the steady-state (particular) solution defined by the response amplitude and the phase shift from the load. The focus here will be to describe the process of solving the 6 DOF coupled equation system that apply for vessel response. Generally, the equation system describing vessel response can be written as:

$$(\mathbf{M} + \mathbf{A})\ddot{\eta} + \mathbf{B}\dot{\eta} + \mathbf{C}\eta = \mathbf{F} \tag{3.43}$$

$$\eta = \begin{bmatrix} \eta_1 & \eta_2 & \eta_3 & \eta_4 & \eta_5 & \eta_6 \end{bmatrix}^T \tag{3.44}$$

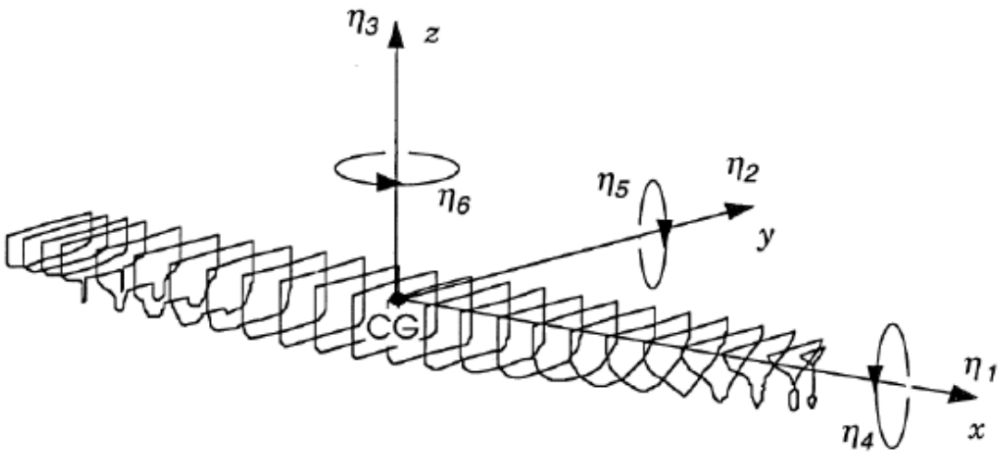

Figure 3.4: 6 DOF system for vessel response (Palmqvist and Hua 1995)

η_{1-3} is translations (surge, sway and heave) and η_{4-6} are rotations (roll, pitch and yaw). Provided that the vessel is symmetric about the xz-plane, the generalised mass matrix, $\mathbf{M}$, may be written as shown in equation 3.45 (Fathi 2014).

$$\mathbf{M} = \rho\nabla \begin{bmatrix} 1 & 0 & 0 & 0 & z_G & 0 \\ 0 & 1 & 0 & -z_G & 0 & 0 \\ 0 & 0 & 1 & 0 & 0 & 0 \\ 0 & -z_G & 0 & R_{44}^2 & 0 & R_{46}^2 \\ z_G & 0 & 0 & 0 & R_{55}^2 & 0 \\ 0 & 0 & 0 & R_{64}^2 & 0 & R_{66}^2 \end{bmatrix} \tag{3.45}$$

Where $\rho\nabla$ is the vessel mass displacement and z_G is the vertical center of gravity. I_{4-6} is the dry mass moment of inertia. The mass moment of inertia is often expressed as:

$$I_{ii} = \rho\nabla R_{ii}^2 \tag{3.46}$$

R_{ii} is called the radius of gyration, and describes how the mass is distributed with regards to the axis of rotation. The inertia for rotational DOFs will increase for increased distance between mass and axis of rotation.

$\mathbf{A}$ is a matrix containing the added mass coefficients. Added mass represents an increase of inertia due to the acceleration of the surrounding fluid. $\mathbf{B}$ contains the damping coefficients. Damping is proportional to the energy dissipation of the system. Added mass and damping forces are steady-state hydrodynamic forces acting on the hull due to rigid body motions when no incident waves are present. Potential theory are commonly applied for finding such coefficients, where the dynamic pressure component and Bernoulli's equation are used. Empirical formulas are also commonly used like seen in section 3.2.4.

$\mathbf{C}$ is the restoring matrix. The restoring coefficients arise due to change in buoyancy and location of center of gravity (COG) relative to center of buoyancy (COB). Restoring forces are proportional to the offset (distance or angle) from the equilibrium position of the vessel.

$\mathbf{F}$ is a 6×1 vector containing the excitation forces and moments for each of the 6 DOFs. Finding the excitation forces from waves is done by examining a fixed vessel exposed

to incident waves. Excitation from waves are divided into two contributions; Froude-Krylov and diffraction forces. Froude-Krylov is the resulting force from the dynamic pressure in the undisturbed wave field, assuming that the vessel or structure has no influence on the incoming waves. Diffraction forces arise due to the presence of the structure, forcing a change in the incident wave pattern. In addition to these forces, floating bodies are also subjected to viscous effects like drag. These forces are small compared to the Froude-Krylov and diffraction pressure forces, and can for most structure geometries be neglected. VERES only accounts for linear pressure forces represented by potential theory, i.e. Froude-Krylov and diffraction as shown in section 3.2.2.

Solving the linear equation system 3.43 results in the vessel responses represented by the steady-state harmonic amplitude and phase shift relative to the excitation force. The response amplitude is given as an RAO as shown in figure 3.5. RAOs are curves for the ratio between the response amplitude and a characteristic load amplitude, wave amplitude ζ_a and wave steepness $k\zeta_a$ are often used for translational and rotational DOFs respectively. Only linear systems results in RAOs as representations of the response process. The ratio between the response amplitude and the characteristic load amplitude is assumed equal for all seastates. Application in steep seastates, where non-linear loading may be of importance, is not recommended.

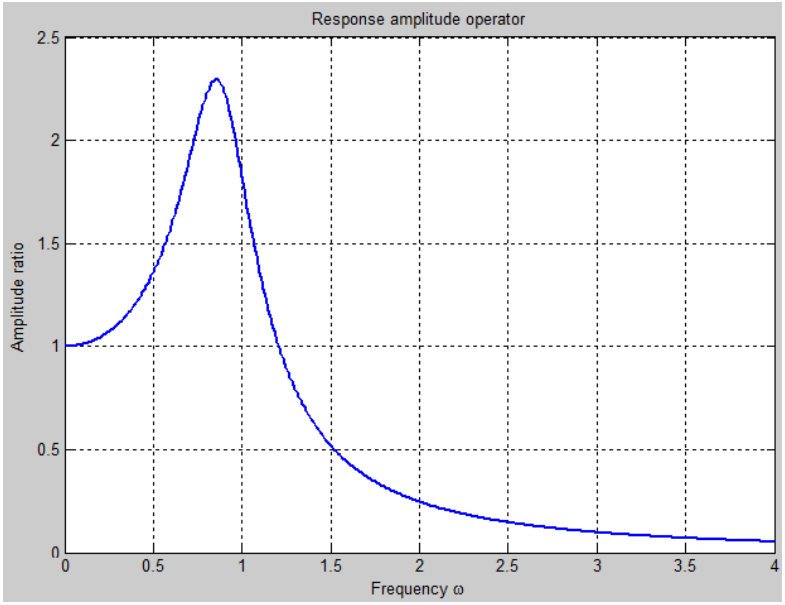

Figure 3.5: RAO for 1DOF system

Rigid body response

The vessel is commonly assumed to have rigid body response. This implies an assumption of no structural deformation of the vessel during motion in waves. This is in reality not the case, but the structural flexing due to wave loading is usually many times smaller than the global ship motion. If the global response is known, defined by η_{1-6}, then the response vector $\mathbf{S}$ may be expressed:

$$\mathbf{S} = \eta_1\mathbf{i} + \eta_2\mathbf{j} + \eta_1\mathbf{k} + \omega \times \mathbf{r} \tag{3.47}$$

Where ω is the angular/rotation vector and $\mathbf{r}$ is the location of a point of interest relative to origo at the center of gravity.

$$\omega = \eta_4\mathbf{i} + \eta_5\mathbf{j} + \eta_6\mathbf{k} \tag{3.48}$$

$$\mathbf{r} = x\mathbf{i} + y\mathbf{j} + z\mathbf{k} \tag{3.49}$$

Solving the crossproduct and adding global translation gives:

$$\mathbf{S} = (\eta_1 + z\eta_5 - y\eta_6)\mathbf{i} + (\eta_2 - z\eta_4 + x\eta_6)\mathbf{j} + (\eta_3 + y\eta_4 - x\eta_5)\mathbf{k} \tag{3.50}$$

$\mathbf{S}$ represent the response in an arbitrary point (x, y, z) relative to the center of gravity in x-, y- and z-direction, indicated by unit vector $\mathbf{i}$, $\mathbf{j}$ and $\mathbf{k}$ respectively. η_{1-6} is here the harmonic response given as:

$$\eta_i = \eta_{ia}\cos(\omega t + \epsilon_i) \tag{3.51}$$

Both amplitude and phase shift are important parameters for determining local response. Phase shifts for different DOFs may give cancellation or amplification of local response depending on whether the response components are in-phase or out of phase. Since the phase shift is a function of the excitation frequency, these effects will also be dependent on frequency.

3.3 Short term statistics

The advantage of linear response analysis is the fast method of doing statistical post-processing based on the RAOs. Combining the RAO $|H_{\eta\eta}(\omega)|$ with a wave spectra $S_{\zeta\zeta}(\omega)$ produce a response spectra $S_{\eta\eta}(\omega)$.

$$S_{\eta\eta}(\omega) = |H_{\eta\eta}(\omega)|^2 S_{\zeta\zeta}(\omega) \tag{3.52}$$

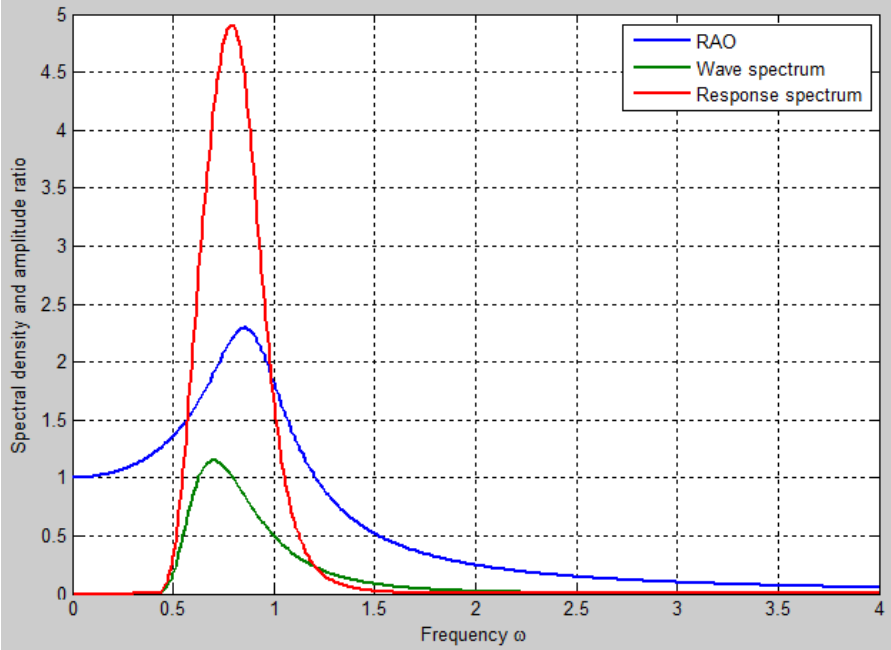

Figure 3.6: RAO, wave spectrum and response spectrum

The wave spectra is the mathematical representation of a seastate, typically with a duration of about 3 hours. The curve represents how the energy is distributed for different wave frequencies. The energy associated with a frequency determines the corresponding wave amplitude. Figure 3.7 shows how an irregular seastate can be created by the summation of regular wave components. This operation is performed as follows (Myrhaug 2007):

The wave spectra is discretized into N intervals with length $\Delta\omega$. On each interval, a harmonic wave component is calculated as:

$$\zeta_{An} = \sqrt{2S_{\zeta\zeta}(\omega_n)\Delta\omega} \tag{3.53}$$

The irregular sea profile may then be calculated as the sum of regular wave components:

$$\zeta(t) = \sum_{n=1}^{N} \zeta_{An} \cos(\omega_n t + \epsilon_n) \tag{3.54}$$

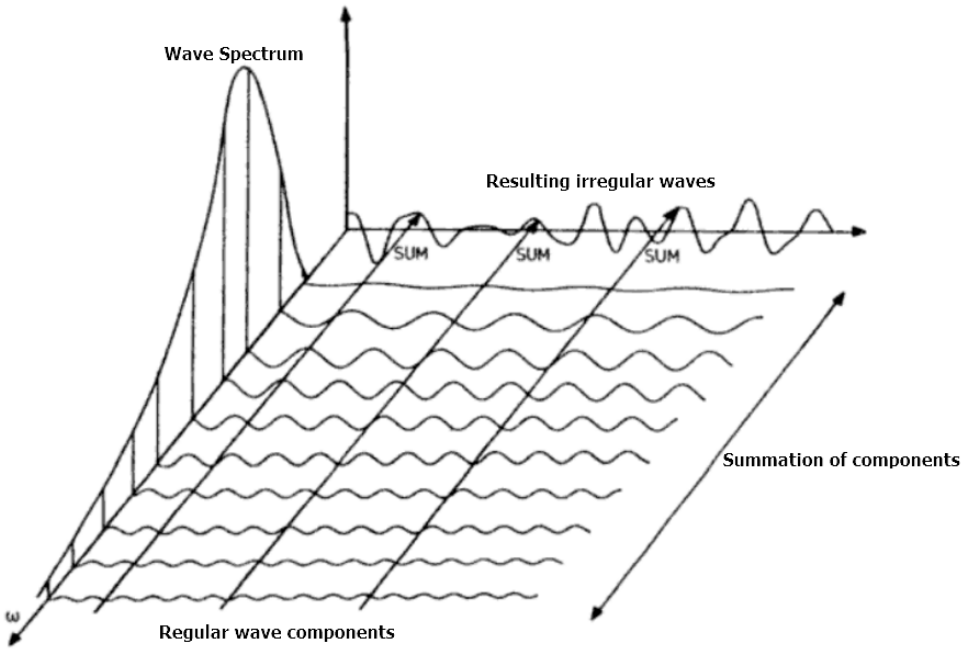

Figure 3.7: Creating irregular waves from regular wave components (Faltinsen 1990)

In equation 3.54 ϵ_n is a random phase shift with a uniform distribution $[0, 2\pi]$ imposed on each wave component. This random property means that irregular waves are stochastic processes since for a given wave spectrum not all properties are deterministically known.

The choice of wave spectra to apply for short term statistics is important for the results. As mentioned earlier, the wave spectra is the mathematical representation of the seastate. Making sure that important physical properties are represented is therefore essential.

- **Joint North Sea Wave Project Spectra (JONSWAP)**

  Developed using data collected in the North Sea, hence it is commonly applied in for studies in this area. It represents a transient seastate. Applies a peakedness parameter, γ, which determines the concentration of seastate energy around the spectral peak period (T_p).

- **Pierson-Moskowitz Spectra (PM)**

  Represents a fully developed, wind generated seastate. Equal to the JONSWAP spectra for $\gamma = 1$. Decreases with ω^{-5} for frequencies higher than the spectral peak frequency according to Phillips relation (Myrhaug 2007).

- **Torsethaugen Spectra**

  Two peaked spectrum which represent both wind and swell generated fully developed seas (Torsethaugen and Haver 2004). Model developed using data from the North Sea.

3.3.1 JONSWAP spectra

JONSWAP spectra is applied for the studies in this thesis. Figure 3.8 show how the JONSWAP spectra are affected by the choice of peakedness parameter γ. For a given seastate, the total energy is constant regardless of choice of wave spectra. Hence, the area under the curves in figure 3.8 and the corresponding significant wave height (H_s) is equal.

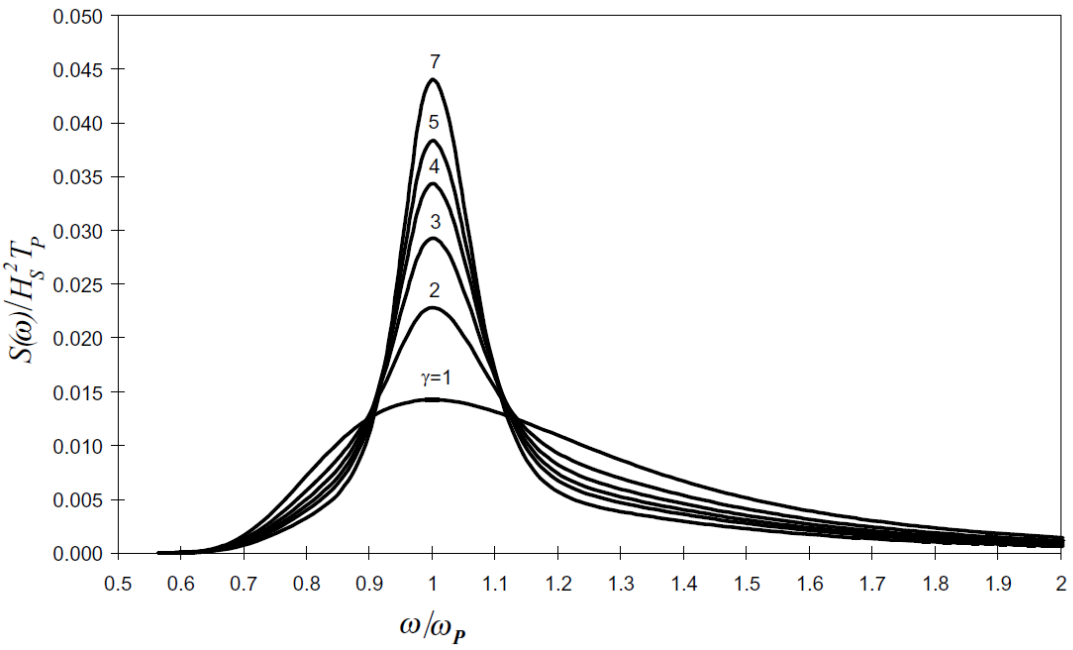

Figure 3.8: JONSWAP spectra for $\gamma = 1 - 7$ (Fathi 2014)

The applicability of JONSWAP spectra is debated. Some scientists question the high peak shape for other areas than the North Sea (Myrhaug 2007). JONSWAP is still often

used for analysis of structures in fully developed seas on deep water. It is assumed to be a good representation of wind generated sea in the JONSWAP interval defined as:

$$3.6\sqrt{H_s} \leq T_p \leq 5\sqrt{H_s} \tag{3.55}$$

γ is often related to H_s and T_p on this interval (Fathi 2014):

$$\gamma = \begin{cases} 5, & T_p/\sqrt{H_s} \leq 3.6 \\ e^{5.75-1.13T_p/\sqrt{H_s}}, & 3.6\sqrt{H_s} \leq T_p \leq 5\sqrt{H_s} \\ 1, & 5 \leq T_p 7\sqrt{H_s} \end{cases} \tag{3.56}$$

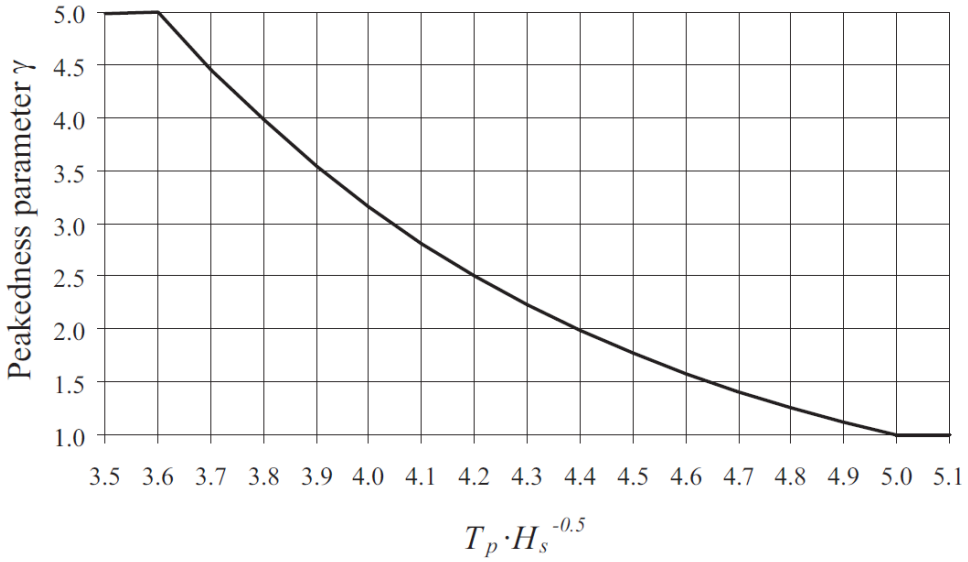

Figure 3.9: γ as a function of H_s and T_p (Fathi 2014)

Figure 3.9 show how γ is modelled as a function of H_s and T_p. Description of a seastate is now complete with values for H_s and T_p.

3.3.2 Limiting seastates

Limiting seastates in this context represents the worst seastates that the vessel is capable of performing the operation. In order to find these environmental limitations, a set of criteria must be defined that reflects the operational limits. As mentioned in section 3.3, the response process in an irregular seastate is a stochastic process. Hence, the criteria needs to be defined as statistical properties with either related to a certain probability of

exceedance or spectral moments.

The basis for computing irregular response characteristics in the frequency domain is the response spectra $S_{\eta\eta}(\omega)$. The kth moment of the response spectra is calculated as:

$$m_k^\eta = \int_0^\infty \omega^k S_{\eta\eta}(\omega) d\omega \tag{3.57}$$

An important parameter for assessing stochastic response is the standard deviation of response σ_η. The interpretation of this value is shown in figure 3.10.

$$\sigma_\eta = \sqrt{m_0^\eta} = \sqrt{\int_0^\infty S_{\eta\eta}(\omega) d\omega} \tag{3.58}$$

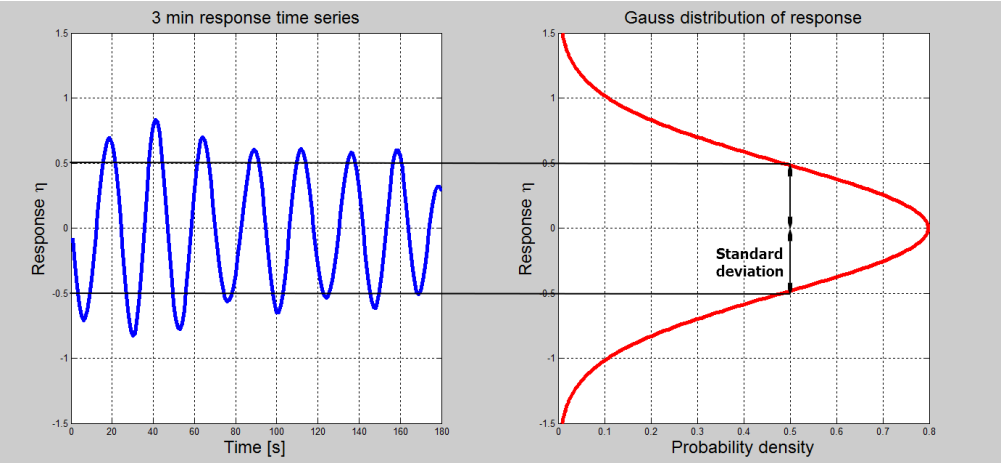

Figure 3.10: Standard deviation of an irregular response process

Statistical values of response can be calculated using the standard deviation. One of the more common values is the significant response amplitude η_{a,m_0}. This value is interpreted as the mean of the $1/3$ largest response amplitudes. $\pm\eta_{a,m_0}$ is also the 95 $\%$ confidence band for the instantaneous response value.

$$\eta_{a,m_0} = 2 \cdot \sigma_\eta \tag{3.59}$$

Another common value is the expected largest response amplitude. This expression is derived assuming Rayleigh distributed individual amplitudes. This assumption is valid for narrow-banded frequency response processes where all amplitudes are assumed in-

dependent. The expected largest amplitude can then be calculated as (Fathi 2014):

$$E(\eta_{a,max}) = \sigma_\eta \left[\sqrt{2 \ln N} + \frac{0.5772}{\sqrt{2 \ln N}} \right] \tag{3.60}$$

Where N is the number of amplitudes during the examined period. Depending on the type of criteria, concrete values are defined for either the standard deviation σ_η or expected maximum $E(\eta_{a,max})$. Other types of statistical values may also be defined as criteria but will not be mentioned here.

Figure 3.11 show the limiting seastates $H_{s,lim}(T_z)$ for two criteria for roll and pitch motion. The example values are 1.5 and 1.0 degrees root mean square (RMS) for roll and pitch respectively. RMS is here equal to the standard deviation σ_η. There is a physical limitation of H_s as a function of T_z indicated by the black line. The area above this line represents seastates that will brake due to steepness.

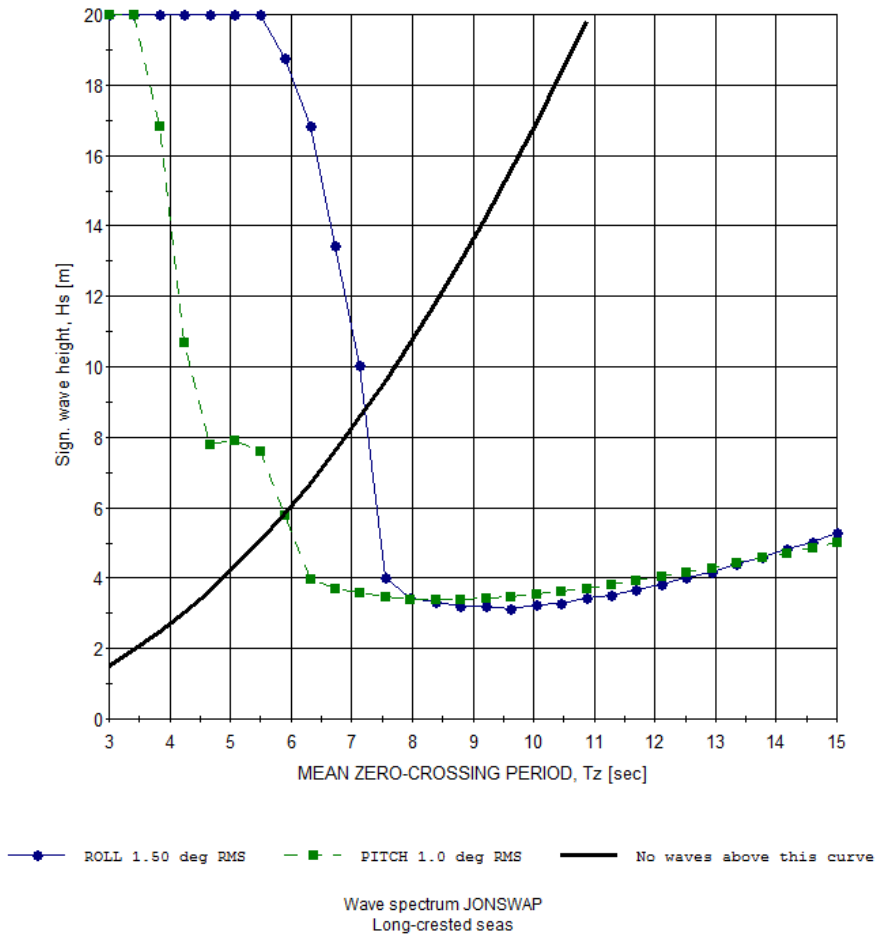

Figure 3.11: Limiting seastates for Roll and Pitch motion

3.4 Long term statistics

Once the limiting seastates are known, the remaining step is to calculate the percentage of time of which these limits are not exceeded. This is done by using scatter diagrams which show the occurrence of seastates for a specific area and in a specified amount of time. Figure 3.12 show the scatter diagram for the North Atlantic Ocean (DNV 2007). The marked area show the seastates which occur 90 % of the time.

SCATTER DIAGRAM FOR THE NORTH ATLANTIC																			
		MEAN ZERO CROSSING PERIOD																Sum	Cum. sum
		3.5	4.5	5.5	6.5	7.5	8.5	9.5	10.5	11.5	12.5	13.5	14.5	15.5	16.5	17.5	18.5		
SIGNIFICANT WAVE HEIGHT	0.5	1.3	133.7	865.6	1186	634.2	186.3	36.9	5.6	0.7	0.1	0	0	0	0	0	0	3050	3050
	1.5	0	29.3	986	4976	7738	5569.7	2375.7	703.5	160.7	30.5	5.1	0.8	0.1	0	0	0	22575	25625
	2.5	0	2.2	197.5	2158.8	6230	7449.5	4860.4	2066	644.5	160.2	33.7	6.3	1.1	0.2	0	0	23810	49435
	3.5	0	0	34.9	695.5	3226.5	5675	5099.1	2838	1114.1	337.7	84.3	18.2	3.5	0.6	0.1	0	19128	68563
	4.5	0	0	6	196.1	1354.3	3288.5	3857.5	2685.5	1275.2	455.1	130.9	31.9	6.9	1.3	0.2	0	13289	81852
	5.5	0	0	1	51	498.4	1602.9	2372.7	2008.3	1126	463.6	150.9	41	9.7	2.1	0.4	0.1	8328	90180
	6.5	0	0	0.2	12.6	167	690.3	1257.9	1268.6	825.9	386.8	140.8	42.2	10.9	2.5	0.5	0.1	4806	94986
	7.5	0	0	0	3	52.1	270.1	594.4	703.2	524.9	276.7	111.7	36.7	10.2	2.5	0.6	0.1	2586	97572
	8.5	0	0	0	0.7	15.4	97.9	255.9	350.6	296.9	174.6	77.6	27.7	8.4	2.2	0.5	0.1	1309	98881
	9.5	0	0	0	0.2	4.3	33.2	101.9	159.9	152.2	99.2	48.3	18.7	6.1	1.7	0.4	0.1	626	99507
	10.5	0	0	0	0	1.2	10.7	37.9	67.5	71.7	51.5	27.3	11.4	4	1.2	0.3	0.1	285	99792
	11.5	0	0	0	0	0.3	3.3	13.3	26.6	31.4	24.7	14.2	6.4	2.4	0.7	0.2	0.1	124	99916
	12.5	0	0	0	0	0.1	1	4.4	9.9	12.8	11	6.8	3.3	1.3	0.4	0.1	0	51	99967
	13.5	0	0	0	0	0	0.3	1.4	3.5	5	4.6	3.1	1.6	0.7	0.2	0.1	0	21	99988
	14.5	0	0	0	0	0	0.1	0.4	1.2	1.8	1.8	1.3	0.7	0.3	0.1	0	0	8	99996
	15.5	0	0	0	0	0	0	0.1	0.4	0.6	0.7	0.5	0.3	0.1	0.1	0	0	3	99999
	16.5	0	0	0	0	0	0	0	0.1	0.2	0.2	0.2	0.1	0.1	0	0	0	1	100000
	Sum	1	165	2091	9280	19922	24879	20870	12898	6245	2479	837	247	66	16	3	1	100000	
	Cum. sum	1	166	2257	11537	31459	56338	77208	90106	96351	98830	99667	99914	99980	99996	99999	100000		

Figure 3.12: Scatter diagram for the North Atlantic Ocean

The probability of occurrence for each seastate, p_{jk}, is first computed by taking the number of occurrences of each seastate and dividing by the total number of seastates. This is shown in figure 3.13. The percentage operability for a given criterion, ship speed and wave heading may then be obtained as a sum of probabilities of seastates satisfying the criterion (Fathi 2014).

$$P_{OP}^{\beta} = \sum_{j=1}^{N_{H_s}} \sum_{k=1}^{N_{T_z}} p_{jk}(H_{sj} < H_{s,lim}, T_{zk}) \tag{3.61}$$

If the study involves several wave headings, the total operability is found by weighting the operability of each heading with the corresponding heading operability, $P(\beta_i)$.

$$P_{OP} = \sum_{i=1}^{N_{\beta}} P_{OP_i}^{\beta} P(\beta_i) \tag{3.62}$$

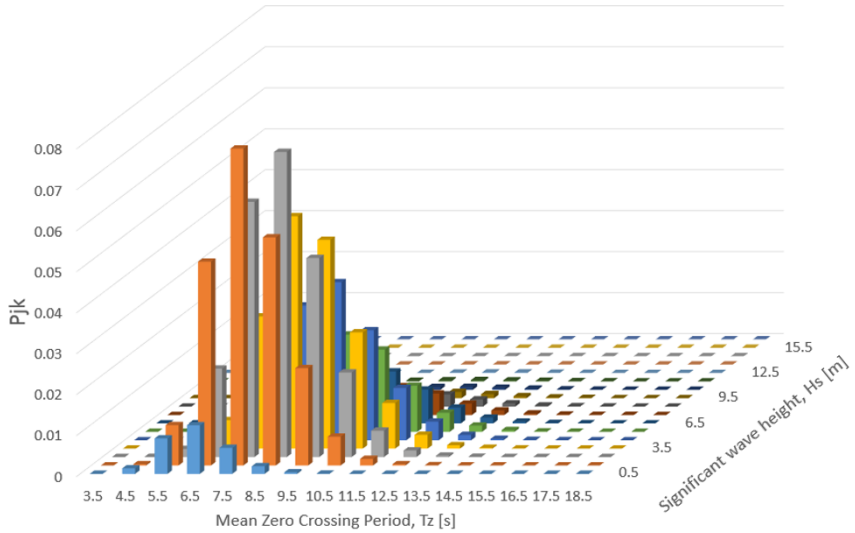

Figure 3.13: Probability of occurrence for seastates in the scatter diagram

The resulting percentage operability is shown in figure 3.14. These values are interpreted as the amount of time the vessel is able to operate without exceeding the previously defined limits.

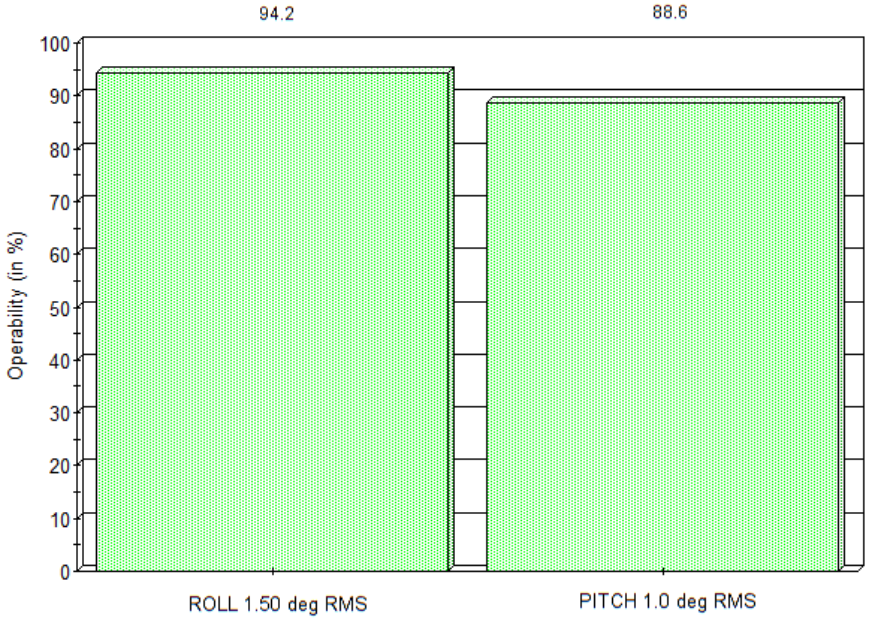

Figure 3.14: Percentage operability by use of long term statistics

Chapter 4

Analysis

This chapter is dedicated to presentation of the analysis set-up. The four vessels that are studied in this thesis is first presented. Then follows the required input to VERES for calculation of response characteristics. The operational areas are presented along with wave statistics. Analysis of required power and change in costs for variation of parameters are presented at the end of the chapter.

4.1 Vessels used in study

This thesis aims to conclude upon general advise concerning design of OSCVs. In order to achieve this, more than one hull design needs to be investigated in order to see if trends found for one design is consistent with trends for other hulls. Hence, the choice was made to study 4 different vessels. This is a compromise between workload and number of data points as the analysis and post-processing work scale linearly with the number of vessels.

All vessels are VARD Design OSCVs designed to perform subsea lifting operations. Since this thesis is publicly available, measures have been taken to conceal the identity of the designs.

4.2 Parameter variation

Characteristic parameters affecting the vessel response is varied for all vessels in order to evaluate changes in operational performance. The chosen parameters represent geometrical changes to the hull and mass distribution inside the vessel.

- *Beam*

  Affects the geometry of the hull directly. Potential roll damping is beam dependent. Also affects building costs and resistance. Applied values based on current design.

- *Length*

  Changes the geometry of the hull directly. Affects building costs and resistance. Not altered for each vessel since the four vessels represent a change in overall length between 100-160m.

- *Draught*

  Affect vessel geometry in water and vessel displacement. May be changed as necessary within the capacity of the ballast tanks. May also change building costs and resistance if design waterline is altered.

- *GM*

  Causes changes in roll stiffness. Altered by changing mass distribution in the vertical direction or changing the waterline second area moment of inertia. Values found by studying the stability manuals of each vessel.

- R_{44}

  Causes changes in roll inertia. Altered by changing the mass distribution towards the sides or in the vertical direction of the vessel (y- or z-direction).

- R_{55}

  Causes changes in pitch inertia. Altered by changing the mass distribution along the length or in the vertical direction of the vessel (x- or z-direction). VARD's experience is that changing the pitch radius of gyration requires moving large amounts of mass along the length of the vessel, which creates difficulties with

general arrangement. The choice was therefore made not to change the pitch radius of gyration based on their experience and advise.

Table 4.1 show the different cases studied in this thesis. Values marked as bold represent the basecases for each vessel. These serve as reference values for comparison of operational performance. Each additional value represent a parametric change of the vessel and subsequently a new VERES-calculation. Note that each parameter is changed independent of other parameters, i.e. coupling effects are neglected. This is discussed further in section 7.2.1.

Table 4.1: Vessel parameter variations

Vessel ID	***1***	***2***	***3***	***4***
Length overall [m]	**100**	**120**	**140**	**160**
variation:+20%B	25.8	27.6	30.0	32.4
variation:+10%B	23.7	25.3	27.5	29.7
Chosen mid value for beam, B [m]	**21.5**	**23.0**	**25.0**	**27.0**
variation:-10%B	19.4	20.7	22.5	24.3
variation:-20%B	17.2	18.4	20.0	21.6
variation:+1.5m	8.0	8.0	9.0	9.5
variation:+1.0m	7.5	7.5	8.5	9.0
variation:+0.5m	7.0	7.0	8.0	8.5
Chosen mid value for draught, D [m]	**6.5**	**6.5**	**7.5**	**8.0**
variation:-0.5m	6.0	6.0	7.0	7.5
variation:-1.0m	5.5	5.5	6.5	7.0
variation:-1.5m	5.0	5.0	6.0	6.5
variation:+1m	3.0	3.0	3.0	3.0
variation:+0.5m	2.5	2.5	2.5	2.5
Chosen mid value for GM [m]	**2.0**	**2.0**	**2.0**	**2.0**
variation:-0.5m	1.5	1.5	1.5	1.5
variation:-1m	1.0	1.0	1.0	1.0
variation:+5%B	40	40	40	40
Chosen mid value for R_{44} [$\%B$]	**35**	**35**	**35**	**35**
variation:-5%B	30	30	30	30
R_{55} [$\%L_{pp}$]	**25**	**25**	**25**	**25**
R_{66} [$\%L_{pp}$]	**25**	**25**	**25**	**25**
R_{64} [$\%L_{pp}$]	**0**	**0**	**0**	**0**
Sinkage [m]]	**0**	**0**	**0**	**0**
Trim [m]	**0**	**0**	**0**	**0**

4.3 VERES response calculations

4.3.1 Vessel data

VERES requires vessel data as input in addition to the section model. Moonpool dimensions, bilge keel data, roll damping tanks data and roll stabilizing foils data be must also be specified in VERES prior to analysis.

- **Moonpools**

  Included in analysis. Data collected manually from general arrangement drawings of each vessel (not listed).

- **Bilge keels**

  Included in analysis. Data collected from experimental study reports at MARINTEK (not listed).

- **Roll damping tanks**

  Not included in analysis. Lifting operations is performed with inactive roll damping tanks.

- **Stabilizing foils**

  Not included in analysis. Not present at vessels.

Including moonpools is important in order to obtain the correct displacement, Froude-Krylov forces, center of buoyancy (COB), added mass and restoring matrices (Fathi 2014). Effects due to resonant motion of the water column inside the moonpool is not accounted for. Including bilge keels is important to for more accurate modelling of roll damping (sec. 3.2.4).

4.3.2 Viscous roll damping

Viscous roll damping is included with a reference wave amplitude of 2.0 m. This value is chosen since it is a suitable reference value for the typically limiting seastates H_s=2.5-4.0m. The application of this value is presented in section 3.2.4. A sensitivity study on the importance of the linearization wave amplitude on operability is found in section 7.3.3.

4.4 Area of operation

Areas along the Norwegian coast is assessed for application in the operability study. Wave statistics is collected from *Global Wave Statistics* by Hogben, Dacunha, and Olliver 1986.

- **Area 1 - Barents Sea**

  An area more known for fishing than oil and gas production, but more fields is currently being developed. The perhaps most famous installation is the Goliat bucket design FPSO currently operating outside Hammerfest.

- **Area 4 - Norwegian Sea**

  Much activity related to oil and gas production in this area. Heidrun, Draugen, Njord and Åsgard are some of the many fields located at Haltenbanken north-west of Trondheim. Also Ormen Lange (sec. 1.1.1) is located in this area.

- **Area 11 - North Sea**

  This is the most extensively developed area along the Norwegian coast. Ekofisk, Draupner, Statfjord, Oseberg and Troll are famous fields in this area.

The geographical location of the areas is shown in figure 4.1. Wave statistics is gathered as annual scatter diagrams based on hindcast data (Appendix A).
The difference in the occurrence of seastates is most clear by computing the marginal distributions for H_s and T_z as seen in figure 4.2.

- **Distribution of H_s**

  H_s is directly proportional to the energy of the seastate. The linear short term response scales linearly with H_s regardless of vessel size and parameter configuration. This means that for a constant T_z, an increase in H_s will reduce operability for all vessels.

- **Distribution of T_z**

  Whether a distribution of T_z is favourable or not is not known until it is compared to the vessel's natural periods. Parametric changes that alters the natural periods will affect the operability by moving the natural periods relative to the most frequent T_z.

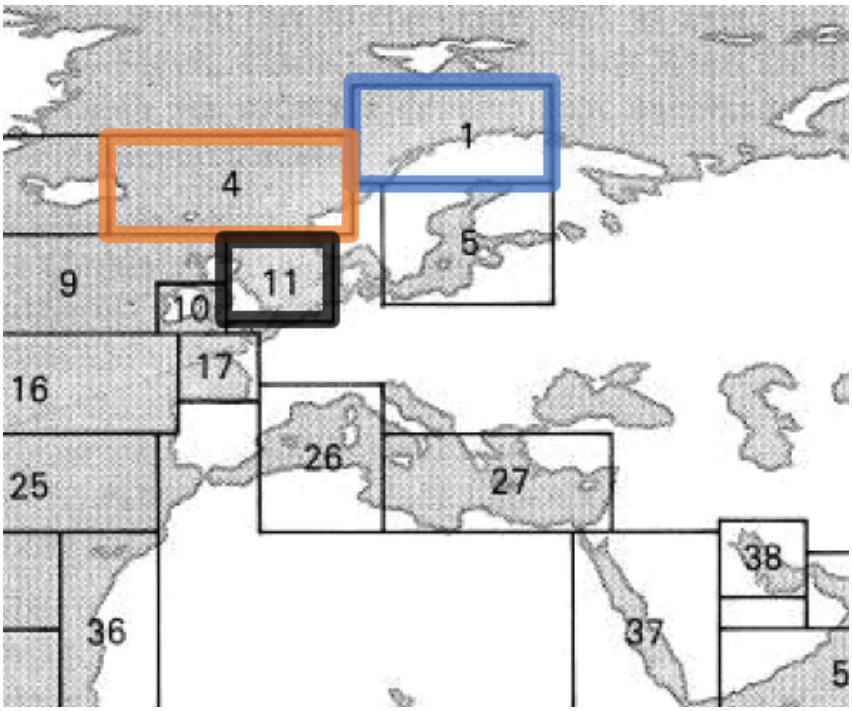

Figure 4.1: Operational areas (Hogben, Dacunha, and Olliver 1986)

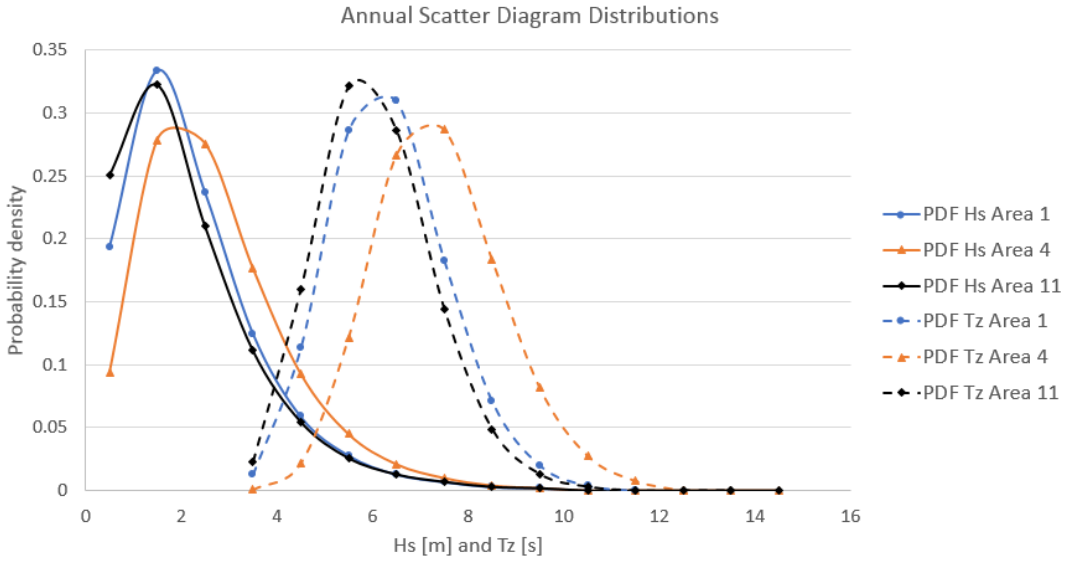

Figure 4.2: Empirical scatter diagram marginal distributions for H_s and T_z

As mentioned above, increased H_s lead to reduced operability. Figure 4.2 shows that the Norwegian Sea (area 4) is the worst area, when only H_s is considered, due to a thicker tail in the H_s distribution. Whether it is the worst area for all vessels and parametric configuration is however not known. The Norwegian Sea and the North Sea has the highest and lowest expected T_z respectively. These two areas are therefore chosen to be applied in the operability analysis.

4.4.1 Seastates

If the vessel is not in close vicinity to other structures, the vessel heading is normally bow towards the weather. This will give unrealistic low roll motion in VERES which is not suitable for comparing vessel seakeeping performance. A wave heading of 15 degrees is therefore chosen to include both roll and pitch motion and be comparable to realistic lifting scenarios. Long-crested sea is applied. The evaluation points is at the lee side of the vessel, which is in compliance with normal operational procedures.

The JONSWAP spectra with varying γ as a function of H_s and T_p is applied in the short term statistics as described in section 3.3.1.

4.5 Estimating change in cost

As mentioned in section 1.2, it is important to evaluate other aspects of the design than operability when doing a parametric study. Changes in cost may also be of importance for decision making. An estimate of the change in cost for different parametric configurations is therefore performed.

4.5.1 Required power

Required power is highly dependent on the choice of main dimensions. In this thesis, the beam and draught are altered to optimize operational performance. Both parameters affect the resistance of the vessel which lead to differences in the cost of main machinery and fuel. An estimate of required power is therefore included.

Resistance prediction

One of the main challenges of resistance prediction is to determine the resistance due to wave making, reflected in the residuary resistance coefficient C_R. The residuary resistance coefficient is the remaining part of the total resistance coefficient C_T after all non-Froude scaling coefficients $\bar{C}$ have been subtracted.

$$C_R = C_T - \sum \bar{C} \tag{4.1}$$

$\bar{C}$ is usually calculated using empirical formulas. Main contributions are:

- Frictional resistance coefficient C_F
- Air resistance coefficient C_{AA}
- Submerged transom coefficient C_{BD}
- Added resistance due to hull roughness ΔC_F

To accurately determine the resistance of an OSCV hull, either experimental tests in a towing tank or numerical methods, preferably CFD, is required. Both methods are too time-consuming and expensive for the number of hulls evaluated in this thesis. An alternative approach is therefore adopted.

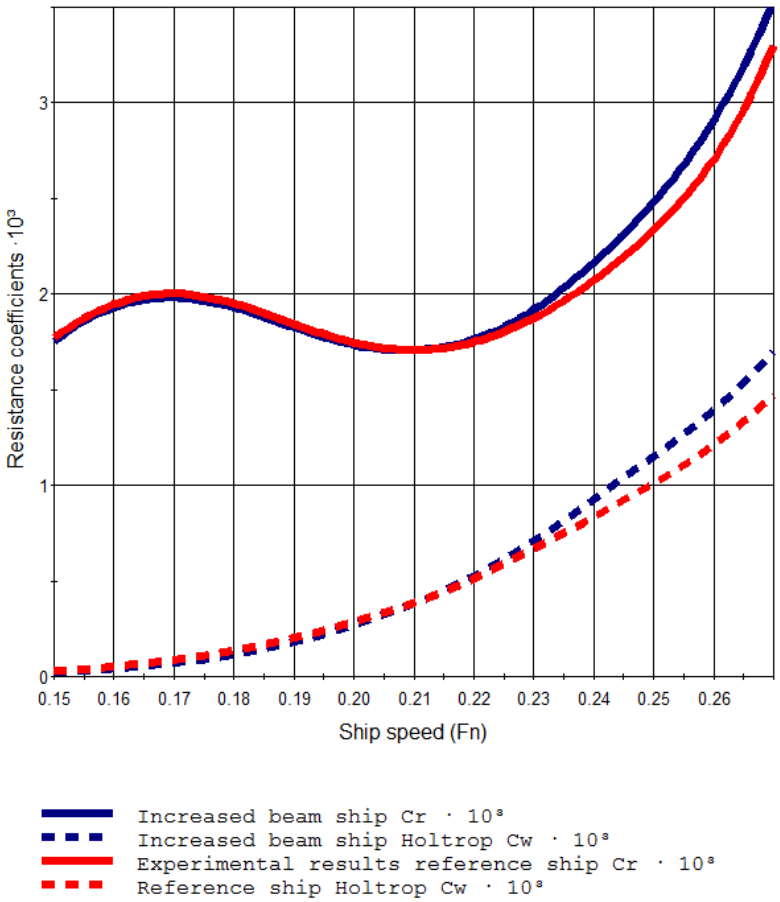

Figure 4.3: Predicting C_R using experimental data and Holtrop 84

Figure 4.3 illustrates how C_R is predicted using experimental results from towing tests at MARINTEK and the empirical method Holtrop 84. The red solid line represent the

experimental results obtained for the vessel at design condition (basecase). To obtain C_R for a vessel with increased beam (solid blue line), C_R is predicted for both vessels empirically using Holtrop 84 (dotted lines). The difference from the empirical predictions are then added to the experimental results for the basecase. This methods allow the use of accurate experimental results while being fast and cheap to apply. Another option is to apply factors calculated from the empirical predictions and apply to the experimental results. This produced untrustworthy results for low Froude numbers. The reason is that C_W approaches zero for low Froude numbers, which resulted in large factors for small differences in C_W. The choice were therefore made to add the difference in C_W directly as seen above. Holtrop 84 was chosen over Hollenbach 98 because Holtrop 84 is based on a larger database of vessels.

The method's ability to reflect differences in C_R for changes in beam and draught was studied. Figure 4.4 show how C_R is affected by changes in beam and draughts for the presented method.

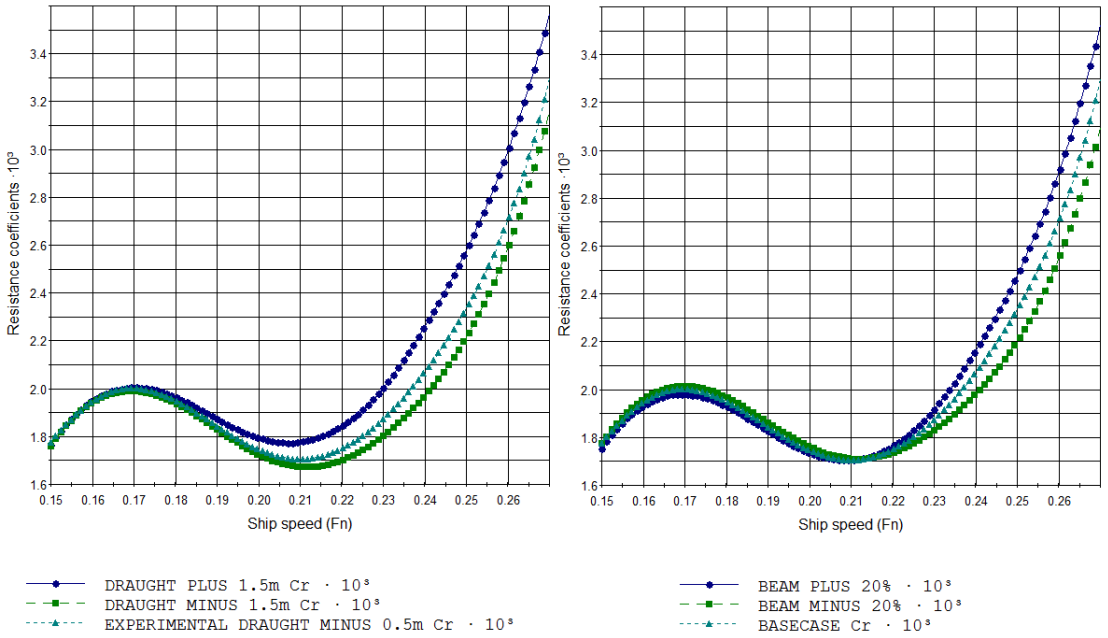

Figure 4.4: C_R prediction for change in beam and draught

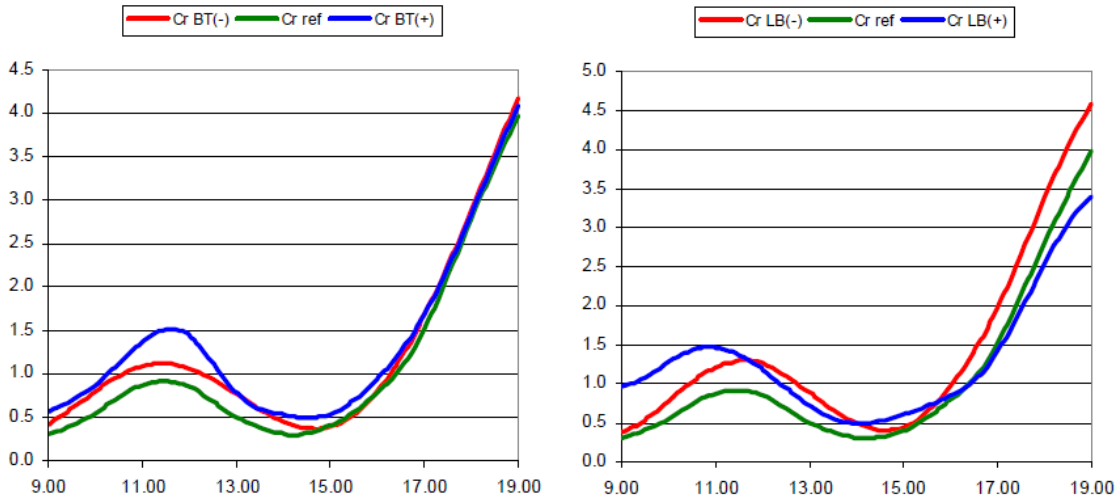

Figure 4.5: $C_R \cdot 10^3$ for change in B/T and L/B (MARINTEK AS 2009)

Figure 4.5 show results from a project on offshore vessels conducted by MARINTEK AS in 2009. These graphs are based on towing tests of OSCV models with different B/T- and L/B-ratios. Note that the B/T- and L/B-variations are not pure. Variation of B/T-ratio is studied on models which also has a varying L/B-ratio and vice versa.

- **Beam variation**

  An increase of beam implies an increase of B/T (blue curve left figure 4.5) and decrease of L/B (red curve right figure 4.5). The trend of increasing C_R for increasing beam at high speed is captured by the presented method as seen on the right plot in figure 4.4. At lower speeds, vessels with smaller beams is predicted to have a higher C_R. This is also consistent with MARINTEK's findings.

- **Draught variation**

  An increase of draught implies a decrease of the B/T-ratio (red curve left figure 4.5). MARINTEK's results show that an increased draught results in C_R between the reference model and the model with decreased draught for all tested speeds. This is not consistent with the presented method, which predicts increasing C_R for increasing draught for all calculated speeds.

Holtrop 84 is based on statistical analysis of model tests on a large number of vessels. It is an empirical method based on main dimensions and is not expected to capture details as well as towing tests. The influence of non-pure B/T and L/B-variations is also not known. The presented method is assumed to be valid for design comparison purposes, and is used to predict differences in resistance in this thesis.

ShipX was found to give inconsistent values for the submerged transom area for variation of beam in the Ship Speed and Powering plug-in. A model for estimating the area was therefore adopted.

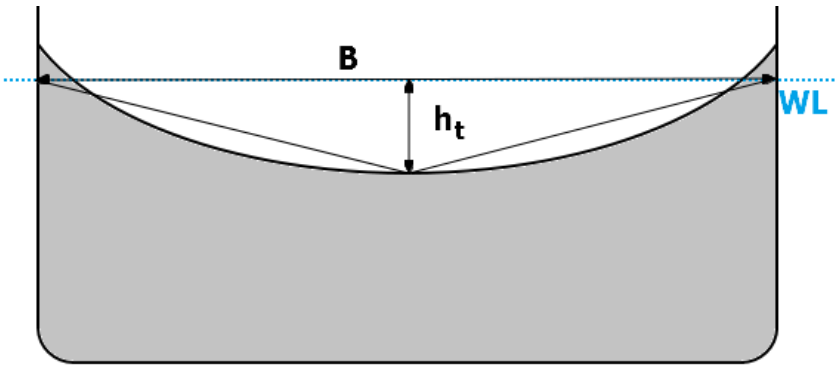

Figure 4.6: Model for calculating submerged area

$$S_{BD} = \frac{1}{2} \cdot B \cdot h_t \cdot \alpha \tag{4.2}$$

Where α is a scale factor obtained to match the original transom stern area and kept equal for all beam variations. Submerged transom area was kept as calculated by Ship Speed and Powering for variation of draught.

The area above the waterline was modelled to include air resistance. Applied values from the towing tests at MARINTEK were used to create the model.

$$A_T = B \cdot (30 + D_{DWL} - D) \tag{4.3}$$

Where D_{DWL} is the design draught. Since no data is found for variation of beam, the area above the waterline is assumed to be directly proportional to the beam. The default air resistance coefficient in ShipX were applied.

Propulsion data

To find the required power, the propeller characteristics and propulsor data must be defined. Open water and propulsion tests at performed at MARINTEK were applied in order to have a good comparison basis.

The following procedure was applied for all parametric variations:

1. **Open water characteristics kept constant**
   Open water characteristics equal to results from open water tests. This assumption involves maintaining equal:
   - Propeller diameter
   - Number of blades
   - Pitch ratio
   - Blade area ratio
2. **Propulsive coefficients kept constant**
   Propulsive coefficients are applied as constants for all calculated speeds. The values were taken as the experimental results at the speed used as reference for transit for each vessel. This assumption involves maintaining equal:
   - Wake fraction
   - Thrust deduction factor
   - Relative rotational efficiency
   - Mechanical efficiency

4.5.2 Hull steel costs

A common way of estimating the building costs of a ship is to apply a rate for cost pr. unit ton of steel. There are several theories concerning how such rates may be defined. One of the methods is based on statistical analysis of empirical data, which estimate the rate based on the main dimensions of the vessel. Kerlen's formula for the specific hull steel costs is based on the block coefficient and vessel length (Schneekluth 1987).

$$k_{st} = k_0 \cdot \left(\frac{3}{\sqrt[3]{L}} + \frac{3}{L} + 0.2082 \right) \cdot \left(\frac{3}{2.58 + C_B^2} - 0.07 \frac{0.65 - C_B}{0.65} \right) \tag{4.4}$$

k_0 is taken to represent the production cost of a ship 140 m in length and with a block coefficient of 0.65. This equation is a result of statistical analysis of the building costs of vessels with block coefficients between 0.5 and 0.8 and length between 80 m and 200 m. Figure 4.7 show the factor applied to k_0 to determine the change in specific hull costs. It shows that the vessel length is the main variable for determining specific hull costs. The dotted lines represent the domain of the OSCV's studied in this thesis.

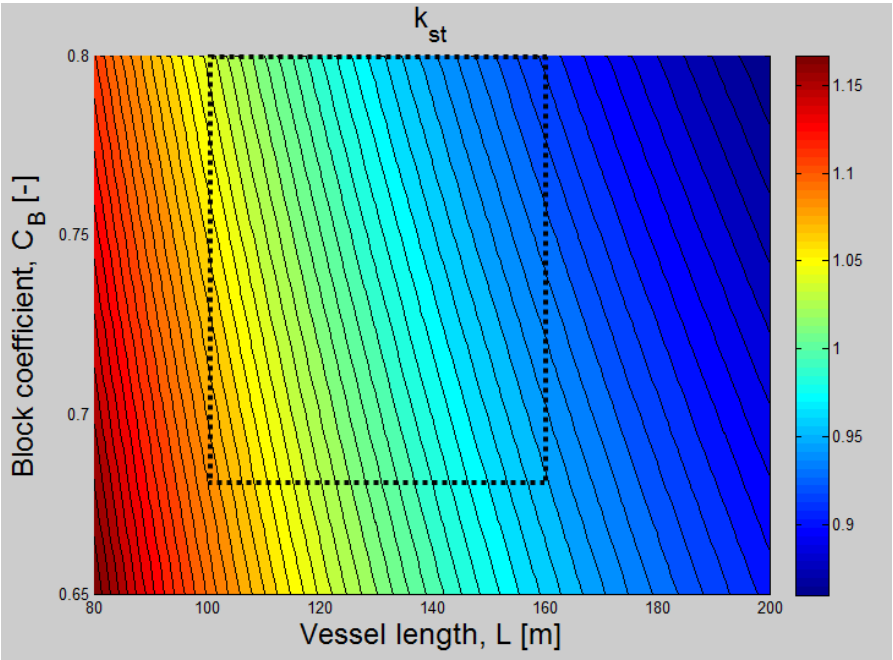

Figure 4.7: Specific hull costs according to Kerlen, k_{st}

Costs from similar projects were obtained from VARD and used to estimate k_0.

4.5.3 Machinery costs

Generator sets vary in price depending on required capacity and quality. When the required propulsion power changes, the capacity of the installed generators must change accordingly. It is common to have several generators for propulsion in order to have a broader range of efficient power modes. It is here assumed a configuration of 4 identical generators for propulsion. Power supply for other systems on the vessels is assumed not to vary.

Jose Jorge Garcia Agis is a PhD Candidate at NTNU and has provided data for the prices on generators based on their power output. The data along with a curve fitting is presented in figure 4.8.

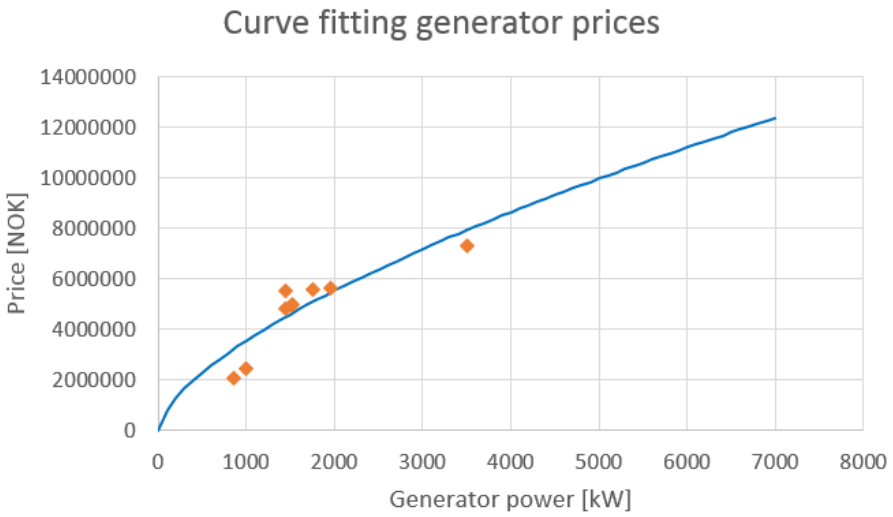

Figure 4.8: Cost of generator set as a function of power output

Table 4.2: Trendline generator prices

Trendline	$41510 \cdot x^{0.6434}$
R^2	0.7882

Prices always increase when the power output increases. Typically, the change in price decreases for higher levels of output power. A much applied model is therefore $a \cdot x^n$, where a and n are constants found through curve fitting and x is the required power output in kW. Results are shown in table 4.2. In reality this curve is discrete and step-wise increasing due to the fixed number of generators available on the market. This model

is however applicable towards estimating the trend of machinery cost and studying the differences in price for the vessels.

The calculations are based on the required propulsion power for varying beam and draught. Since these are calm water calculations, a factor must be applied to account for the increase of required power in waves, wind and current and due to degradation and marine growth on the hull. For the North Atlantic, a typical factor of 1.25 - 1.30 is applied (Hultgreen et al. 2011). A factor of 1.3 is therefore added to the propulsion power in calm water as an estimate of the installed power.

4.5.4 Fuel costs

A case study is performed to evaluate the difference in fuel costs. The scenario is that the vessels are set to install equipment on the Ormen Lange gas field described in section 1.1.1. The distance to Ormen Lange is 120 km from Kristiansund, equivalent to 64.8 nautical miles. The reference transit speed is set to 80% of the contract speed.

Table 4.3: Transit Froude numbers

Vessel ID	***1***	***2***	***3***	***4***
F_N	0.205	0.186	0.183	0.183

The specific fuel consumption is found in Bergen Engines fact sheet for generator plants as 185 g/kWh (Bergen Engines AS 2016). The fuel price were found from Bergen Bunker AS on July 25 2016 as 460 USD/ton for MGO in Bergen port. The exchange rate between USD and NOK were at the same time 8.22 NOK/USD.

Chapter 5

Operability criteria and limits

This chapter presents the background for the applied operational criteria. First the operational setting including the investigated phases and evaluation points is presented. Criteria applied in similar studies are then presented and compared. The last section show how the applied limits are found and how total operability is calculated.

5.1 Operational setting

5.1.1 Operational phases

Out of the phases mentioned in section 2.2.3, the following are assessed with respect to operability:

1. **Lifting over the side (in air)**

   The template is hanging in air over the vessel. Main challenge is to keep the template stable in the horizontal plane.

2. **Splash-zone**

   The template is over the side of the vessel, and is about to be lowered into the water. Main challenge is to keep the template stable in the vertical plane.

3. **Lowering through water column/touch down**

   The template is in the water and being lowered. The crane tip is close to the vessel and low compared to the splash-zone stage. Main challenge is vertical motion.

The choice of phases are based on advice by VARD concerning critical stages of operation dependent on vessel characteristics. Transport to the field and touch-down are also critical phases were extensive planning is required. These phases are however typically limited by the seafastening and DP capacity, which is not considered in this thesis.

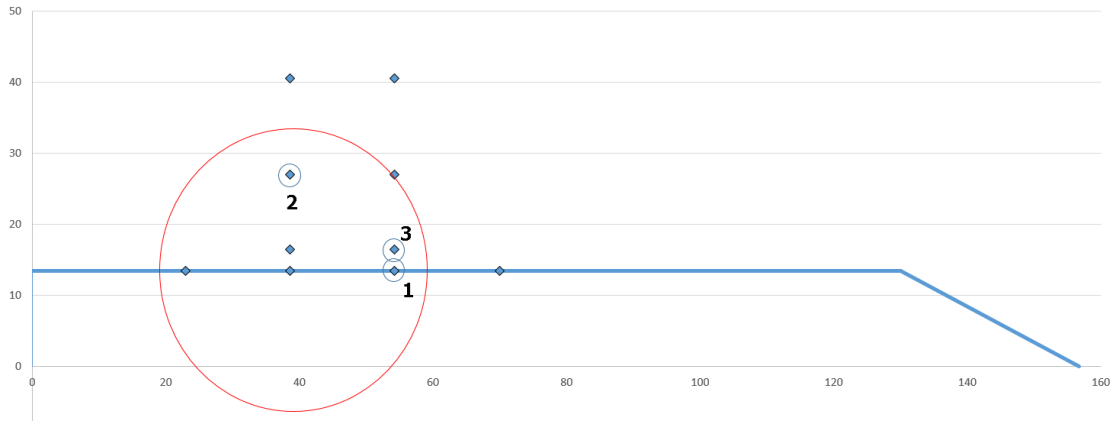

Figure 5.1: Evaluation points lifting operation and 300 ton boom extension limit for crane

Figure 5.1 shows the evaluation points used to calculate the operability of each phase. The red circle is the 300 ton boom extension limit for the crane. Ten points were considered possible early on in the analysis. Points 1, 2 and 3 were chosen because they represent critical points for that phase since the motion of the crane tip is largest in these points for each individual phase. They also represent typical lifting locations. Discussions with VARD provided key information for the choice of relevant evaluation points.

The point coordinates scale linearly according to vessel dimensions. Scaling factors were obtained by studying general arrangement drawings of the vessels. Table 5.1 show the scaling of the evaluation points. The longitudinal position scales with the overall length of the vessel, this coordinate is mainly influenced by the crane position. The transverse and vertical coordinates scales with the beam of the vessel. A wider vessel is assumed capable of lifting larger structures, which often requires higher and longer out over the side lifting positions to maintain clearances to the vessel.

Table 5.1: Scaling of evaluation points relative to the stern

Point	***1***	***2***	***3***
X [m]	$0.4 \cdot L_{OA}$	$0.3 \cdot L_{OA}$	$0.4 \cdot L_{OA}$
Y [m]	$0.5 \cdot B$	$1.0 \cdot B$	$0.5 \cdot B + 3.0$
Z [m]	$1.0 \cdot B$	$1.0 \cdot B$	$0.5 \cdot B$

5.2 Operability criteria

Choosing relevant operability criteria is one of the most critical aspects of an operability study. These criteria is set to represent the exact limit of operation, and have to be quantitative. Fonseca and Soares did a study on the importance of choosing the correct limiting criteria.

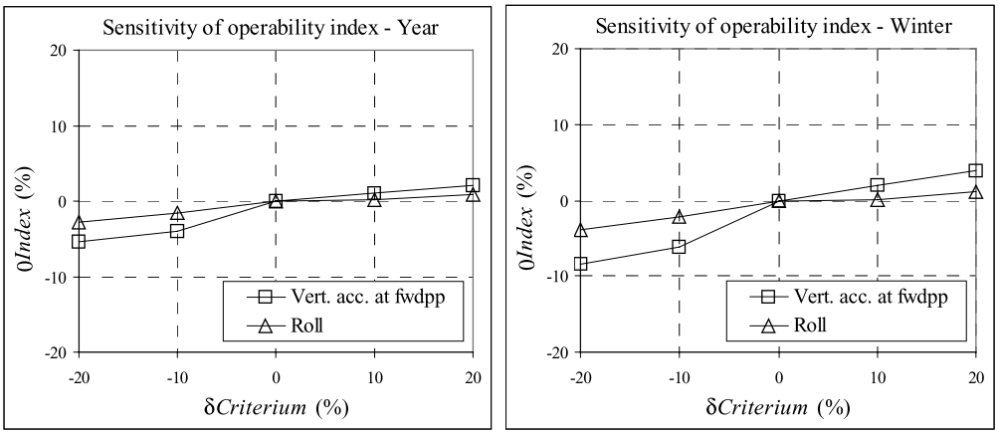

Figure 5.2: Operability sensitivity (Fonseca and Soares 2002)

They found that the operability's sensitivity is dependent on the operability level. Low operability levels have higher sensitivity to the choice of operational limit. This is shown in figure 5.2. The operability sensitivity is higher if only the winter months is considered rather than a full year analysis. This is because operability levels are lower in the winter season due to harsher weather.

5.2.1 Criteria and limits applied in similar studies

A literature study was performed as part of the work towards finding relevant criteria and limitations. Finding similar public studies on offshore vessels turned out to be challenging, so studies involving military vessels, passenger/cruise vessels and fishing

vessels were used. These criteria may not be directly applicable, but seeing how criteria and limits vary with respect to vessel type and operation is valuable learning.

Military vessels

NATO has published a report on the common procedures for seakeeping in the ship design process (H. Eriksen 2000). This report is based on NATO's work for incorporating seakeeping more closely into the ship design procedure from 1995. The operational capability of a warship is stated to be dependent on the following factors:

- Ship Speed
- Weapon and sensor effectiveness
- Ability to launch, recover and handle aircraft
- Replenishment at sea
- Crew effectiveness and safety
- Repair and maintenance work

Criteria related to weapons and aircraft launch and retrieval is considered of little relevance for lifting operations of subsea equipment. Replenishment at sea is done in three ways; connected replenishment (CONREP), fuelling at sea from another ship (FAS) and vertical replenishment from a helicopter (VERTREP). These operations involve loads hanging over the deck, and the same type of challenges is met as for the in-air phase of a subsea lifting operation (sec. 2.2.3).

Figure 5.3, 5.4 and 5.5 show the advised criteria for CONREP, FAS and VERTREP respectively. Criteria for motion induces sickness (seasickness) and motion induced interruptions is included for all types of operation. Also criteria related to the limitation of necessary equipment is included (missile dolly and pallet truck). The most interesting criteria is however the helicopter-to-ship criteria for comparison to a subsea lifting operation.

Limiting Factor	Performance Limitations		
	Motion	Limit*	Location
Equipment: Pallet truck slip angle	Roll	2.2°	
	Pitch	2.2°	
Personnel	Motion Induced Interruption (MII)	0.5/min	CONREP Station
	Motion Sickness Incidence (MSI)	20% of crew @ 4 hr	CONREP Station
	Wetness Index	0.5/hr	CONREP Station

*Note: Roll and pitch limits are given in terms of root-mean-square amplitude.

Figure 5.3: CONREP criteria (H. Eriksen 2000)

Limiting Factor	Performance Limitations		
	Motion	Limit	Location
Personnel	Motion Induced Interruption (MII)	0.5/min	FAS Station
	Motion Sickness Incidence (MSI)	20% of crew @ 4 hr	FAS Station
	Wetness Index	0.5/hr	FAS Station

Figure 5.4: FAS criteria (H. Eriksen 2000)

Limiting Factor	Performance Limitations		
	Motion	Limit*	Location
Helicopter	Relative Wind	±30° off head seas, 15-30 kts	
Helicopter-to-ship	Vertical Displacement	0.7m	VERTREP Station
	Vertical Velocity	1.05m/sec	VERTREP Station
Equipment: missile dolly slip angle	Roll	1.6°	
	Pitch	1.6°	
Personnel	Motion Induced Interruption (MII)	0.5/min	VERTREP Station
	Motion Sickness Incidence (MSI)	20% of crew @ 4 hr	VERTREP Station
	Wetness Index	0.5/hr	VERTREP Station

*Note: Roll, pitch, vertical displacement and velocity limits are given in terms of root-mean-square amplitude.

Figure 5.5: VERTREP criteria (H. Eriksen 2000)

Cruise/passenger vessels

Tezdogan, Incecik, and Turan investigates how the operability is affected by adopting high speed vessels for meeting increasing demand for passenger transportation at sea. The most critical aspect of a cruise vessel is passenger safety and comfort. Many passengers have limited amount of previous time at sea, which make them easily exposed to seasickness and discomfort. Criteria is therefore centred around assuring passenger comfort as seen in table 5.2.

Table 5.2: Operability criteria Tezdogan, Incecik, and Turan 2014

Criterion	***Prescribed maximum value***
Vertical acceleration	2 h exposure 0.05G
Motion Induced Interruptions (MII)	0.5 MII/min
Motion Sickness Incidence (MSI)	35%MSI in 2 h
Lateral acceleration	0.025G RMS

Results show that the operability is mainly governed by the vertical acceleration criterion. The vessel apparently has no problem of meeting the other criteria. Sensitivity analysis show that the operability of all criteria is significantly affected by the choice of seasonal scatter diagram.

Fishing vessels

Mata-Álvarez-Santullano and Souto-Iglesias researched the link between stability, safety and operability on small fishing vessels after 5 vessels tragically capsized due to loss of stability in Spain between 2004 and 2007. These were all new vessels set to replace vessels operating in the same area with the same crew. The new vessels had been designed to improve the operability compared to their predecessors, which raised the question if there is a link between operability and safety. An operability study was performed based on the criteria in table 5.5.

The criteria related to vessel motions have been established as a limit for the crew's ability to work. Fishing involves staying on deck and do heavy work for long periods of time, which is difficult and may also be dangerous in rough weather. The study finds that the operability and stability for the two generations of vessels has opposite trends.

Table 5.3: Operability criteria Mata-Álvarez-Santullano and Souto-Iglesias 2014

Criterion	*Prescribed maximum value*
Roll	6 deg RMS
Pitch	3 deg RMS
Lateral acceleration	0.1G RMS
Vertical acceleration	0.2G RMS
Propeller emergence	15% Prob.
Green water on deck	5% Prob

The predecessors had in general higher stability and less operability than the newer vessels. Lower GM for the new vessels is found to be the main cause of this effect.

Comparison

To see how operational limits vary for different vessel types is valuable with respect to comparison towards OSCVs. The following criteria and limits is gathered from similar studies performed on different vessel types.

Table 5.4: Comparison of different operational criteria for different vessel types

Criterion	*Military vessel*	*Passenger vessel*	*Fishing vessel*
Vertical displacement	0.7 m RMS	Not Limited	Not Limited
Vertical velocity	1.05 m/s RMS	Not Limited	Not Limited
Vertical acceleration	Not Limited	2 h at 0.05G	0.2G RMS
Lateral acceleration	Not Limited	0.025G RMS	0.1G RMS
ROLL	1.6-2.2 deg RMS	Not Limited	6 deg RMS
PITCH	1.6-2.2 deg RMS	Not Limited	3 deg RMS
Motion Induced Interruptions	0.5 MII/min	0.5 MII/min	Not Limited
Motion Sickness Incidence	20%MSI in 4 h	35%MSI in 2 h	Not Limited

Table 5.4 show that there are differences in criteria and limits depending on vessel type. The military vessel has the strictest limits in general. Limits in roll and pitch is several times stricter for the military vessel compared to the fishing vessel. This is because these limits represent different operational scenarios. The military vessel is doing replenishment at sea with objects hanging in the air. Avoiding unintended contact between deck

and lifted object is the reason for choosing such a strict limit. The fishing vessel allow much higher values of roll and pitch since operability of these vessels are limited by the crew's ability to work on deck. Evaluating the operation the vessel is intended to perform is key to develop operational criteria.

These values are not directly applicable as operational limits for a subsea lifting operation using an OSCV. The closest vessel of the ones mentioned above is the military vessel do to the similar nature of the operation. These values will therefore serve as a basis of comparison to the limits applied for the lifting operation in this thesis.

5.2.2 Applied operability criteria

Each phase is analysed separately based on its own set of criteria. This allow evaluation of critical phases in detail as well as global evaluation of vessel operational performance.

- **Lifting in air**

  The main concern is horizontal motion of the lifted object. Lifts are often performed with little clearance to surrounding structures. Horizontal movement of the object is induced as a result of movement of the crane tip due to vessel motion. The dynamic system is similar to a pendulum hanging in a massless string excited by the movement of the change in equilibrium position. Horizontal movements of the crane tip is therefore studied by calculating operability based on the following criteria:

  - Sway displacement
  - Sway velocity
  - Surge displacement
  - Surge velocity
  - Horizontal acceleration

  Notice that the total horizontal acceleration is considered. This is because an extension to the VERES code was provided by the developer, Senior Research

Scientist Dariusz Eirik Fathi at MARINTEK, that allow calculation of the total acceleration.

- **Splash-zone**

  Main concern is vertical motion. Vertical hydrodynamic loads may give slack in the lifting line if the relative motion, velocity and acceleration between the water and the object gets too high (sec. 2.2.3). VERES does not account for diffraction of the wave field when applying 2D strip theory. Relative motion, velocity and acceleration between the lifted object and water on the lee side of the vessel is therefore not included in the analysis in order to maintain the validity of the results. The following criteria is studied for the splash-zone phase:

  - Vertical displacement
  - Vertical velocity
  - Vertical acceleration

- **Lowering**

  Lowering the object out of the splash-zone reduces the hydrodynamic loading. Added mass, viscous damping and current forces are the main loads during this phase of lifting. Vertical motion is induced by the crane tip and determines the hydrodynamic loading during lowering. The following criteria is therefore considered limiting for this phase:

  - Vertical displacement

- **Global criteria for all phases of operation**

  Criteria for global response are also included in the analysis. These affect the above mentioned criteria by rigid body coupled response as described in section 3.2.5. These criteria are included to see how they compare to the local criteria established for each phase. It is of particular interest to see whether operability can be assessed based on global criteria alone. The included global criteria are:

  - Roll
  - Pitch

5.3 Operational limits

5.3.1 Pendulum motion

As mentioned in section 5.2.2, a lifted object suspended from the crane tip is a dynamic system similar to a pendulum hanging in a massless string. The lifting gear is of course not weightless, but it is valid to assume that the main concentration of the mass is at the lifted object. The equation of motion for a pendulum exposed to horizontal harmonic base excitation $x_0(t) = A\cos\Omega t$ may be written as (Zhang and Ma 2015):

$$\ddot{\theta} + \xi\dot{\theta} + \sin\theta = p\cos\omega\tau\cos\theta \tag{5.1}$$

Where θ is the angular displacement and τ is a non-dimensional time variable defined as $\tau = \omega_n t$ where $\omega_n = \sqrt{\frac{g}{L}}$. The amplitude and frequency of the excitation are normalized by $p = \frac{A\Omega^2}{g}$ and $\omega = \frac{\Omega}{\omega_n}$. $\xi = \frac{c}{m\omega_n}$ is the non-dimensional damping ratio.

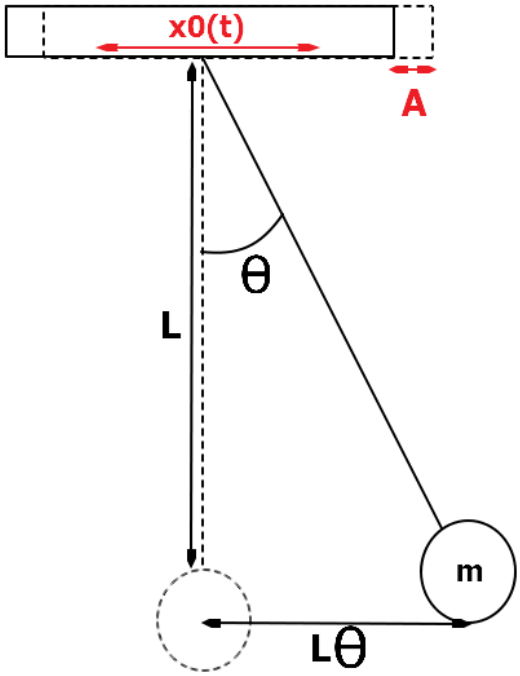

Figure 5.6: Pendulum exposed to horizontal harmonic base excitation

Equation 5.1 is a non-linear differential equation that describes the dynamic behaviour of an object hanging in air while being subjected to harmonic base excitation as seen in figure 5.6. As the base moves, the equilibrium position of the pendulum moves with it a distance A. The resulting restoring force causes excitation. Solving this equation is

difficult due to the non-linear behaviour, and simplified analytical solutions or iterative methods like the ones used by Zhang and Ma are often adopted. A linearized equation is adopted to estimate the limits of operation with regards to pendulum motion.

$$mL^2\ddot{\theta} + c\dot{\theta} + mgL\theta = mgL\theta_A \cos\omega t \tag{5.2}$$

Where mL^2 is the moment of inertia. Notice that the excitation term is equal in formulation as the restoring term. It is here assumed small values of θ, giving $\sin\theta \approx \theta$ and $\cos\theta \approx 1$. θ_A may be formulated as $\frac{A}{L}$ in the excitation, and substituting $c = \xi mL^2\omega_n$ allow removal of the mass m in the equation yielding:

$$L^2\ddot{\theta} + \xi L^2\omega_n\dot{\theta} + gL\theta = gA\cos\omega t \tag{5.3}$$

Equation 5.3 is a linearized differential equation of phenomena often strongly influenced by non-linear contributions to both restoring and excitation. It must therefore be used with the simplifications clearly in mind. A subsea module swinging as a pendulum from a crane is a low damped process. A damping ratio of 0.01 is therefore assumed. A length L=15m is applied as a reference length.

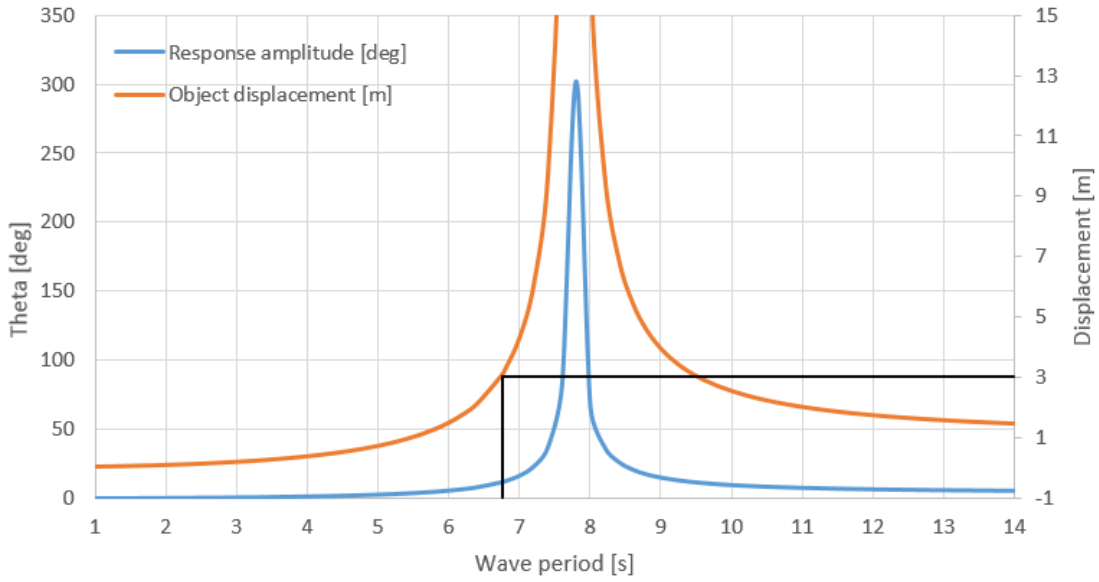

Figure 5.7: Pendulum exposed to horizontal harmonic base excitation

Figure 5.7 show the response θ and displacement $L\theta$ as a function of wave amplitude. The first thing to notice is the large responses at resonance, almost 300 degrees. Such

high values are not physical, and can not be used to find operational limits. Wave periods between 7.5-8.5 seconds are therefore disregarded. In DNV OS-H205 (DNV 2014) section 2.3.3 it is recommended to have a minimum distance of 3 m between lifted objects and surrounding structures. This value is adopted as the maximum allowed displacement $L\theta$.

Excitation frequency, ω

A reference excitation frequency was adopted in order to evaluate the pendulum response. This was chosen using the T_z PDFs for area 11 and 4 shown in figure 4.2. The PDFs are discretely defined according to the scatter diagram. Each discrete value was used as a weight to calculate the weighted average.

$$T_z^{mf} = \frac{1}{2}\left(\sum_{i=1}^{n_{T_z}} PDF_{11}(T_{zi}) \cdot T_{zi} + \sum_{i=1}^{n_{T_z}} PDF_4(T_{zi}) \cdot T_{zi}\right) \tag{5.4}$$

Where PDF_{11} and PDF_4 is the empirical PDFs of the North Sea and the Norwegian Sea respectively. T_z^{mf} was calculated to be 6.73 seconds, meaning that the reference excitation frequency by this method is ω_{mf} = 0.93.

The offset value A corresponding to surge and sway displacement at the crane tip was then adjusted to obtain the prescribed limit of 3 m object displacement. A= 1.0m was found to be the limit. This corresponds to a normalized excitation amplitude p of 0.082 in equation 5.1.

In order to avoid pendulum motion, displacements and velocities in sway and surge and horizontal accelerations are limited. These limits have to correspond to the same level of pendulum motion excitation in order to be consistent. The normalized excitation amplitude p is used as a measure of pendulum motion excitation.

$$p = \frac{A\Omega^2}{g} = \frac{\eta_{1,2}\omega^2}{g} = \frac{\dot{\eta}_{1,2}\omega}{g} = \frac{\ddot{\eta}_{1,2}}{g} \tag{5.5}$$

Equation 5.5 exploits the linear response process and the relation between displacement, velocity and accelerations in harmonic systems. In order to find corresponding values,

a reference excitation frequency had to be chosen. This implies that the chosen limits are only consistent for a specific value of T_Z.

$$\eta_{1a,2a}^{lim} = \frac{p \cdot g}{\omega_{mf}^2} = 1.00m$$
$$\dot{\eta}_{1a,2a}^{lim} = \frac{p \cdot g}{\omega_{mf}} = 0.86m/s$$
$$\ddot{\eta}_{hor}^{lim} = p \cdot g = 0.80m/s^2$$

5.3.2 Splash-zone

In section 2.2.3 the hydrodynamic forces that act on a object in the splash-zone were presented. The main concern at this phase is that the vertical forces exceeds the weight of the object, causing slack in the lifting cable. The vertical hydrodynamic force on the lifted object may be approximated as:

$$F_3 = \rho g \nabla + \rho \nabla \dot{\zeta} + A_{33}(\ddot{\zeta} - \ddot{\eta}_3) + \frac{dA_{33}}{dh}(\dot{\zeta} - \dot{\eta}_3)^2 + B_{33}^1(\dot{\zeta} - \dot{\eta}_3) + B_{33}^2(\dot{\zeta} - \dot{\eta}_3)|\dot{\zeta} - \dot{\eta}_3| \quad (5.6)$$

- $\rho g \nabla$ - buoyancy force
- $\rho \nabla \dot{\zeta}$ - Froude Kriloff force
- $A_{33}(\ddot{\zeta} - \ddot{\eta}_3)$ - diffraction force
- $\frac{dA_{33}}{dh}(\dot{\zeta} - \dot{\eta}_3)^2$ - slamming force
- $B_{33}^1(\dot{\zeta} - \dot{\eta}_3)$ - linear damping due to wave making
- $B_{33}^2(\dot{\zeta} - \dot{\eta}_3)|\dot{\zeta} - \dot{\eta}_3|$ - quadratic damping due to drag

Many of the terms in equation 5.6 depend on the relative motion between the lifted object and the free water surface. Shielding effects must be taken into account to get accurate values for the relative motions. Limiting significant wave height has been found to increase by between 0.5 m and 1.0 m on average if shielding is taken into account (Olsen 2015). Only the crane tip vertical displacement, velocity and acceleration is

analysed in this thesis due to the limitation of ShipX regarding diffraction of the wave field.

Two cases are studied to find limiting crane tip motions as seen in figure 5.8.

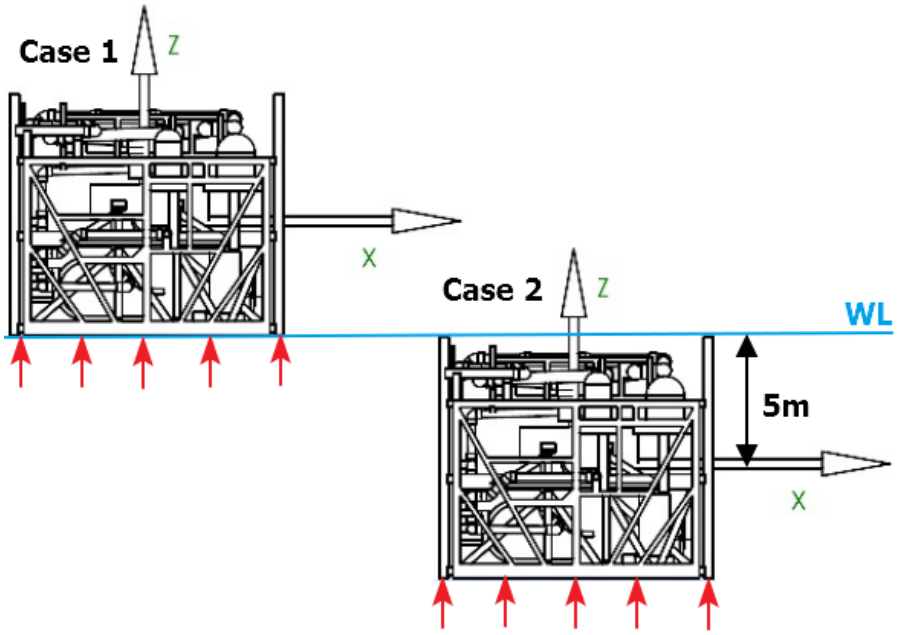

Figure 5.8: Cases for finding limiting crane tip motions (adapted from Selvåg 2013)

- **Case 1 - Slamming force**

  At water entry, an object may be subjected to slamming forces if the relative motion between the water surface and the object is large.

- **Case 2 - Mass and drag forces**

  Fully submerged, the object is subjected to drag and mass forces due to the relative motion between the object and water particles.

Case 1

In section 3.2.9.4 in DNV RP-H103 it is stated that during the initial water entry, the slamming force may be assumed to dominate. Hence, buoyancy and viscous drag are neglected in these calculations. The slamming force of an object in still water may be calculated as (DNV 2011b):

$$F_s(t) = \frac{1}{2}\rho C_s A_p v_s^2 \tag{5.7}$$

Where A_p is the slamming area (horizontal projected area), v_s is the slamming velocity and C_s is the slamming coefficient defined by

$$C_s = \frac{2}{\rho A_p v_s} \frac{dA_{33}^{\infty}}{dt} = \frac{2}{\rho A_p} \frac{dA_{33}^{\infty}}{dh} \tag{5.8}$$

$\frac{dA_{33}^{\infty}}{dh}$ is the rate of change of high frequency added mass with submergence. Hydrodynamic coefficients like added mass are difficult to obtain due to the complex geometry of subsea modules. Anders Selvåg did his master thesis on wave impact forces on complex structures in 2013. He studied the agreement on hydrodynamic forces during lowering through the wave zone using numerical methods (Orcaflex and SIMA) and experimental results on a subsea compressor. The compressor module and results from his thesis is used in case study 1 and 2.

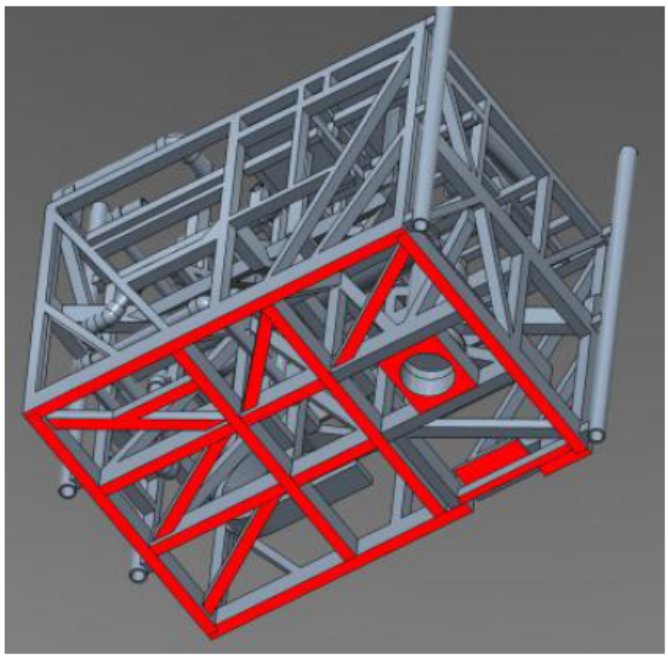

Figure 5.9: Compressor and slamming area (Selvåg 2013)

Table 5.5: Experimental slamming results (Selvåg 2013)

Slamming velocity	***Slamming load***	***Slamming coefficient***
1.5 m/s	205.5 kN	6.0
3.0 m/s	787.5 kN	5.8

A slamming area of 29.6 m^2 and a slamming coefficient of 6.0 will here be used to find a limit for the vertical crane tip velocity in case 1. The compressor has an estimated dry

weight of 333 tons, meaning that the static load due to weight is 3266.7 kN in the lifting cable.

DNV RP-H103 section 4 lists a simplified method of assessing forces on structures lowered through the wave zone. The characteristic wave amplitude may be taken as:

$$\zeta_a = 0.90 \cdot 1.10 \cdot H_s \tag{5.9}$$

A factor of 1.10 is to be applied if the duration of the lift exceeds 30 minutes. This is included in the analysis. The characteristic wave particle velocity at the surface may then be calculated.

$$v_w = \zeta_a \frac{2\pi}{T_z} \tag{5.10}$$

The impact slamming velocity is then taken as:

$$v_s = v_c + \sqrt{v_{ct}^2 + v_w^2} \tag{5.11}$$

Where v_{ct} is the single amplitude vertical velocity of the crane tip and v_c is the hook lowering velocity. v_c = 0.50 m/s is listed in DNV RP-H103 section 4.3.5 as a common value.

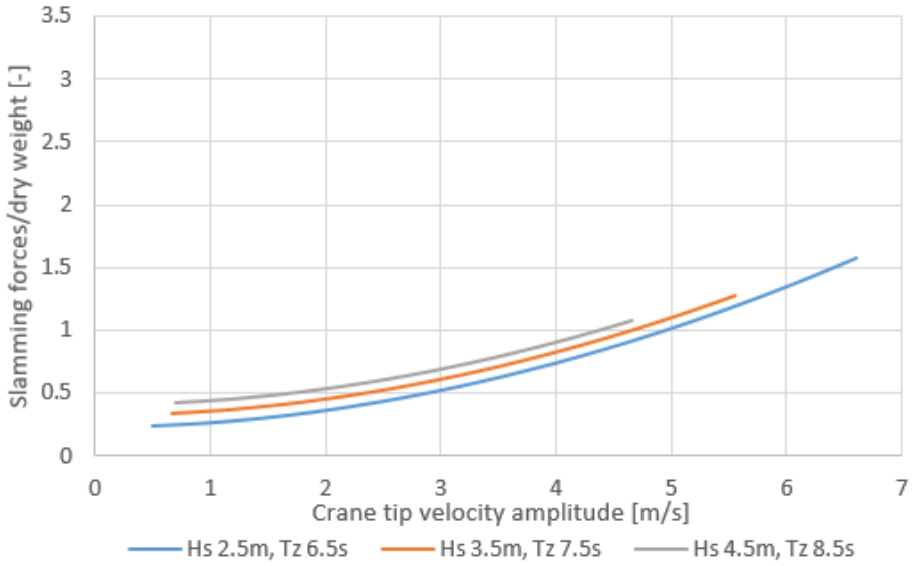

Figure 5.10: Results case 1 H_s = 2.5 - 4.5 m T_z = 6.5 - 8.5 s

Case 2

The compressor is assumed to be completely submerged and subject to mass and drag forces. The term mass force in DNV RP-H103 is to be understood as a combination of the inertia force and the hydrodynamic contributions from Froude Kriloff forces and diffraction. Selvåg did experiments to find the added mass and drag coefficients for the compressor module due to the complex geometry. The results are shown in figure 5.11.

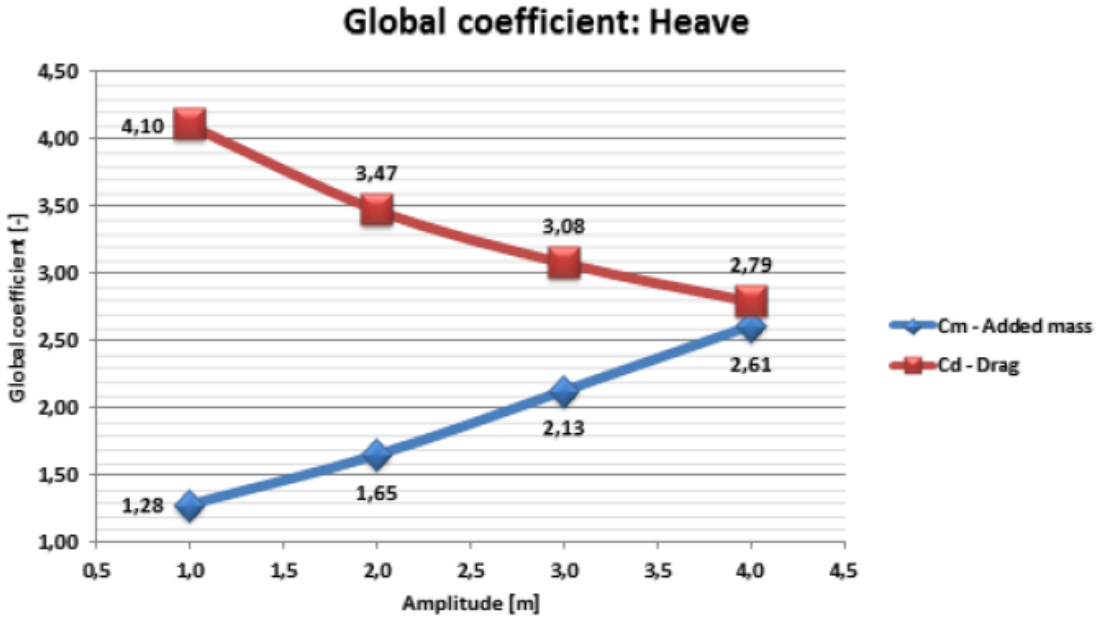

Figure 5.11: Hydrodynamic coefficients for compressor module (Selvåg 2013)

The heave coefficients are functions of the displacement amplitude. This is to be expected for porous structures in infinite water according to Selvåg. This means that the forces corresponding to crane tip vertical displacement, velocity and acceleration are coupled, and is treated accordingly here. Characteristic mass and drag forces are calculated as follows:

$$F_{mi} = \sqrt{[(M_i + A_{33i}) \cdot a_{ct}]^2 + [(\rho V_i + A_{33i}) \cdot a_w]^2} \tag{5.12}$$

Where M_i is the mass of the object in air, A_{33i} is the heave added mass, V_i is the submerged volume, a_{ct} is the crane tip acceleration and a_w is the fluid particle acceleration. $A_{33i} = \rho V_i \cdot C_m$.

$$F_{Di} = \frac{1}{2}\rho C_D A_{pi} v_r^2 \tag{5.13}$$

Where C_D is the drag coefficient, A_{pi} = 84.1 m^2 is the reference drag area and v_r is the characteristic relative velocity between the object and the water particles.

$$v_r = v_c + \sqrt{v_{ct}^2 + v_w^2} \tag{5.14}$$

It is assumed that the module is completely submerged with a volume displacement V_i = 84.7 m^3. The module is 10 m high, so the reference depth is taken at z = 5 m. This corresponds to the center of the module at the same moment that the module is being completely submerged. The characteristic particle displacement, velocity and acceleration are found as:

$$\zeta = \zeta_a \cdot e^{-\frac{4\pi^2}{T_z^2 g}z} \tag{5.15}$$

$$v_w = \frac{2\pi}{T_z} \cdot \zeta_a \cdot e^{-\frac{4\pi^2}{T_z^2 g}z} \tag{5.16}$$

$$a_w = \left(\frac{2\pi}{T_z}\right)^2 \cdot \zeta_a \cdot e^{-\frac{4\pi^2}{T_z^2 g}z} \tag{5.17}$$

The characteristic relative displacement and velocity between the compressor and the fluid particles are then found as:

$$\eta_r = \sqrt{\zeta^2 + \eta_{ct}^2} \tag{5.18}$$

Due to the linear response process, the following relation applies for the crane tip displacement, velocity and acceleration amplitudes

$$\ddot{\eta}_{ct} = \omega\dot{\eta}_{ct} = \omega^2\eta_{ct}$$

This allow calculation of the drag and mass forces as a function of the crane tip displacement. The characteristic combined drag and mass force amplitude may then be calculated as:

$$F_{hyd} = \sqrt{F_D(\eta_{ct})^2 + F_M(\eta_{ct})^2} \tag{5.19}$$

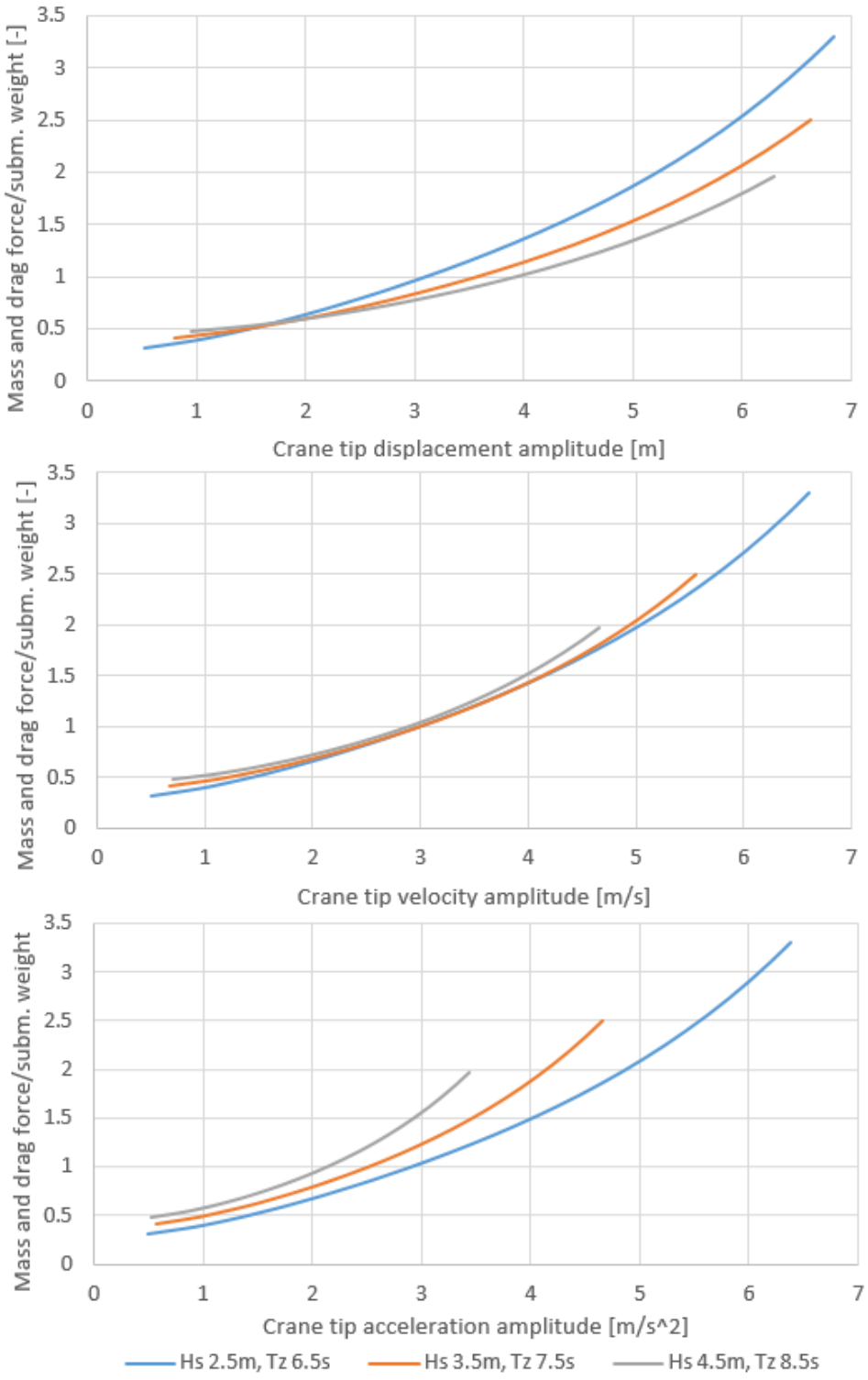

Figure 5.12: Results case 2 H_s = 2.5 - 4.5 m T_z = 6.5 - 8.5 s

Instead of subtracting the buoyancy of the compressor, F_{hyd} is compared to the submerged weight. The submerged weight corresponds to the tension in the line if the compressor is fully submerged and no dynamic forces are present. The characteristic

slamming force is compared to the dry weight since it is assumed not to have buoyancy at water entry. Results from case 1 and 2 are shown in figure 5.10 and 5.12. The seastates have different domain sizes to stay within the domain analysed by Selvåg in figure 5.11.

The results show that the risk of a slack line is higher for when the compressor is submerged than at the water surface. Slamming can cause large forces on structural members mounted at the bottom of the compressor seen in figure 5.9. This is not taken into account when deciding the operational limits here. Assuming then that slack line is the limiting phenomena, case 2 is the limiting part of the splash-zone phase since the crane tip vertical velocity is lower in case 2 than in case 1 for a given force ratio. This holds for all calculated seastates.

All seastates calculated are common in the North Sea and Norwegian Sea. They represent what is to be expected for normal operation. The blue line represent the most steep seastate, but with the least amount of energy. The grey line is the least steep seastate, with the most energy.

The limit of operation is set to when the ratio between mass and inertia forces and submerged displacement is equal to 0.5. This is chosen due to the simple method of analysing the forces acting on the compressor. The main uncertainty is the calculated values for the relative motion, velocity and acceleration between the compressor and the water particles. Since all calculated seastates are common, the worst seastate is chosen for each physical unit.

$$\eta_{ct}^{lim} = 1.2m$$

$$\dot{\eta}_{ct}^{lim} = 0.9m/s$$

$$\ddot{\eta}_{ct}^{lim} = 0.6m/s^2$$

5.3.3 Lowering through the water column

As mentioned in section 5.3.3, the lowered object and the stiffness of the lifting cable create mass-spring dynamical system. This system is excited by movements in the crane tip as seen in figure 5.13. This can cause large forces in the lifting cable as well as slack.

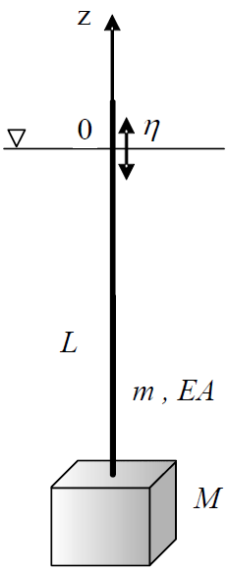

Figure 5.13: Mass-spring system of object during lowering (DNV 2011b)

The following is assumed during calculation of this phase:

- **Same compressor and coefficients as phase 2**

  The same coefficients is applied for drag coefficients and added mass. Constant values for an amplitude of 2.0 m is applied.

- **Water surrounding the structure is not moving in the vertical direction**

  The compressor has been lowered out of the wave-zone and is located in water with low vertical movement.

- **The compressor has been completely filled with water**

  Filling the compressor is assumed completed. 10 $\%$ is added to M_i compared to phase 2 and submerged weight adjusted accordingly.

- **Horizontal motions of the crane tip is insignificant**

  The tension in the cable may be calculated by assessing vertical motions only.

The differential equation governing the module vertical motion η_{3m} is

$$(M_i + \alpha \cdot mL + A_{33})\ddot{\eta}_{3m} + \frac{1}{2}\rho C_D A_P \dot{\eta}_{3m}|\dot{\eta}_m| + k\eta_{3m} = k\eta_{ct} \tag{5.20}$$

Where M_i is the compressor dry mass, α is a factor to account for cable mass, m is mass of cable per meter, A_{3m} is heave added mass for the compressor and k is vertical stiffness. The system is damped by drag as discussed in phase 2. According to DNV RP-H103 section 5.3.5 α may be assumed to be 1/3 if the cable stiffness dominates.

The following parameters are assumed for the lifting equipment and compressor

Table 5.6: Parameters lowering study

Parameter	***Value***
Cable diameter	0.05 m
EA	$4.0 \cdot 10^8$ N
Depth	400 m
M_i	366.3 tons
m	30 kg/m
Subm. weight cable	250 N/m
A_{33}	147.07 tons
C_D	3.491
A_P	81.5 m^2

The drag term is linearised in order to solve the differential equation. This was done using DNV RP-H103 section 5.3.7.5, which give the linear damping coefficient as:

$$B_l = \frac{4}{3\pi}\rho C_D A_p \omega \eta_{3ma} \tag{5.21}$$

Since the damping is a function of the vertical response, an iteration procedure is required. First, $\omega\eta_{3ma}$ = 1 was assumed and the response calculated. A new set of damping coefficients was then calculated as a function of the wave period. This procedure was repeated 50 times. To obtain a stable solution, the new damping was represented as in equation 5.22.

$$B_l^i = \frac{1}{2} \cdot (\frac{4}{3\pi}\rho C_D A_p \omega \eta_{3ma}^i + \frac{4}{3\pi}\rho C_D A_p \omega \eta_{3ma}^{i-1}) \tag{5.22}$$

In figure 5.14 the blue line represent the damping for $\omega\eta_{3ma}$ = 1. The black line is the applied damping. As expected, the damping peak is close to the natural period of the system due to the large motion amplitudes.

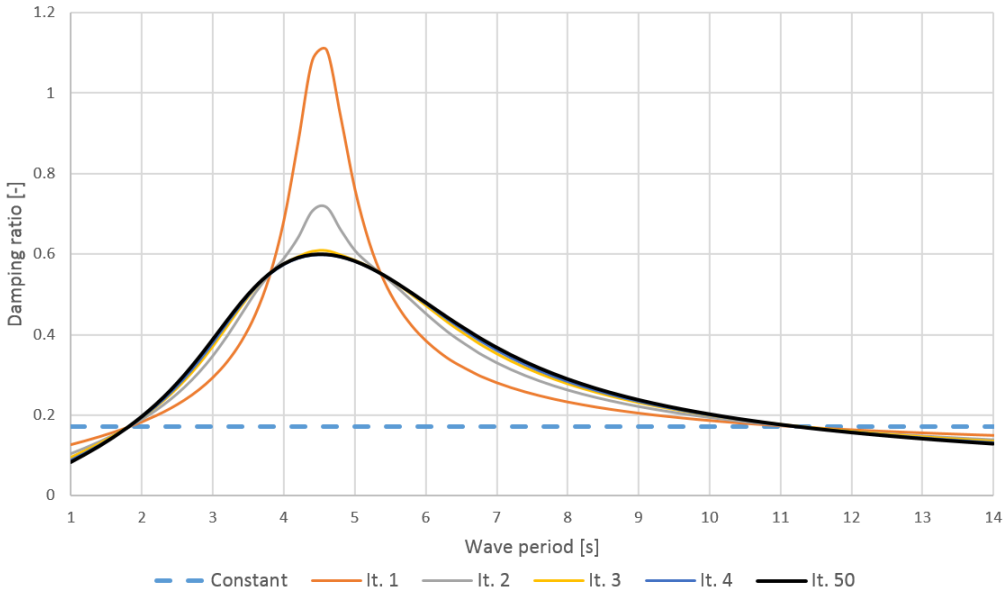

Figure 5.14: Convergence of iteration procedure to determine damping for η_{cta}=1

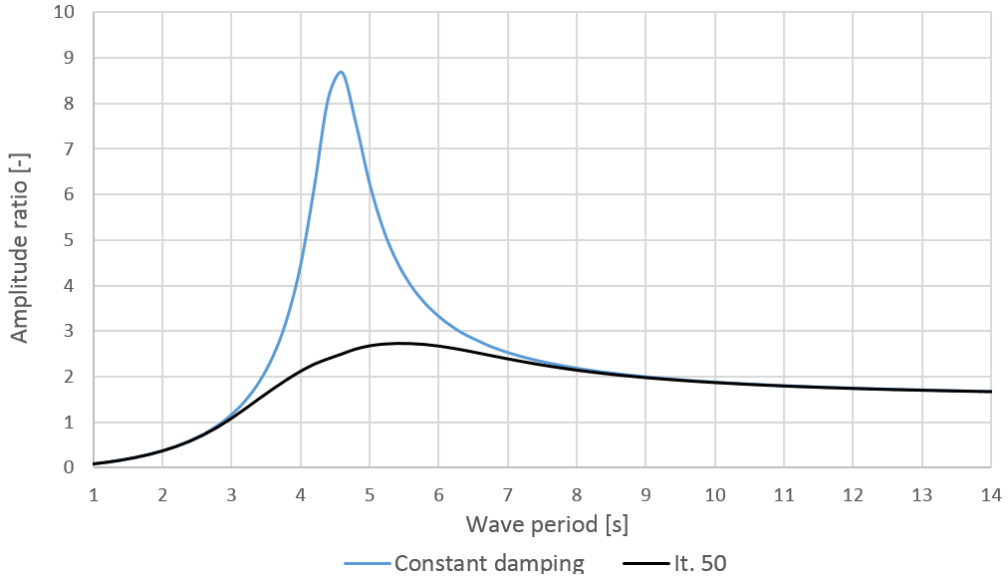

Figure 5.15: RAO for vertical compressor motions for constant and varying damping for η_{cta}=1

Figure 5.15 show the obtained RAOs for constant damping and damping applied after iteration method. The figure illustrates the importance of drag for the vertical motions

of the compressor at resonance. The next step towards finding the corresponding forces is to calculate the RAO for the relative motion between the compressor and the crane tip.

The phase shift between the crane tip and compressor vertical motion is an important factor for the relative motion. If the movement of the crane tip is given as $\eta_{cta} \cos \omega t$, the response of the compressor may be expressed as (Larsen 2012):

$$\eta_{3m} = A \cdot \cos \omega t + B \cdot \sin \omega t = \sqrt{A^2 + B^2} \cdot \cos(\omega t - \epsilon) \tag{5.23}$$

Where ϵ is the phase shift between the response and excitation. Since it is the crane tip motion that excites the motion of the compressor, ϵ represent the phase difference between the crane tip motion and the compressor motion.

$$\epsilon = \tan^{-1}\left(\frac{B}{A}\right) \tag{5.24}$$

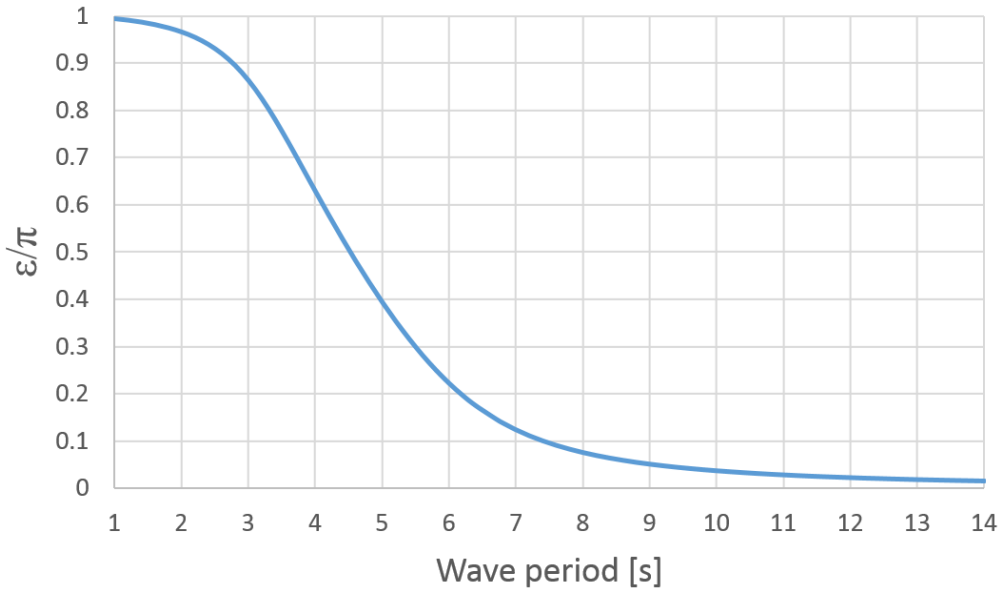

Figure 5.16: Phase shift of motion between crane tip and compressor for η_{cta}=1

Figure 5.16 show the calculated phase shift. As expected the phase difference is high for low periods and converges to zero for high periods. The relative motion RAO can now be derived.

The relative motion between the crane tip and the compressor can be expressed as:

$$\eta_{rel}(t) = \eta_{3m} - \eta_{ct} = \eta_{3ma}\cos(\omega t - \epsilon) - \eta_{cta}\cos(\omega t)$$

The relation between η_{3ma} and η_{cta} is known through the RAO $|H_{3ma}(\omega)| = \frac{\eta_{3ma}}{\eta_{cta}}$.

$$\begin{aligned}\eta_{rel}(t) &= |H_{3ma}(\omega)|\eta_{cta}\cos(\omega t - \epsilon) - \eta_{cta}\cos(\omega t) \\ &= \eta_{cta}\left(|H_{3ma}(\omega)|\cos(\omega t - \epsilon) - \cos(\omega t)\right)\end{aligned}$$

Expressing $\cos(\omega t - \epsilon) = \cos(\omega t)\cos(\epsilon) + \sin(\omega t)\sin(\epsilon)$ yields:

$$\eta_{rel}(t) = \eta_{cta}\left(\left(|H_{3ma}(\omega)|\cos(\epsilon) - 1\right)\cos(\omega t) + |H_{3ma}(\omega)|\sin(\omega t)\sin(\epsilon)\right)$$

$$\begin{aligned}\frac{\eta_{rel}(t)}{\eta_{cta}} &= \left(|H_{3ma}(\omega)|\cos(\epsilon) - 1\right)\cos(\omega t) + |H_{3ma}(\omega)|\sin(\omega t)\sin(\epsilon) \\ &= A_{rel}\cos(\omega t) + B_{rel}\sin(\omega t) \\ &= |H_{rel}(\omega)|\cos(\omega t - \epsilon^{rel})\end{aligned}$$

$$\begin{aligned}A_{rel} &= |H_{3ma}(\omega)|\cos(\epsilon) - 1 \\ B_{rel} &= |H_{3ma}(\omega)|\sin(\epsilon)\end{aligned}$$

It can be shown using trigonometric identities that

$$\begin{aligned}|H_{rel}(\omega)| &= \sqrt{A_{rel}^2 + B_{rel}^2} \\ &= \sqrt{\left(|H_{3ma}(\omega)|\cos(\epsilon) - 1\right)^2 + \left(|H_{3ma}(\omega)|\sin(\epsilon)\right)^2}\end{aligned}$$

Since the damping is a function of the displacement in equation 5.21, an RAO for η_{cta} = 1 m is not valid for all η_{cta}. The change in damping for different displacement levels affect the vertical motion RAO and phase shift, similar to the non-linear roll damping in section 3.2.4. Hence, the iteration procedure is applied to find $|H_{3ma}(\omega)|$ and ϵ for each

analysed η_{cta}. The relative motion amplitude is calculated as:

$$\eta_{rela} = |H(\eta_{cta}, \omega)_{rel}| \cdot \eta_{cta} \tag{5.25}$$

In DNV RP-H103 section 5.3.8 it is stated that slack occur if the relative motion between the crane tip and the lifted object exceeds the static stretch of the cable. The static stretch is calculated as

$$\eta_{st} = L_s - L = \frac{WL + \frac{1}{2}wL^2}{EA} \tag{5.26}$$

The following criterion is applied

$$|\eta_{st} - \eta_{rela}| > 0.1 \cdot \eta_{st} \tag{5.27}$$

This approach is based on the static solution of the force in the lifting line. Dynamic load effects occur locally along the cable that are not taken into account. Analysing it can be done by analysis in time domain software such as SIMA. The results are however a good indication of the crane tip's effect on the dynamics of lowered objects, and hence valid for the purpose of this master thesis.

Figure 5.17 show the relative motion between the crane tip and the compressor, and the tension in the cable at the compressor. The tension is taken as a ratio compared to the static tension at the compressor if the crane tip was stationary. The relative motion is assumed harmonic, but only the lowest tension is plotted since slack is the limiting phenomena. A crane tip amplitude of 1.5 m has 10 $\%$ remaining tension at resonance. The lift is therefore on the limit if heave compensation devices are not applied. $\pm$1.5 seconds around resonance the remaining tension is 20 $\%$. Heave compensation is typically applied near resonance, before the risk of slack is substantial. It is difficult to accurate estimate how much relative motion the heave compensator is able to cancel out. It will depend on the compensator and the lifted object. As mentioned above, it is also difficult to estimate the local tension at the cable with this approach.

A maximum crane tip amplitude of 1.5 m is assumed for comparing the vessels in this

thesis. The analysis above show that this limit represent a typical operational limit for lowering operations.

$$\eta_{cta}^{lim} = 1.5m \tag{5.28}$$

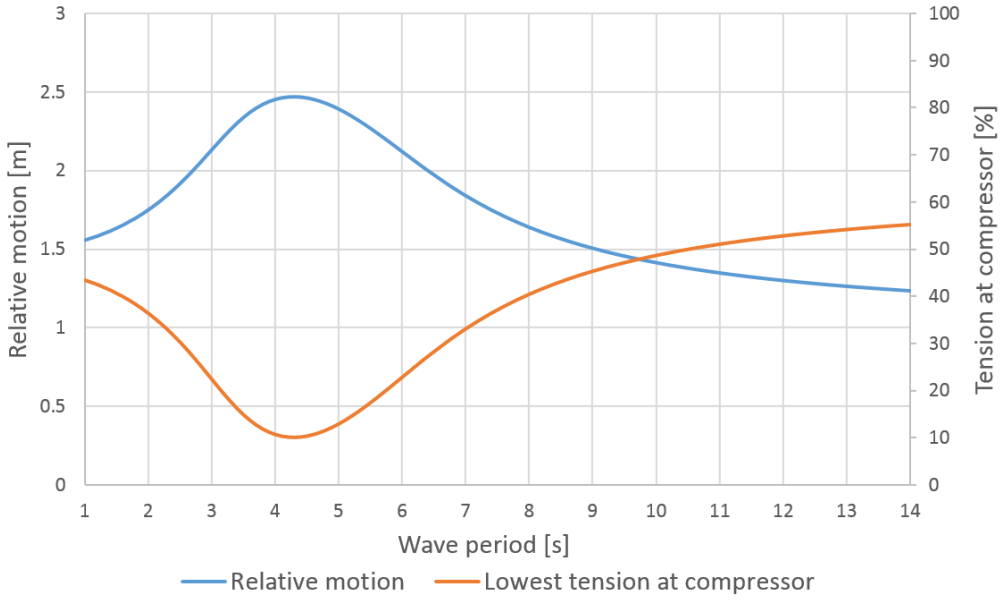

Figure 5.17: Relative motion and cable tension for η_{cta}=1.5

5.4 List of criteria and limits

As mentioned in section 3.4, operability is calculated using the limiting seastates for each criteria. This means that the limits have to be formulated statistically in order to evaluate the performance. The limits have been chosen in a way that allows continuous operation in a 3 hour seastate. As a statistical equivalent, the significant amplitude is assumed to represent the limits. This is the statistical equivalent of the mean of the 1/3 largest values. It is calculated as:

$$\eta_a^{sign} = 2 \cdot \sigma_\eta = limit \tag{5.29}$$

Where σ is formulated in equation 3.58, and corresponds to the root-mean-square (RMS) value. Hence, the limits found in section 5.3 are divided by 2 in table 5.7, 5.8 and 5.9.

Table 5.7: Criteria and limits point 1

Criterion	***Amplitude limit***
Sway displacement	0.50 m RMS
Sway velocity	0.43 m/s RMS
Surge displacement	0.50 m RMS
Surge velocity	0.43 m/s RMS
Horizontal acceleration	0.40 m/s^2 RMS

Table 5.8: Criteria and limits point 2

Criterion	***Amplitude limit***
Vertical displacement	0.60 m RMS
Vertical velocity	0.45 m/s RMS
Vertical acceleration	0.30 m/s^2 RMS

Table 5.9: Criteria and limits point 3

Criterion	***Amplitude limit***
Vertical displacement	0.75 m RMS

5.5 Assessing operability

Each criterion result in a operability level representing the expected percentage of time the vessel is able to meet the criterion limit. It is assumed that the lifting operation will not start until the lifted object can be lifted from the deck, lowered and installed without stop. This requires that all criteria are met for operation to commence.

The total operability is therefore defined as the minimum operability level for all phases and criteria. This implies that the limiting criterion may vary between vessels.

$$OP_{TOT} = min\{OP_1, OP_2, OP_3 \ldots, OP_n\} \tag{5.30}$$

Chapter 6

Results

This chapter presents the results of the analysis performed regarding operability and costs. First the operability levels in different points along with the standard deviation is presented. Then the total operability for parametric variations for operation in the North Sea and Norwegian Sea is presented. Results for the estimates of costs is presented at the end of the chapter.

6.1 Operability

6.1.1 Evaluation points and criteria

The mean operability of the basecase vessels 1-4 has been calculated for all criteria for operation in the Norwegian Sea and North sea.

Point 1 - Pendulum motion

Figure 6.1 show the mean operability of basecase vessel 1-4 regarding pendulum motion in the North Sea and Norwegian Sea. The operability levels for sway and surge displacement and velocity are found to be similar in magnitude, while the operability levels for horizontal acceleration are lower. This is to be expected since the horizontal acceleration calculation in ShipX is the total acceleration, while the displacement and velocity is the x- and y- component.

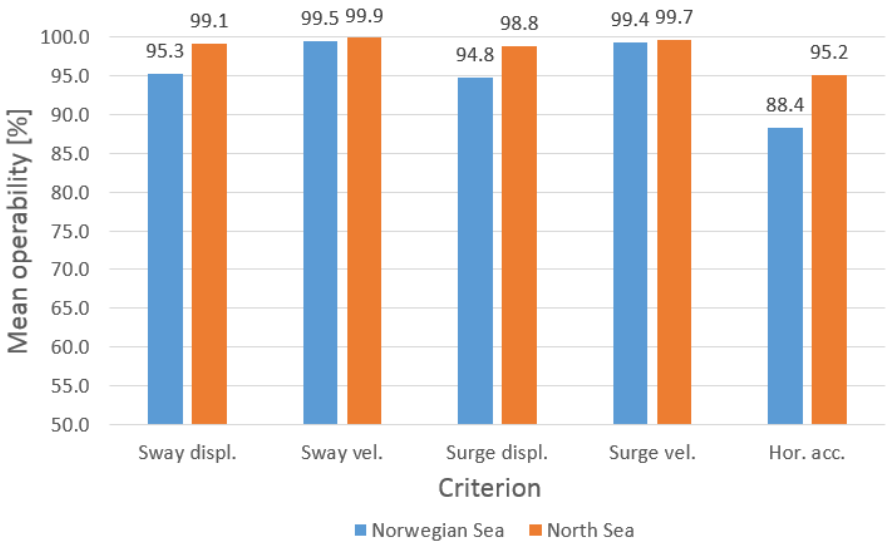

Figure 6.1: Mean operability vessel 1-4 point 1

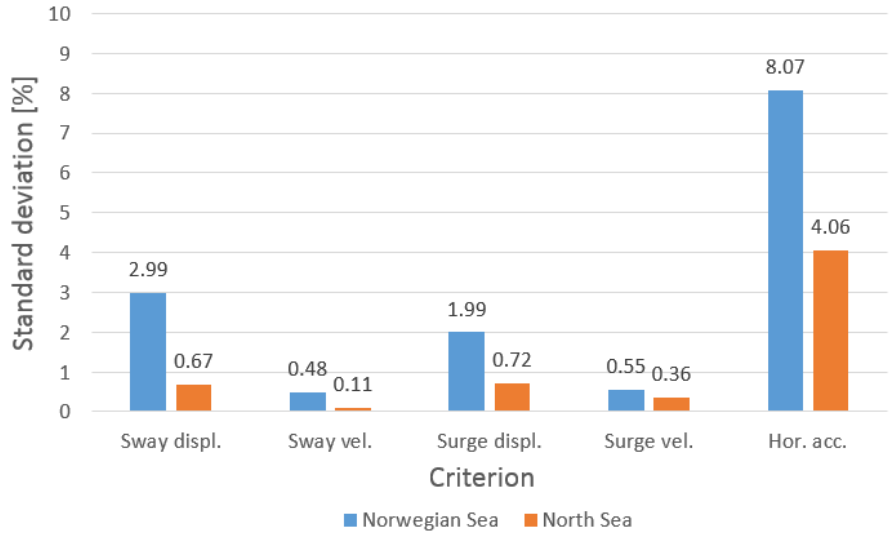

Figure 6.2: Standard deviation operability vessel 1-4 point 1

Figure 6.2 show the standard deviation of the operability levels. The criteria resulting in the lowest operability tend to have the highest standard deviation. This is expected since a mean value close to 100% implies that all four vessels must have close to 100% operability for that particular criterion.

Point 2 - Splash-Zone

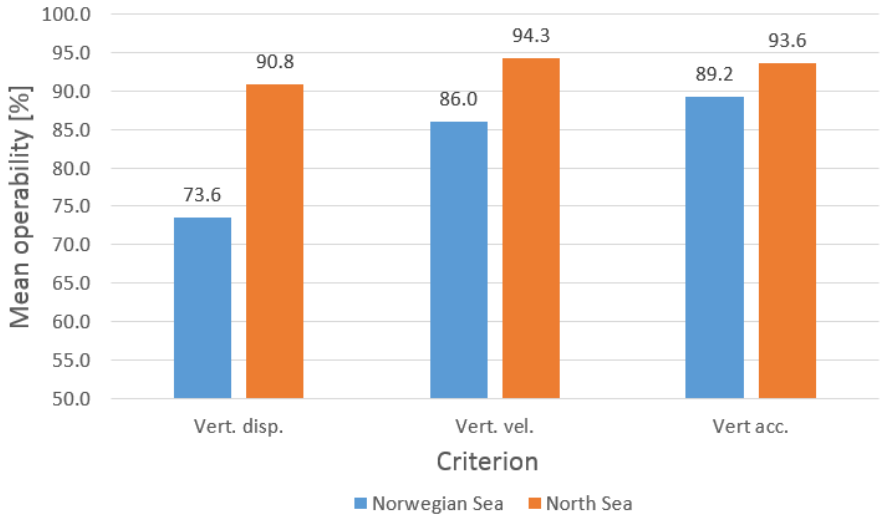

Figure 6.3: Mean operability vessel 1-4 point 2

Figure 6.3 show the mean operability of basecase vessel 1-4 for point 2. The vertical displacement criterion result in the lowest average operability in both the Norwegian Sea and North Sea.

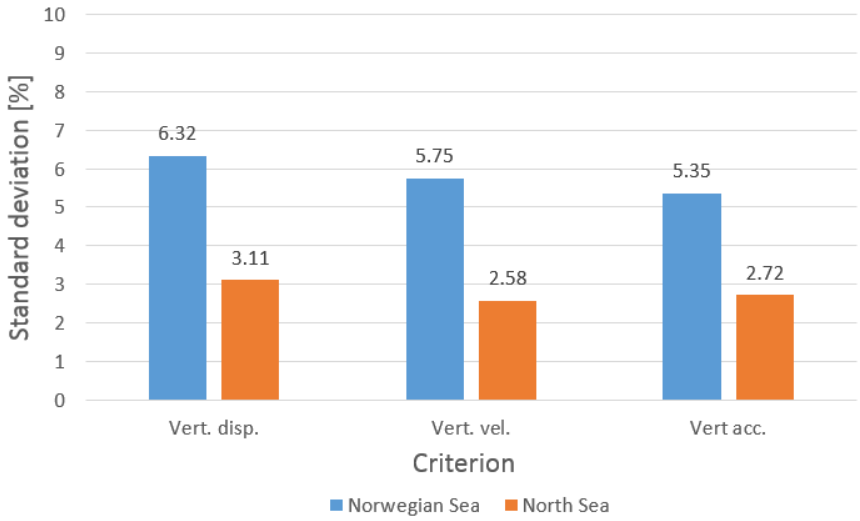

Figure 6.4: Standard deviation operability vessel 1-4 point 2

Figure 6.4 show that the standard deviation is more evenly distributed between the criteria in point two than in point 1. The deviation is also higher on average, meaning there is a larger difference in operability for the four vessels in this phase of the lift.

Point 3 - Lowering

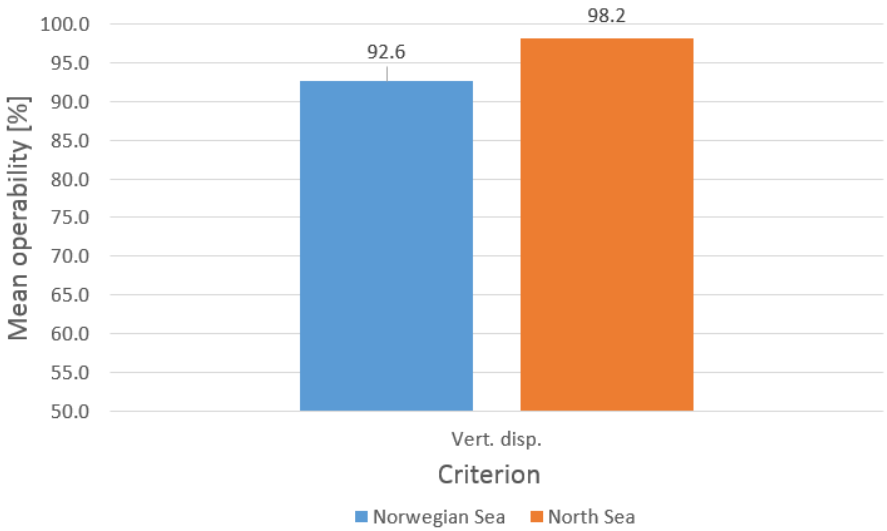

Figure 6.5: Mean operability vessel 1-4 point 3

Figure 6.5 show the mean operability for vertical crane tip displacement in point 3. The operability is found to be higher in the North Sea than in the Norwegian Sea, similar to point 1 and 2.

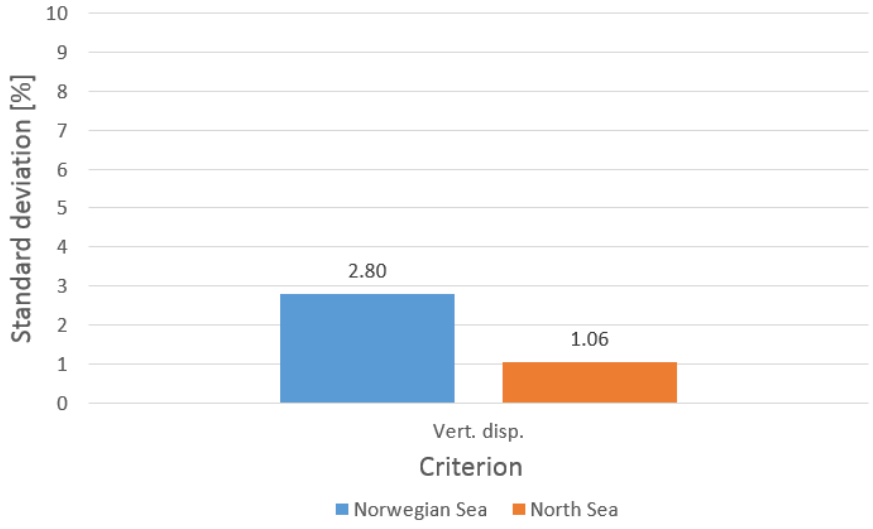

Figure 6.6: Standard deviation operability vessel 1-4 point 3

Figure 6.6 show that the standard deviation of vessel operability is larger in the Norwegian Sea than in the North Sea.

6.1.2 Length variation

The influence of length on operability is assessed by comparing the basecase of vessel 1-4, which have lengths between 100-160 m. The difference is taken with respect to vessel 1. Figure 6.7 show the operability difference in point 1. It is found that longer vessels can operate more often without experiencing pendulum motion.

Figure 6.8 show how the length influences a vessel's ability to carry out operations involving lowering through the splash-zone. An increase in length is found to increase operability, except from vessel 2 in the Norwegian Sea which show a small reduction compared to vessel 1.

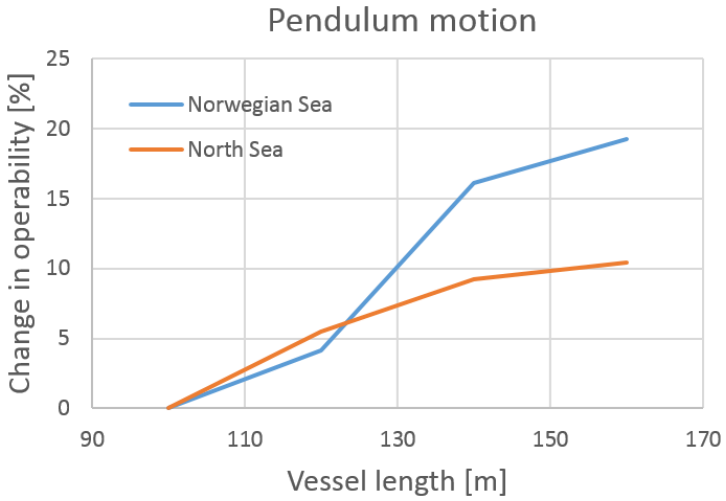

Figure 6.7: Difference in operability for the pendulum motion phase vessel 1-4 compared to vessel 1

Figure 6.9 show how the length influences operability for the lowering phase. Operability is found to be proportional to the length. The increase of operability is not as severe as for pendulum motion and splash-zone.

Figure 6.10 show the difference in total operability compared to vessel 1. Point 2 is limiting for all basecase vessels, so the total operability is equal to the operability for lowering through the splash-zone seen in figure 6.8. Results are presented for total operability for the remaining parametric variations. Parametric variations is applied to all vessels, so the influence on operability of a parametric variation is presented as a mean value and corresponding standard deviation.

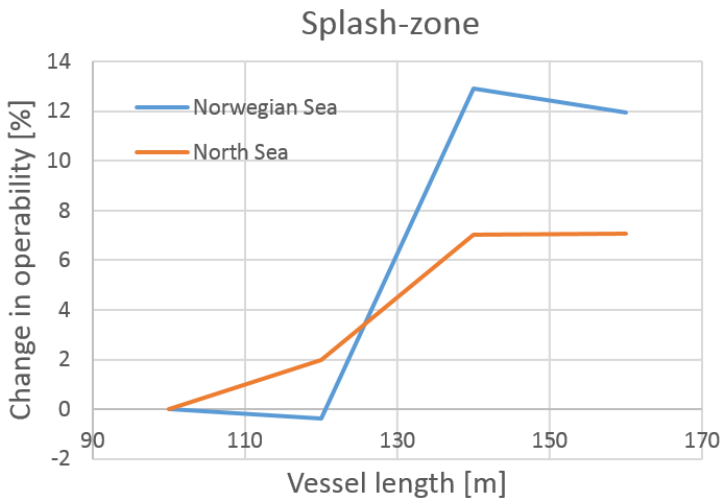

Figure 6.8: Difference in operability for the splash-zone phase vessel 1-4 compared to vessel 1

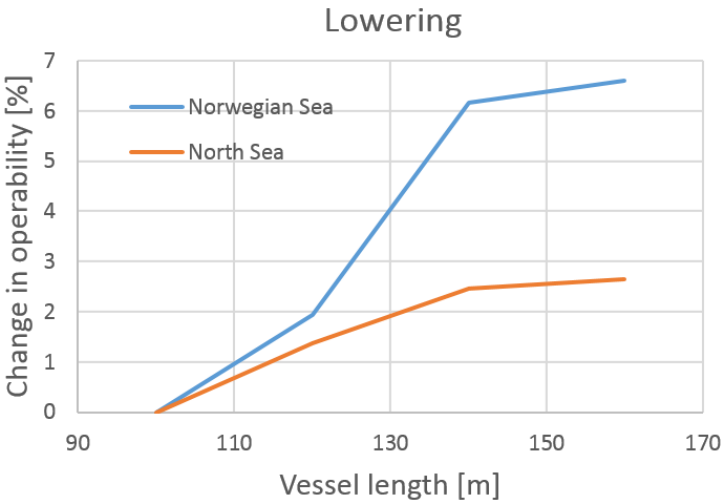

Figure 6.9: Difference in operability for the lowering phase vessel 1-4 compared to vessel 1

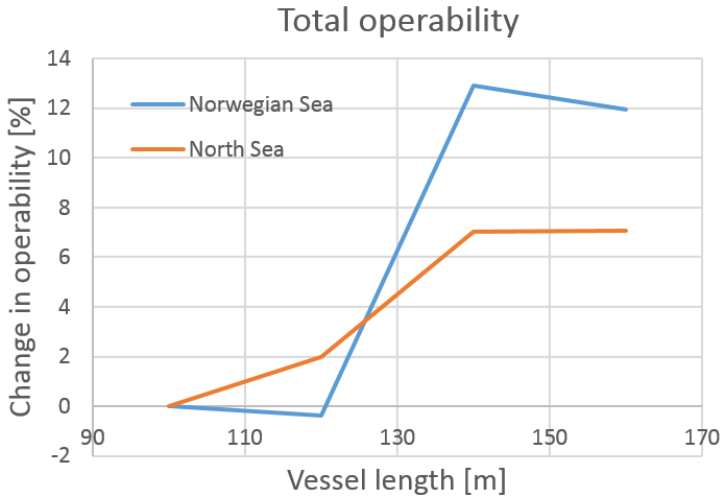

Figure 6.10: Difference in total operability vessel 1-4 compared to vessel 1

6.1.3 Beam variation

The beam is varied between ±20 % of the design beam of each vessel, and the corresponding effect on operability is calculated. Figure 6.11 show the difference in operability compared to the basecase vessels. The largest differences in operability is found to be for operations in the Norwegian Sea. Notice that the change in operability is different in the two areas. This is shown by the statistics listed in table 6.1.

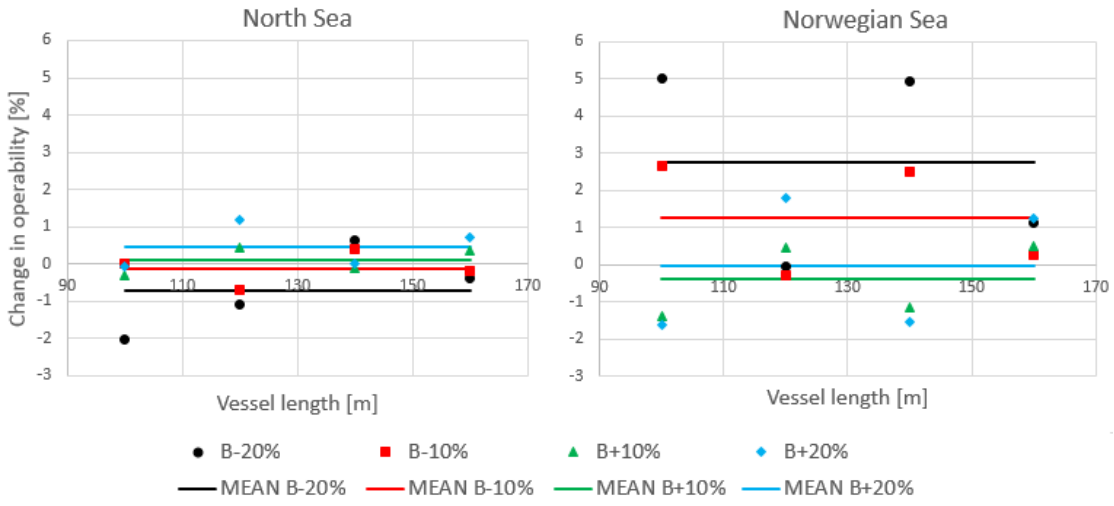

Figure 6.11: Difference in operability beam variation compared to the basecase vessels

Table 6.1: Statistical properties of change in operability for beam variation compared to the basecase vessels

Beam variation	***-20*** %	***-10*** %	***+10*** %	***+20*** %
Norwegian Sea				
Mean	+2.76 %	+1.28 %	-0.39 %	-0.02 %
Std. dev.	2.26 %	1.31 %	0.87 %	1.56 %
North Sea				
Mean	-0.72 %	-0.12 %	+0.09 %	+0.46 %
Std. dev.	0.97 %	0.40 %	0.32 %	0.51 %

The difference in operability as a function of the beam variation is plotted in figure 6.12 using the data in table 6.1. In the North Sea, the trend is an increase of operability for increasing beam, while the opposite trend is found for the Norwegian Sea. The standard deviation of the change in operability is higher in the North Sea than the Norwegian Sea,

which indicates that the vessel respond differently to the beam variation with respect to operability.

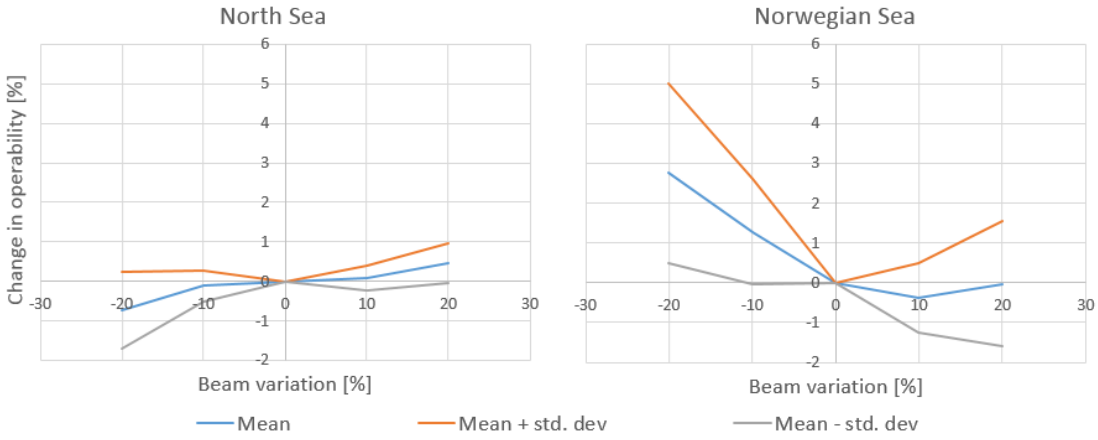

Figure 6.12: Trend for change in operability for beam variation

Table 6.2: Limiting criteria for beam variation

Vessel	***1***	***2***	***3***	***4***
Norwegian Sea				
B-20 %	Point 2, displ.	Point 2, displ.	Point 2, displ.	Point 2, displ.
B-10 %	Point 2, displ.	Point 2, displ.	Point 2, displ.	Point 2, displ.
B+10 %	Point 2, displ.	Point 2, displ.	Point 2, displ.	Point 2, displ.
B+20 %	Point 2, displ.	Point 2, displ.	Point 2, displ.	Point 2, displ.
North Sea				
B-20 %	Point 1, acc.	Point 2, displ.	Point 2, displ.	Point 2, displ.
B-10 %	Point 1, acc.	Point 2, displ.	Point 2, displ.	Point 2, displ.
B+10 %	Point 2, displ.	Point 2, displ.	Point 2, displ.	Point 2, displ.
B+20 %	Point 2, displ.	Point 2, displ.	Point 2, displ.	Point 2, displ.

Table 6.2 show that it is the phase of lowering the object through the splash zone that limits the operability for almost all vessels and beam configurations. The smallest vessel is limited by the horizontal acceleration criterion for pendulum motion when the beam is reduced in the North Sea.

6.1.4 Draught variation

The draught is varied between ±1.5 m, and the corresponding change in operability is calculated. Figure 6.13 show the data points of the operability differences and mean values for each level of draught variation for the North Sea and Norwegian Sea. The influence of draught variation on operability appears to be different for each vessel depending on the magnitude of draught change and operational area. For the North Sea, the smallest vessel has increased operability for both positive and negative draught changes while the three larger vessels are distributed around zero. The opposite is observed for the Norwegian Sea. The lowest operability is found for the lowest draught for all vessels in the North Sea. In the Norwegian Sea, the lowest operability is found for different draught variations depending on the vessel.

Table 6.3 show the statistical properties derived from the data in figure 6.13. Figure 6.14 show the data in table 6.3 plotted to illustrate the trend in the North Sea and Norwegian Sea. For the North Sea, a clear trend for increased operability for deeper draught is observed. For the Norwegian Sea, the operability increases for all draught variations, with higher operability values for deep draughts.

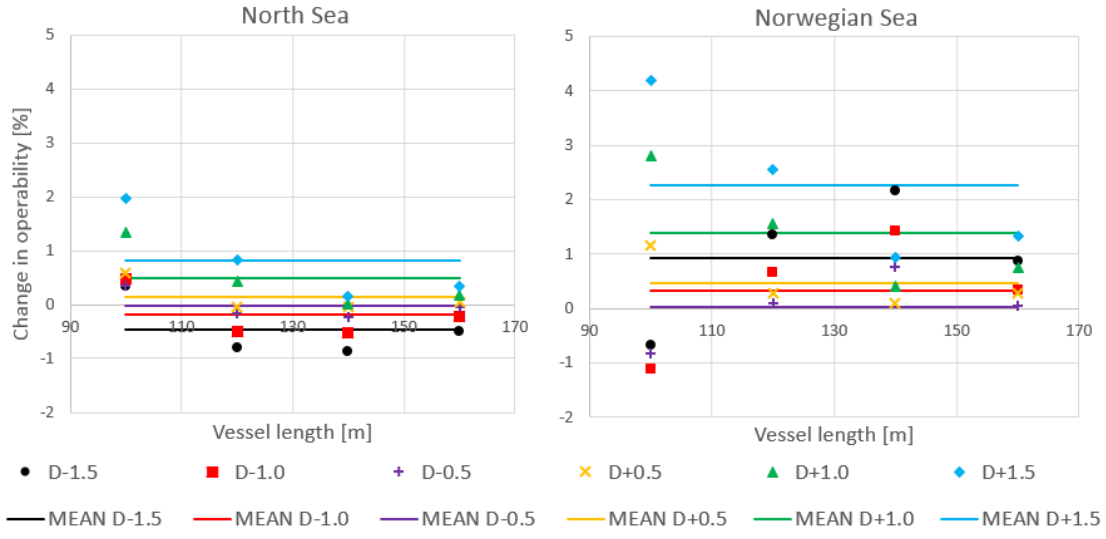

Figure 6.13: Difference in operability for draught variation compared to basecase vessels

Table 6.3: Statistical properties for the change in operability compared to the basecase vessels for draught variation

Draught variation	*-1.5 m*	*-1.0 m*	*-0.5 m*	*+0.5 m*	*+1.0 m*	*+2.5 m*
Norwegian Sea						
Mean	+0.92 %	+0.33 %	+0.02 %	+0.45 %	+1.38 %	+2.25 %
Std. dev.	1.03 %	0.93 %	0.56 %	0.42 %	0.92 %	1.26 %
North Sea						
Mean	-0.45 %	-0.19 %	-0.03 %	+0.13 %	+0.49 %	+0.82 %
Std. dev.	0.48 %	0.41 %	0.22 %	0.26 %	0.52 %	0.71 %

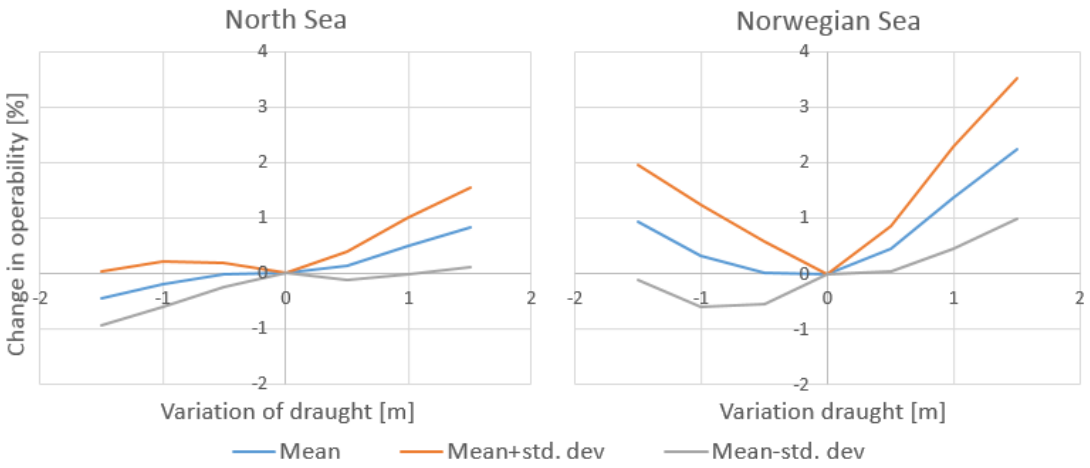

Figure 6.14: Trend for change in operability for draught variation

Table 6.4 show the limiting criteria for vessel draught variations. All vessels are limited by the vertical crane displacement during lowering through the splash-zone for all draught variations.

Table 6.4: Limiting criteria for draught variation

Vessel	*1*	*2*	*3*	*4*
Norwegian Sea				
D-1.5m	Point 2, displ.	Point 2, displ.	Point 2, displ.	Point 2, displ.
D-1.0m	Point 2, displ.	Point 2, displ.	Point 2, displ.	Point 2, displ.
D-0.5m	Point 2, displ.	Point 2, displ.	Point 2, displ.	Point 2, displ.
D+0.5m	Point 2, displ.	Point 2, displ.	Point 2, displ.	Point 2, displ.
D+1.0m	Point 2, displ.	Point 2, displ.	Point 2, displ.	Point 2, displ.
D+1.5m	Point 2, displ.	Point 2, displ.	Point 2, displ.	Point 2, displ.
North Sea				
D-1.5m	Point 2, displ.	Point 2, displ.	Point 2, displ.	Point 2, displ.
D-1.0m	Point 2, displ.	Point 2, displ.	Point 2, displ.	Point 2, displ.
D-0.5m	Point 2, displ.	Point 2, displ.	Point 2, displ.	Point 2, displ.
D+0.5m	Point 2, displ.	Point 2, displ.	Point 2, displ.	Point 2, displ.
D+1.0m	Point 2, displ.	Point 2, displ.	Point 2, displ.	Point 2, displ.
D+1.5m	Point 2, displ.	Point 2, displ.	Point 2, displ.	Point 2, displ.

6.1.5 GM variation

GM is varied between 1-3 m and the corresponding change in operability calculated. Figure 6.15 show the change in operability for all vessels and GM variations along with the mean change in operability for each level of GM variation. For the North Sea, the change in operability is distributed around zero, except vessel 3, with low GM resulting in the highest operability. For the Norwegian Sea, the operability difference is positive for most GM variations except GM = 1.5 m and 2.5 m. The highest operability is found for high GM for vessel 1 and 3, and low GM for vessel 2 and 4.

Table 6.5 show the statistical properties derived from the data in figure 6.15. It shows that the average operability difference is positive for all GM variations in the Norwegian Sea, and that low GM results in higher operability in the North Sea.

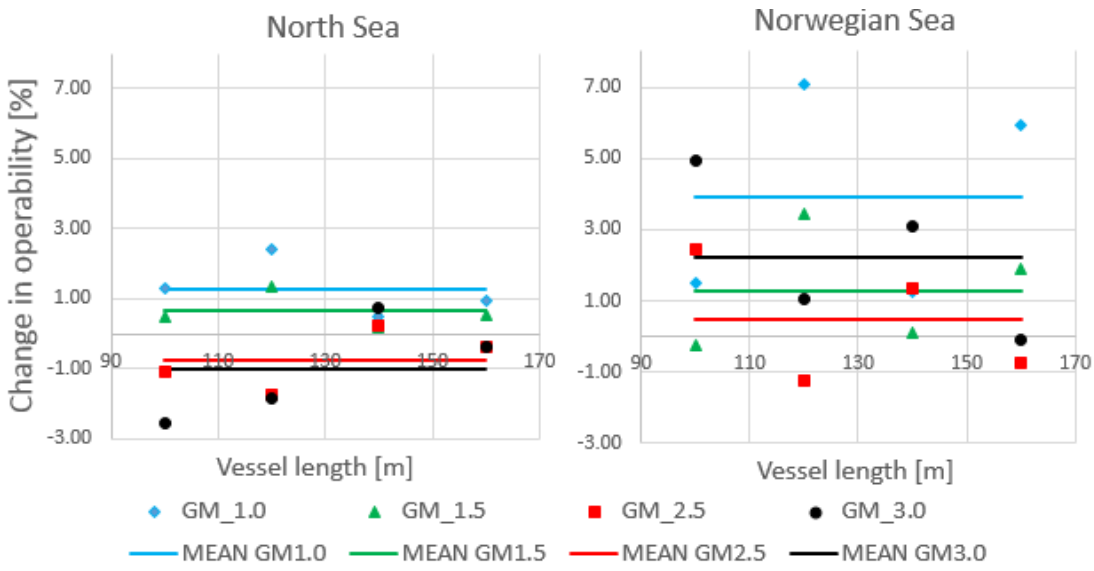

Figure 6.15: Difference in operability compared to basecase vessels for GM variation

Figure 6.16 show the resulting trend for change in operability by varying GM. Low GM result in increased operability in the North Sea. In the Norwegian Sea, all variations of GM result in increased operability.

Table 6.5: Statistical properties for the change in operability compared to the basecase vessels for GM variation

GM	***1.0 m***	***1.5 m***	***2.5 m***	***3.0 m***
Norwegian Sea				
Mean	+3.93 %	+1.29 %	+0.46 %	+2.24 %
Std. dev.	2.60 %	1.10 %	1.50 %	1.93 %
North Sea				
Mean	+1.28 %	+0.65 %	-0.74 %	-1.00 %
Std. dev.	0.70 %	0.43 %	0.76 %	1.27 %

Table 6.6 show that it is the vertical crane tip displacement during the lowering through the splash-zone that limits all four vessels for all values of GM. The exceptions are the high GM values for vessel 1 in the North Sea, where the criterion for horizontal acceleration with respect to pendulum motion is limiting operability.

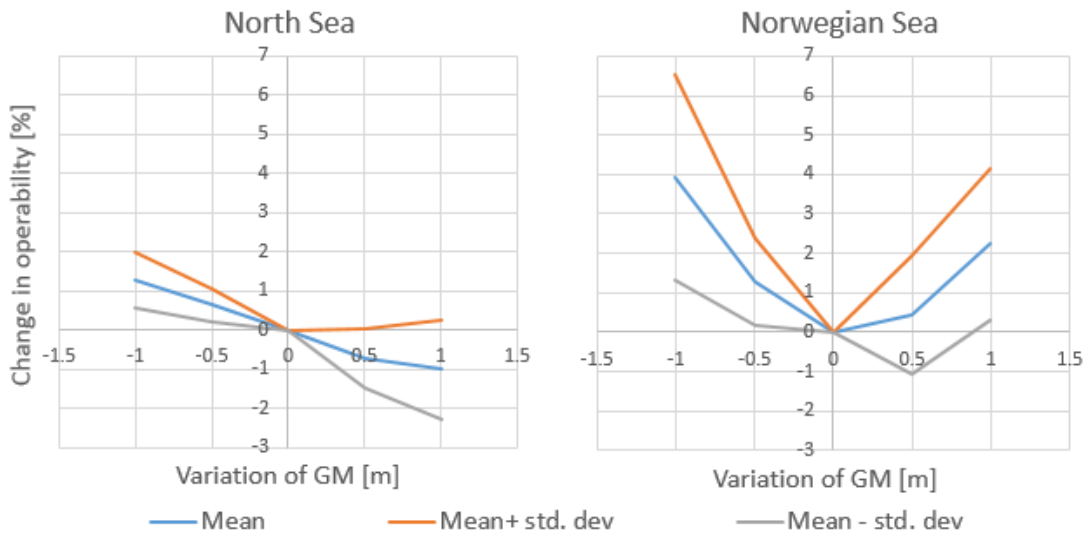

Figure 6.16: Trend for change in operability for GM variation

Table 6.6: Limiting criteria for GM variation

Vessel	***1***	***2***	***3***	***4***
Norwegian Sea				
GM 1.0 m	Point 2, displ.	Point 2, displ.	Point 2, displ.	Point 2, displ.
GM 1.5 m	Point 2, displ.	Point 2, displ.	Point 2, displ.	Point 2, displ.
GM 2.5 m	Point 2, displ.	Point 2, displ.	Point 2, displ.	Point 2, displ.
GM 3.0 m	Point 2, displ.	Point 2, displ.	Point 2, displ.	Point 2, displ.
North Sea				
GM 1.0 m	Point 2, displ.	Point 2, displ.	Point 2, displ.	Point 2, displ.
GM 1.5 m	Point 2, displ.	Point 2, displ.	Point 2, displ.	Point 2, displ.
GM 2.5 m	Point 1, acc.	Point 2, displ.	Point 2, displ.	Point 2, displ.
GM 3.0 m	Point 1, acc.	Point 2, displ.	Point 2, displ.	Point 2, displ.

6.1.6 R_{44} variation

The roll radius of gyration is varied between 30%-40% of the vessel beam and the corresponding change in operability is calculated. Figure 6.17 show the differences in operability for all vessels and R_{44} variations and the mean operability difference for each level of R_{44} variation. Results for both the Norwegian Sea and the North Sea show that the operability is increased by increasing the roll radius of gyration. As R_{44} only influences roll motion, it must be due to an increased natural period for roll.

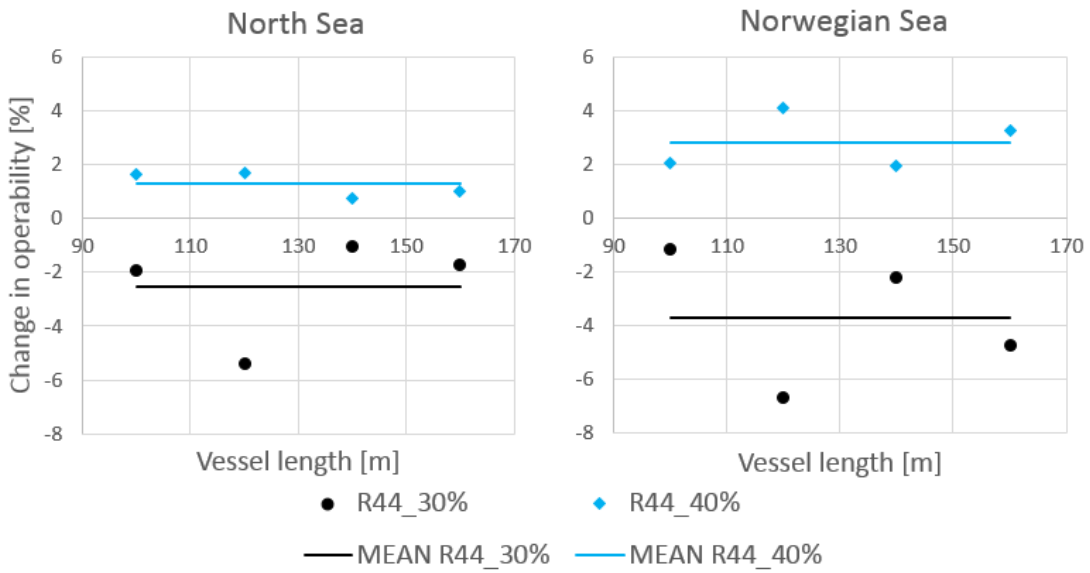

Figure 6.17: Difference in operability compared to the basecase vessels for R_{44} variation

Table 6.7 show the statistical properties derived from the data in figure 6.17. The trend is similar in both areas, with expected positive difference in operability for increasing R_{44}.

Table 6.7: Statistical properties of the change in operability compared to the basecase vessels for GM variation

R_{44}	***30*** $\%B$	***40*** $\%B$
Norwegian Sea		
Mean	-3.69 %	+2.82 %
Std. dev.	2.17 %	0.89 %
North Sea		
Mean	-2.51 %	+1.26 %
Std. dev.	1.69 %	0.42 %

The trends for the Norwegian Sea and the North Sea based on the data in table 6.7 are shown in figure 6.18. These trends are more consistent compared to the trends of the previously presented parameter variations. An increase of the natural period in roll improves operability for all vessels in both areas.

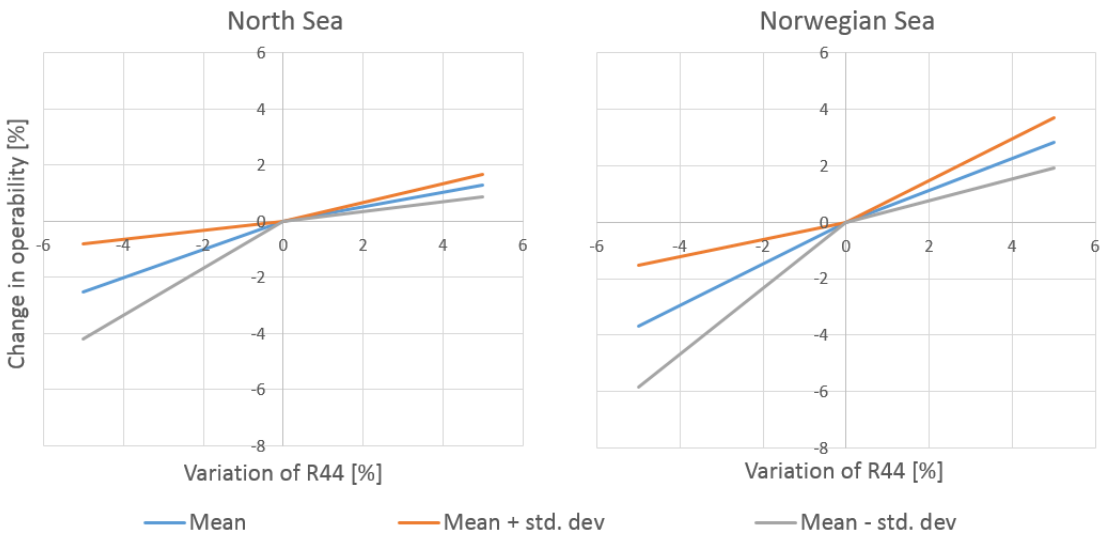

Figure 6.18: Trend for change in operability compared to basecase vessels for R_{44} variation

Table 6.8: Limiting criteria R_{44} variation

Vessel	***1***	***2***	***3***	***4***
Norwegian Sea				
R44 30 $\%B$	Point 2, displ.	Point 2, displ.	Point 2, displ.	Point 2, displ.
R44 40 $\%B$	Point 2, displ.	Point 2, displ.	Point 2, displ.	Point 2, displ.
North Sea				
R44 30 $\%B$	Point 1, acc.	Point 2, displ.	Point 2, displ.	Point 2, displ.
R44 40 $\%B$	Point 2, displ.	Point 2, displ.	Point 2, displ.	Point 2, displ.

Table 6.8 show the limiting criteria for variations of R_{44}. All vessels and configurations are limited by the vertical crane displacement during lowering through the splash-zone except vessel one with R_{44} = 30 $\%$B in the North Sea.

6.2 Power prediction

Estimation of required power were performed for all parametric variations influencing the hull geometry as mentioned in section 4.5. For comparison and trend observations, most of the results are shown as non-dimensional values. The presented results are the required power at the transit Froude numbers listed in table 4.3.

6.2.1 Beam variation

The required power for vessel 1-4 was calculated for beam variation. The results are shown in figure 6.19. Increase of beam is found to have a steeper change of required power than decreasing the beam. A trendline with curvature is therefore required to have a good fit. The trendline is shown in figure 6.19 and the expression is listed in table 6.9. R^2 = 0.9728 indicates a reasonably good fit. Maximum deviation is found to be 6%.

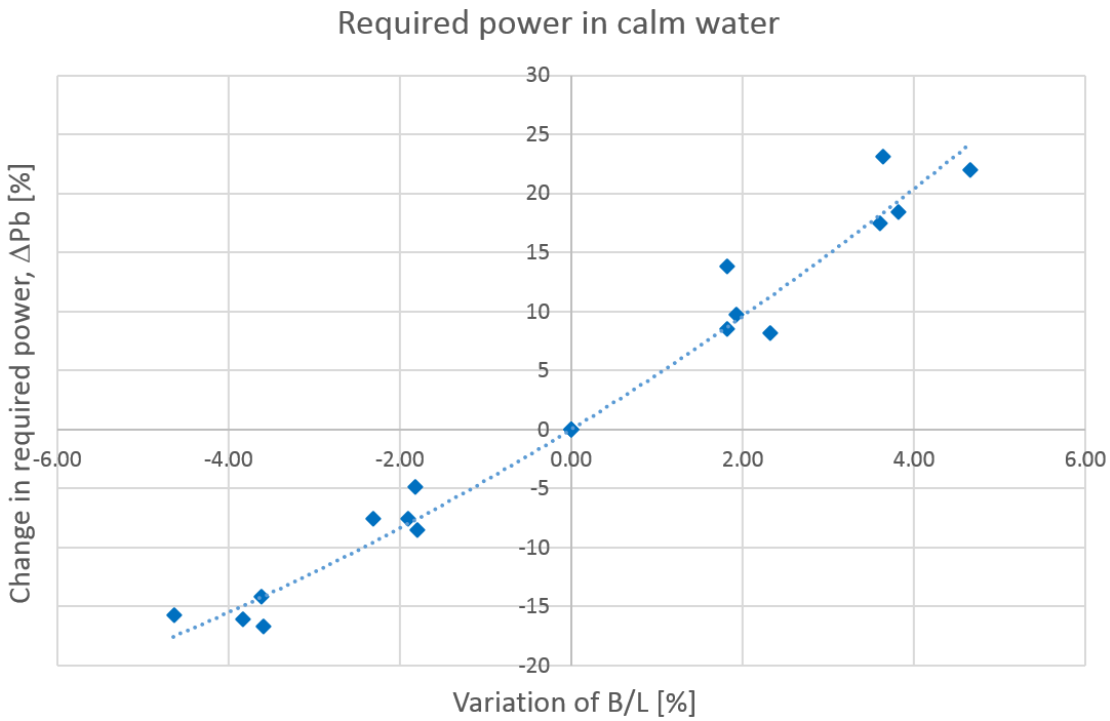

Figure 6.19: Change in required power compared to the basecase vessels for beam variation

A common way of indicating vessel performance is the admiralty coefficient C_{adm}. It is a function of the brake power, volume displacement and vessel speed, and is an indication of the economical performance of the vessel. The admiralty coefficient is

Table 6.9: Trendline for change in required power compared to basecase vessels for beam variation

Trendline	$0.1526x^2 + 4.4875x$
R^2	0.9728

calculated as:

$$C_{adm} = \frac{\nabla^{2/3} \cdot V_s^3}{P_B} \tag{6.1}$$

Since it is proportional to volume displacement and the vessel speed, and inversely proportional to the required break power, higher values of C_{adm} indicate better performance. Figure 6.20 show the change in admiralty coefficient as a function of beam variation. The change of admiralty coefficient appear to be unique for each vessel, which result in a poor fit for the trendline. An increase of C_{adm} for decreasing beam, and a decrease for increasing beam is observed for all vessels and beam variations but one. For a beam reduction of 10%, ShipX predicts an increase of C_{adm} for vessel 4. Since the speed is equal to the basecase, this implies lower reduction of required power than volume displacement to the power of 2/3.

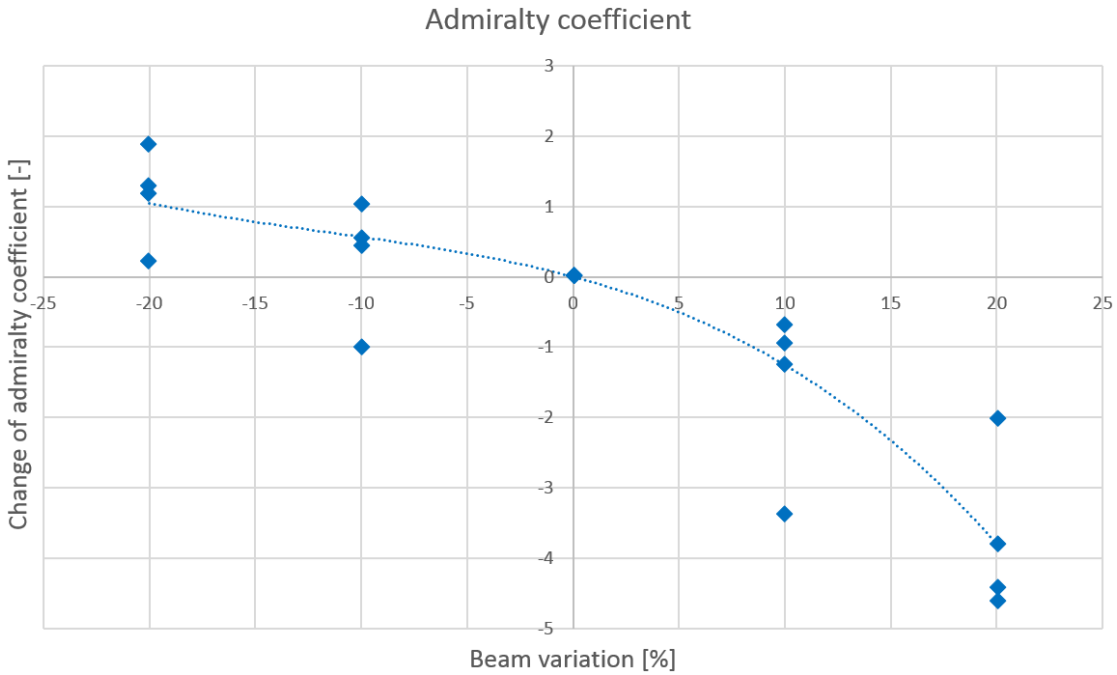

Figure 6.20: Change in admiralty coefficient compared to the basecase vessels for beam variation

The fitted trendline is presented in table 6.10. With R^2 = 0.8117 for a third degree polynomial trendline, the change of admiralty coefficient is inconsistent for beam variation compared to the other parametric variations.

Table 6.10: Trendline for change in admiralty coefficient compared to the basecase vessels for beam variation

Trendline	$-0.0001x^3 - 0.0034x^2 - 0.0808x$
R^2	0.8117

6.2.2 Draught variation

The change in required power for draught variations are shown in figure 6.21. Due to the curvature of the scatter, a second degree polynomial were used to fit a trendline. The trendline is a reasonably good fit with R^2 = 0.9659. Deviations are largest for draught increases, with a maximum of 9 %. The expression for the trendline is presented in table 6.11.

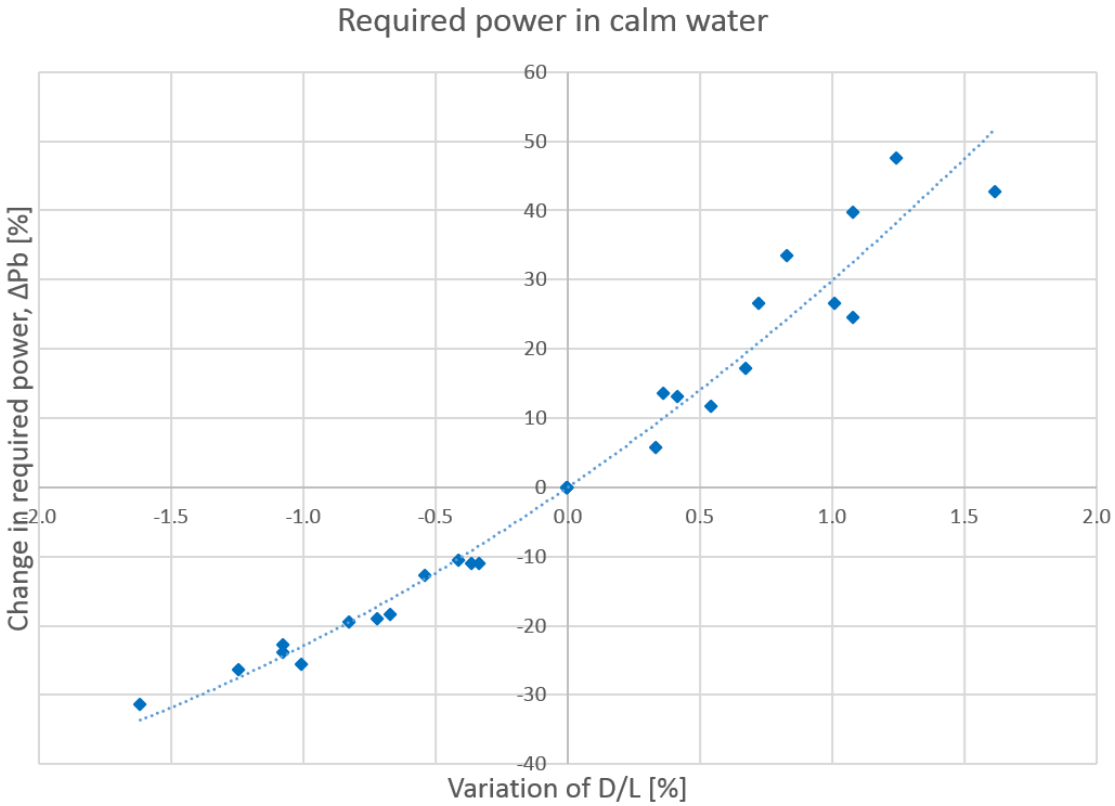

Figure 6.21: Change in required power compared to the basecase vessels for draught variation

Table 6.11: Trendline for change in required power compared to the basecase vessels for draught variation

Trendline	$3.4681x^2 + 26.414x$
R^2	0.9659

The admiralty coefficient has a more clear trend for draught variations compared to beam variations, as can be seen in figure 6.22 and 6.20. An increase of draught result in a reduction of C_{adm} for all vessels, and opposite for draught reductions. With $R^2 = 0.9366$ and a maximum deviation of 2.5 (-), results must be expected to deviate significantly from the trendline if similar studies are performed. It appears that, similar as to the beam variation, the change of admiralty coefficient for draught variation is unique to each vessel.

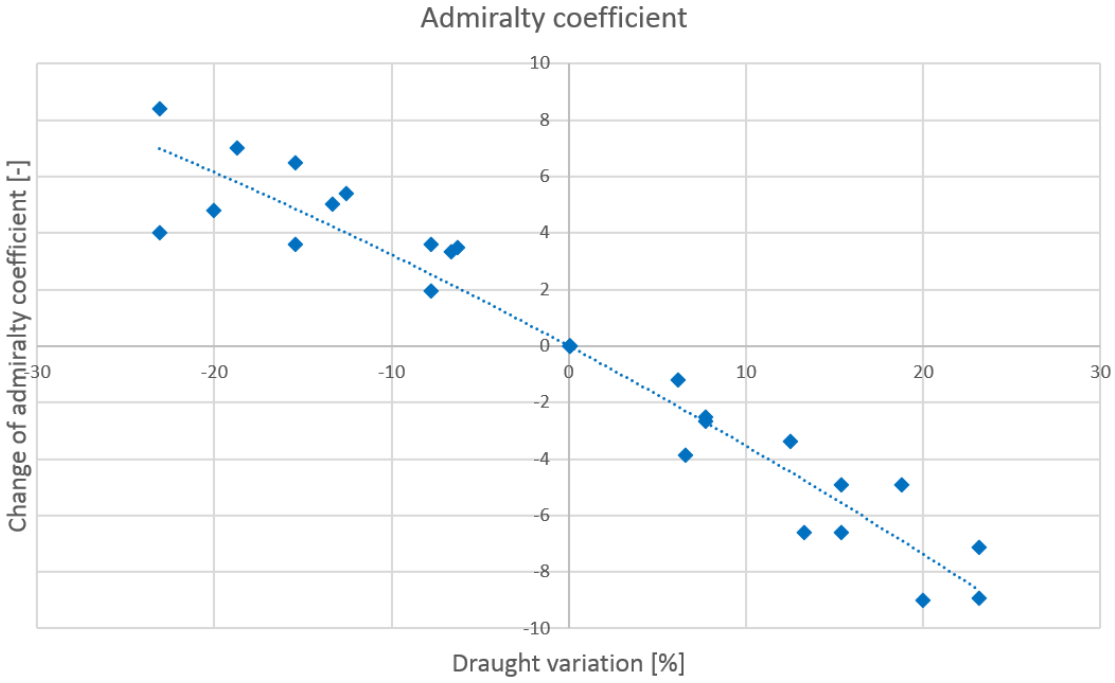

Figure 6.22: Change in admiralty coefficient compared to basecase vessels for draught variation

Table 6.12: Trendline for change in admiralty coefficient compared to basecase vessels for draught variation

Trendline	$-0.0015x^2 - 0.3381x$
R^2	0.9366

6.3 Costs

6.3.1 Machinery costs

The investment cost of generators have been analysed according to the methodology in section 4.5.3.

Variation of length

The difference in propulsion machinery cost has been analysed for the basecase vessels to determine the effect of vessel length. Figure 6.23 show the increase of generator costs compared to the smallest vessel. The required power is found to increase rapidly with vessel length in figure 6.29. The same trend is found for the change in machinery costs, although the increase is not as severe as for the increase of required power.

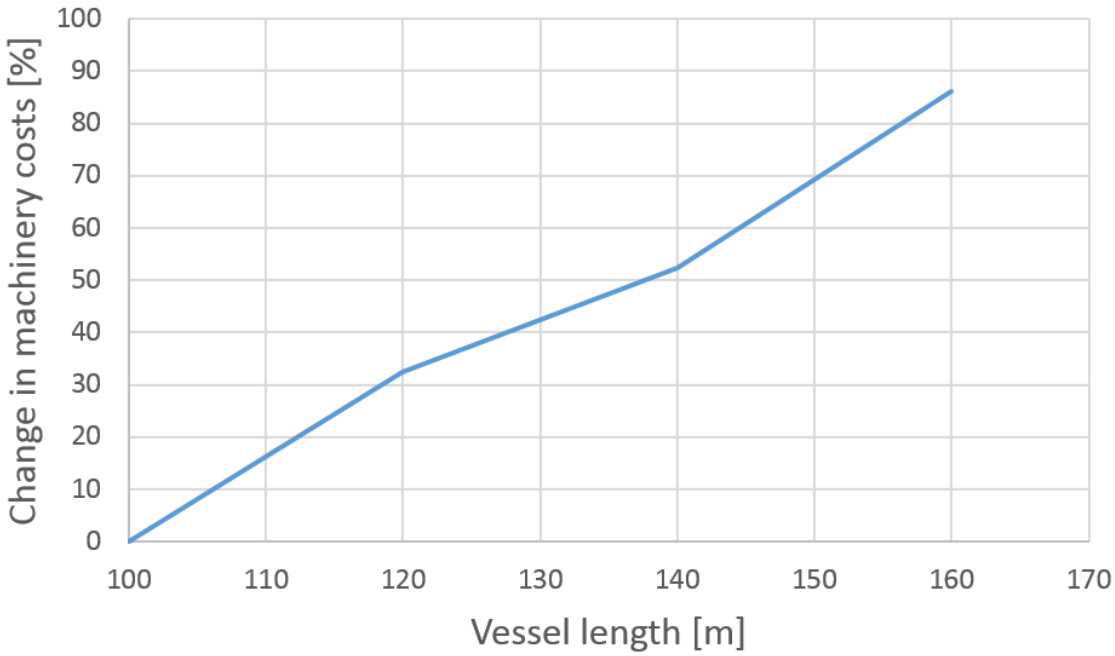

Figure 6.23: Change in generator costs for varying length compared to vessel 1

Variation of beam

Since the required installed power has been obtained from the calculated required propulsion power, the figures and trends appear similar to section 6.2.1. They are however different due to the added factor to account for increased resistance in weather and the applied model for generator price. Figure 6.24 show the change in machinery costs for beam variations compared to the basecase vessels. With R^2 = 0.9736 and a maximum deviation of less than 5%, the results seem to follow the same trend. The expression for the trendline is found in table 6.13.

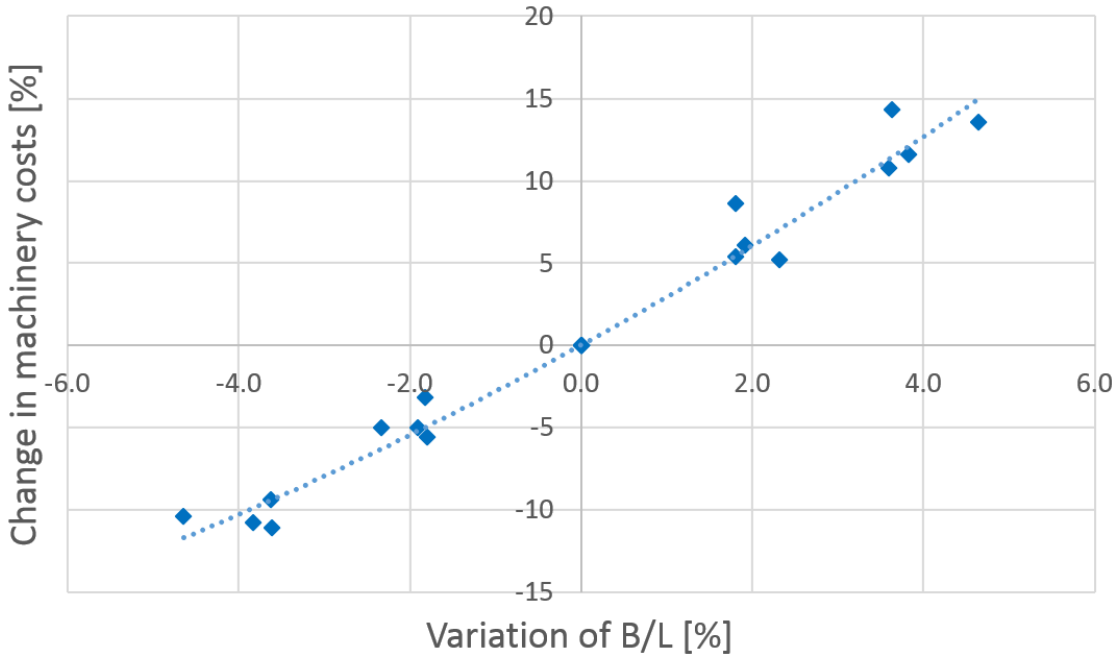

Figure 6.24: Change in machinery costs compared to basecase vessels for beam variation

Table 6.13: Trendline for change in machinery costs compared to basecase vessels for beam variation

Trendline	$0.0754x^2 + 2.8715x$
R^2	0.9736

Variation of draught

Figure 6.25 show the results obtained for the generator prices for draught variation. The trendline agrees especially well with the results for reduced draught. Maximum deviation is 7 %. The expression for the trendline is listed in table 6.14.

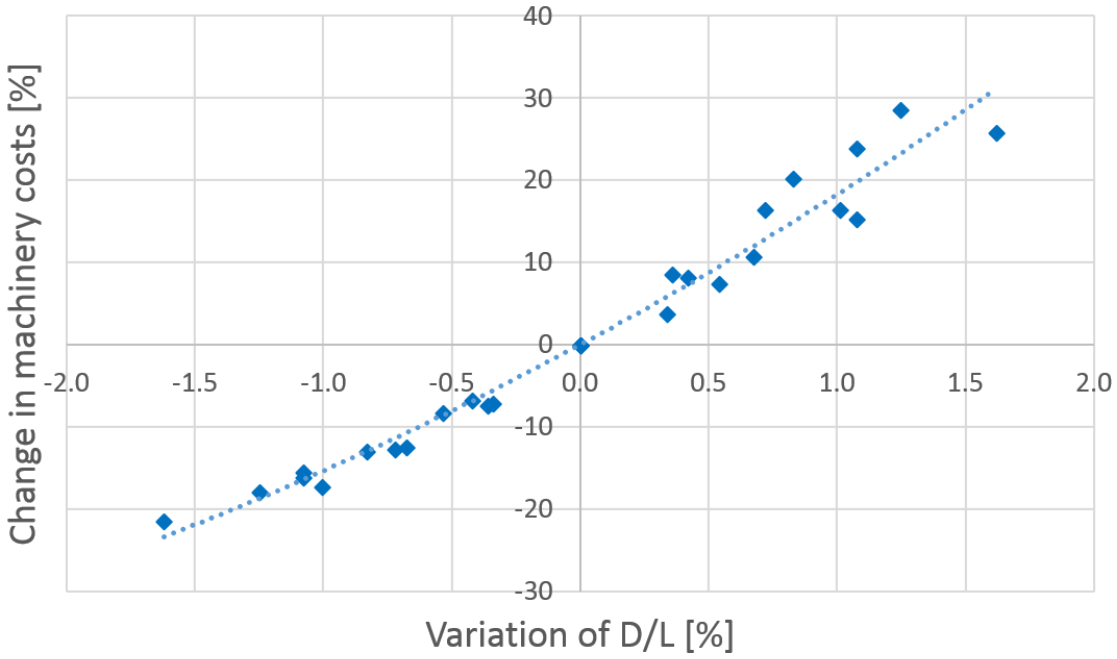

Figure 6.25: Changes in machinery costs for varying draught compared to basecase vessels

Table 6.14: Trendline for change in machinery costs compared to basecase vessels for draught variation

Trendline	$1.492x^2 + 16.81x$
R^2	0.9696

6.3.2 Hull steel costs

Variation of length

The vessel length is often the governing parameter for building costs of ships. Figure 6.26 show the increase of hull steel costs compared to the smallest vessel calculated using the methodology presented in section 4.5.2. The results show that the length of the vessel has a large influence on the building costs.

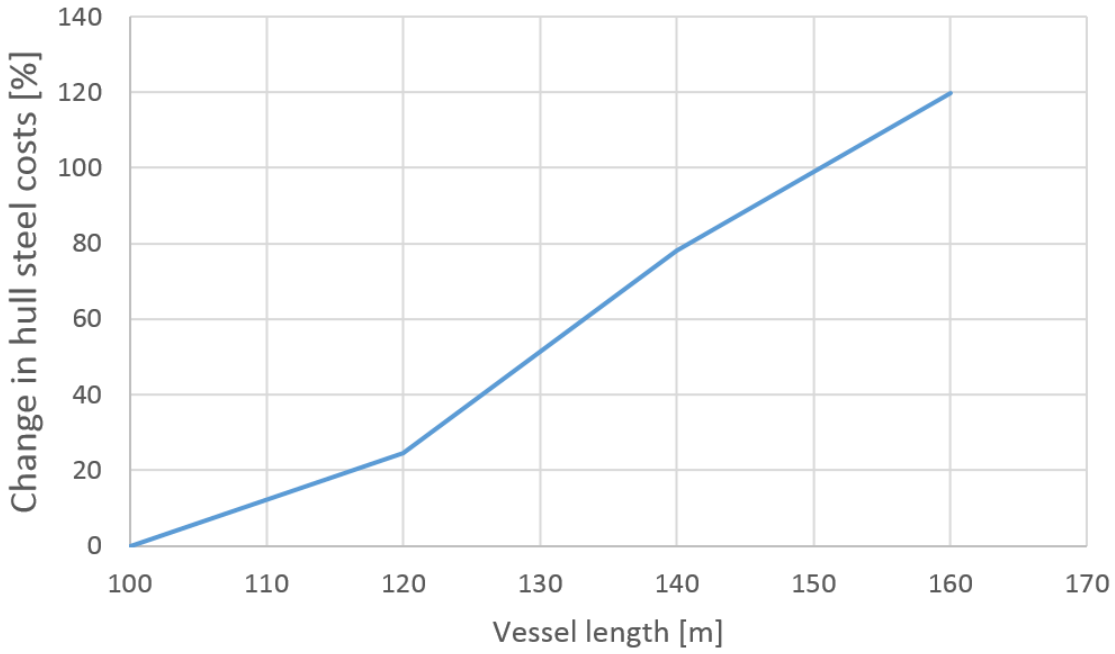

Figure 6.26: Change of hull steel costs for variation of length compared to vessel 1

Variation of beam

The empirical model adopted for estimating the specific hull costs is not a direct function of the vessel beam. C_B is kept constant for beam variations in ShipX. k_{st} is therefore constant for all beam variations for each vessel. The change of hull steel price is therefore equal to the change of displacement for the applied methodology. Figure 6.27 show the obtained data and the fitted trendline. Table 6.15 lists the expression for the trendline. R^2 = 0.984 indicates a satisfactory fit.

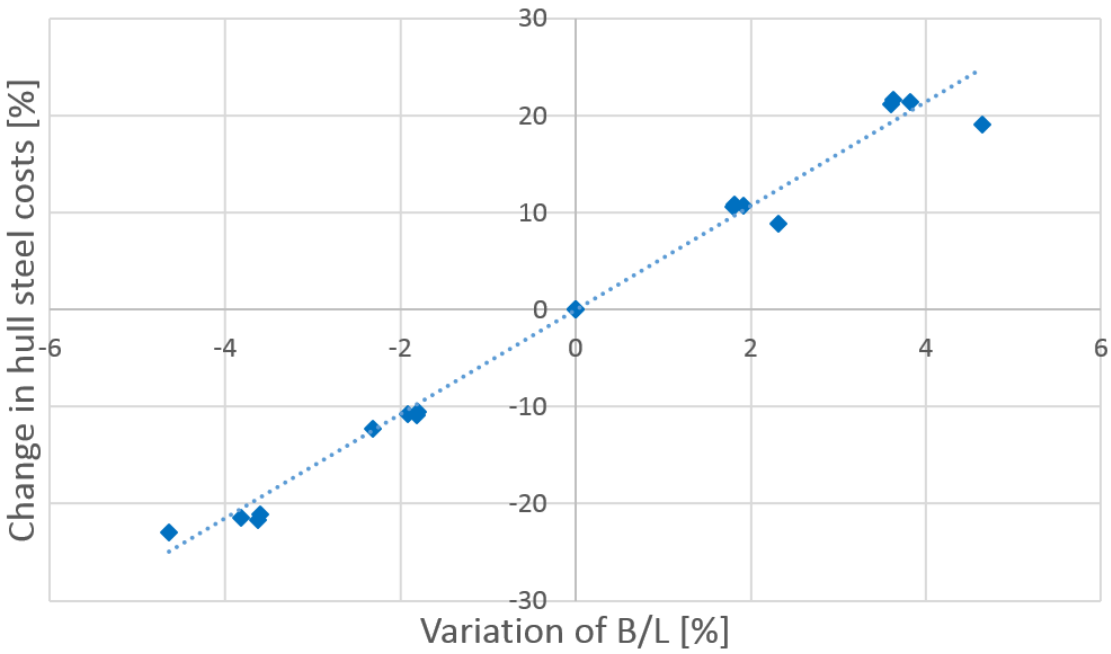

Figure 6.27: Change in hull steel costs compared to basecase vessels for beam variation

Table 6.15: Trendline for change in hull steel costs compared to basecase vessels for beam variation

Trendline	$5.3648x$
R^2	0.984

Variation of draught

The draught variations changes the displacement and C_B. These calculations are performed to indicate the change in hull steel cost for variation of design draught. Results and trendline are shown in figure 6.28. Table 6.16 lists the expression for the trendline shown in figure 6.28. R^2 = 0.9857 indicates a well fitting trendline.

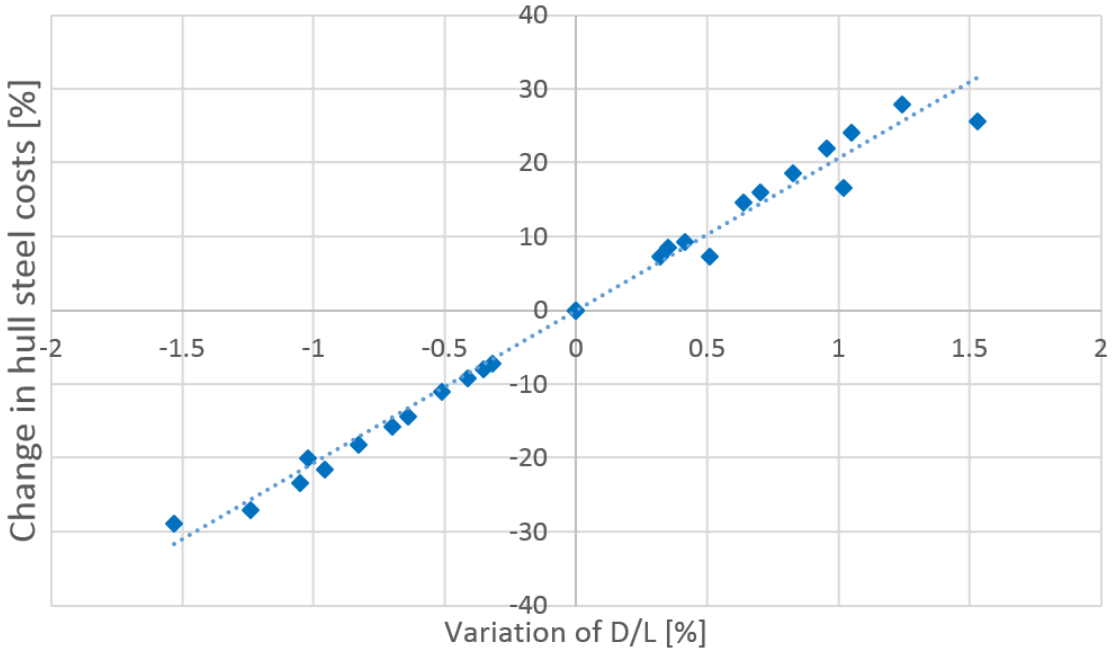

Figure 6.28: Change in hull steel costs compared to basecase vessels for draught variation

Table 6.16: Trendline for change in hull steel costs compared to basecase vessels for draught variation

Trendline	$20.666x$
R^2	0.9857

6.3.3 Fuel costs

Since the same transit speed is assumed for all parametric variations for each vessel and the specific fuel consumption is kept constant, the difference in fuel costs is equal to the difference in required power for the parametric variations of each vessel. The difference in fuel costs for draught and beam variations is therefore given in figure 6.19 and 6.21.

The difference in fuel costs between vessel 1-4 will not be equal to the difference in power since the transit speed varies. The longer vessels require more power, but the transit speed is higher, which implies a shorter transit period to Ormen Lange. The same specific fuel consumption is assumed for all vessels.

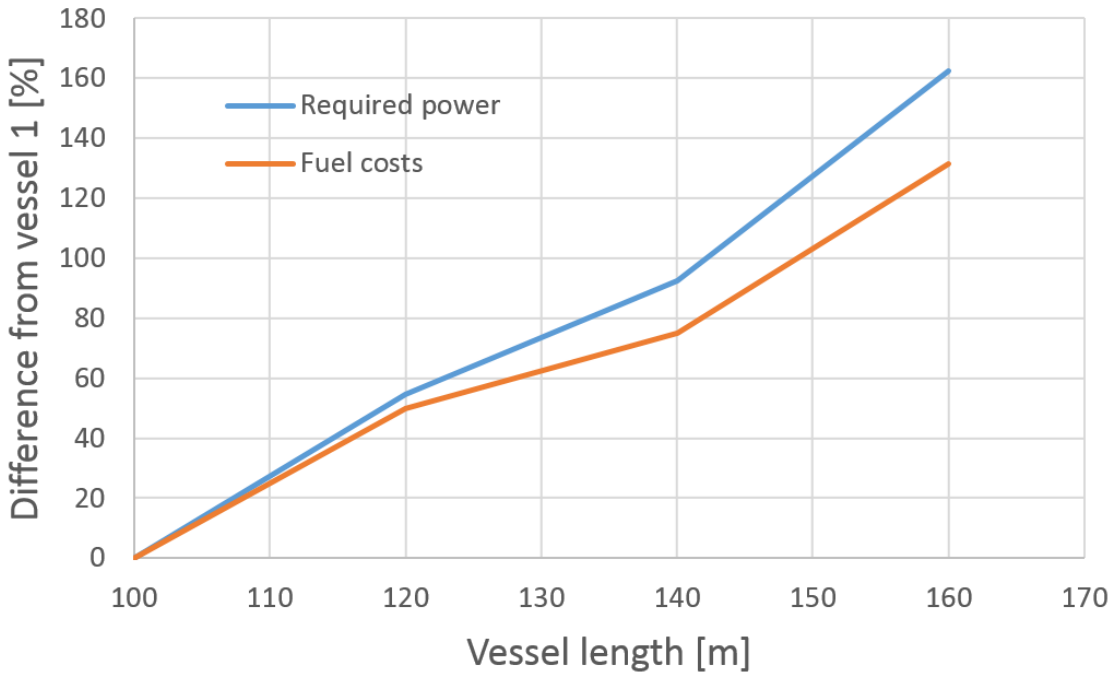

Figure 6.29: Fuel cost increase compared to vessel 1

Figure 6.29 show the increase of required power and fuel costs for basecase vessel 2, 3 and 4 compared to basecase vessel 1.

Chapter 7

Discussion

This chapter presents a discussion concerning methods and assumptions applied in this thesis. The aim is to give clarity to the applicability and validity of the results that has been obtained. Recommendations towards design based on the obtained results is presented at the end of the chapter.

7.1 Unexpected operability trends

Results from the operability analysis is presented in chapter 6. Some unexpected results are found for the change in operability for beam, draught and GM variations. They show that the operability increase for all parametric variations for some of the vessels in the Norwegian Sea.

As previously mentioned in section 4.4, the distribution of T_z relative to the natural periods of the vessel is one of the main factors of operability. How often seastates with waves that have energy at periods close to the natural periods occur, is the main issue when designing vessels optimized with respect to operability. If the operability increase for all parametric changes, it is suspected to be because the original vessel often had resonant motions. To investigate further some additional operability studies were performed.

Vessel 3 is one of the vessels that show an increased operability for all parametric variations. This vessel is found to always be limited by the vertical crane tip motions when lowering through the splash-zone. By re-arranging the evaluation point of the crane tip position, it is possible to evaluate each vertical motion component's impact on operability separately. By moving the crane tip to $y = 0$, the effect of roll is removed. By moving the crane tip to the pitch center, the effect of pitch is removed. Since pitch is mostly dominated by stiffness, the center of pitch is close to the longitudinal center of the water plane area. Global heave motion can not be removed, but by examining the point were roll and pitch is zero the effect of global heave can be assessed.

Vertical motion of 0.6 m RMS is applied as criteria in all points. The difference in operability with respect to the basecase vessel 3 is shown in table 7.1.

- **Point a**

  The influence of pitch is removed. Local vertical motion governed by heave and roll motion.

- **Point b**

  The influence of roll is removed. Local vertical motion governed by heave and pitch motion.

- **Point c**

  The influence of roll and pitch is removed. Local vertical motion equal to the global heave motion.

Table 7.1: Vertical motion component influence on operability

Evaluation point	***Original point 2***	***Point a***	***Point b***	***Point c***
GM-1 m	+1.2 %	+5.8 %	+0.1 %	0 %
GM+1 m	+3.1 %	+3.5 %	0 %	0 %
D-1.5 m	+2.1 %	+3.2 %	-0.7 %	+0.2 %
D+1.5 m	+0.9 %	+3.0 %	-0.3 %	+0.1 %
B-20%	+4.9 %	+5.5 %	-0.1 %	-0.3 %
B+20%	-1.5 %	-0.1 %	+0.4 %	+0.2 %

- **GM**

  Both GM variations results in an increase of operability when the criterion is evaluated at the original location for the crane tip. The same is found point a. Almost no change in operability is found at point b. No change in operability for at point c. The conclusion is therefore that the operability is increased because the basecase vessel encounter roll resonance more often than after GM variations.

- **Draught**

  Both draught variations result in increased operability when the criteria is evaluated at the original location for the crane tip. The same is found at point a. The operability reduces at point b. Point c show an increase of operability for both draught variations. Roll is therefore found to be the governing motion component of the crane tip for draught variations. Pitch is found to have larger effect than for beam and GM variations.

- **Beam**

  The operability is found to decrease for increasing beam when the criteria is evaluated at the original location for the crane tip. The same is found for point a. In point b and c, the operability increases with increasing beam. The reduction in operability due to increased roll motion appear to be larger than the increase of operability due to less pitch and global heave motion. This indicates that the roll motion dominates the operability also for beam variations.

Table 7.1 show that roll is the dominating vertical motion component affecting total operability. The y-coordinate of the evaluation point in phase 2 is the largest of all the evaluation points, equal to the beam of the vessel. The vertical motion component due to roll is therefore largest in phase 2. Since phase 2 is found to be the limiting phase for most vessels, it is therefore not surprising that the total operability is closely linked to roll motion.

7.2 Parameter variation

7.2.1 Neglecting parameter coupling

An assumption made during the parameter variation of the vessels is that a single parameter may be altered freely without coupling to other parameters. This assumption was introduced to be able to distinguish parameter impact on operability.

However, designers may not always choose parameters independently of each other. Equation 7.1 show how GM changes as a function of vertical center of buoyancy from the keel (KB), geometry in the waterline and vertical center of gravity from the keel (KG).

$$GM = KB + \frac{I_{wl}}{\nabla} - KG \tag{7.1}$$

- **Beam variation - constant draught and GM**
  Changes the geometrical shape of the waterline area and displacement. May also affect KB. KG changed accordingly to keep GM constant.

- **Draught variation - constant beam and GM**
  Changes displacement and KB. May also affect the geometrical shape of the waterline area. KG changed accordingly to keep GM constant.

To illustrate how assuming constant GM may be problematic, calculations regarding the necessary amount and location of added displacement were performed. These calculations assume that the original general arrangement must be kept equal, and that only the change in displacement (ΔM) may be used to obtain a constant GM. Table 7.2 show the how vertical center of gravity was changed for the beam and draught variations.

Table 7.2: ΔVCG applied to keep constant GM

Case	*Vessel 1*	*Vessel 2*	*Vessel 3*	*Vessel 4*
B+20% [m]	+3.18	+3.53	+3.61	+4.00
B+10% [m]	+1.56	+1.69	+1.72	+1.91
B-10% [m]	-1.35	-1.53	-1.56	-1.74
B-20% [m]	-2.63	-2.91	-2.94	-3.32
D+1.5m [m]	-0.60	-0.67	-0.52	-0.68
D+1.0m [m]	-0.43	-0.48	-0.37	-0.49
D+0.5m [m]	-0.23	-0.25	-0.19	-0.26
D-0.5m [m]	+0.23	+0.26	+0.20	+0.25
D-1.0m [m]	+0.48	+0.58	+0.43	+0.54
D-1.5m [m]	+0.81	+1.00	+0.72	+0.87

Table 7.3 show ΔM in percent of the original configuration (basecase).

Table 7.3: Changes in vessel displacement, ΔM

Case	*Vessel 1*	*Vessel 2*	*Vessel 3*	*Vessel 4*
B+20% [%]	+18.99	+21.41	+21.15	+21.63
B+10% [%]	+8.73	+10.70	+10.57	+10.81
B-10% [%]	-12.28	-10.71	-10.58	-10.82
B-20% [%]	-23.03	-21.42	-21.15	-21.64
D+1.5m [%]	+27.36	+29.70	+25.61	+23.24
D+1.0m [%]	+17.62	+19.75	+17.00	+15.45
D+0.5m [%]	+7.75	+9.84	+8.46	+7.70
D-0.5m [%]	-11.65	-9.71	-8.36	-7.62
D-1.0m [%]	-21.08	-19.20	-16.58	-15.18
D-1.5m [%]	-30.26	-28.42	-24.61	-22.63

Table 7.4 show the necessary VCG of ΔM relative to the original VCG. COG for ΔM is always above and below the original vessel KG for variation of beam and draught respectively. The reason is that an increase of beam is done by $\Delta VCG > 0$ with $\Delta M > 0$, while an increase of draught is done by $\Delta VCG < 0$ with $\Delta M > 0$.

Table 7.4: COG of ΔM relative to basecase VCG

Case	*Vessel 1*	*Vessel 2*	*Vessel 3*	*Vessel 4*
B+20% [m]	+19.95	+19.99	+20.66	+22.47
B+10% [m]	+19.43	+17.44	+18.03	+19.59
B-10% [m]	+9.67	+12.76	+13.22	+14.36
B-20% [m]	+8.80	+10.68	+10.97	+12.02
D+1.5m [m]	-2.77	-2.94	-2.55	-3.58
D+1.0m [m]	-2.89	-2.90	-2.52	-3.68
D+0.5m [m]	-3.17	-2.80	-2.40	-3.65
D-0.5m [m]	-1.78	-2.47	-2.18	-3.01
D-1.0m [m]	-1.80	-2.45	-2.14	-3.02
D-1.5m [m]	-1.86	-2.52	-2.21	-2.96

Studying table 7.4 reveals that changing the beam is much more challenging than changing the draught if a constant GM is required. The reason is that an increase of 20 % for the beam result in an dramatic increase of the $I_{wl} \propto B^3$, giving a large metacentric height. Adding 20 % of vessel displacement 20 m above original VCG is not considered practically feasible. For an increase of the beam, this implies that the general arrangement would have to be altered significantly to increase KG. Varying the draught is considerably easier. The changes in mass must be done below the original VCG, meaning inside the hull. This makes it easier to apply tanks and other forms of dead weight.

The calculations above does not state that varying the beam is practically impossible. They only show that some combinations of parameters are difficult to achieve. This thesis aims to show the possible benefits of ship designs obtained by optimizing operability. The trends resulting from changing beam and draught are still valid although some of the combinations may be considered theoretical.

7.3 Operability analysis

7.3.1 Operability measurements

The methodology presented in chapter 3 is often applied for assessing the operational capability of vessels. It results in an estimate of the percentage of time the vessel is expected to be able to operate. However, when marine and subsea lifting operations are considered, the chosen methodology is a simplification.

One of the key differences is the duration of operation. In section 2.3.1 the importance of the operational period was discussed. Performing marine operations requires weather windows, often significantly longer than 3 hours which is the duration considered in this thesis. Applying scatter diagrams with seastates occurring independently means that the ability to study weather windows is lost.

Another difference is that the start-up of the operation is based on the forecast weather. Natskår, Moan, and Alvær discussed the difference between forecast and experienced weather, which is the basis for the α-factor.

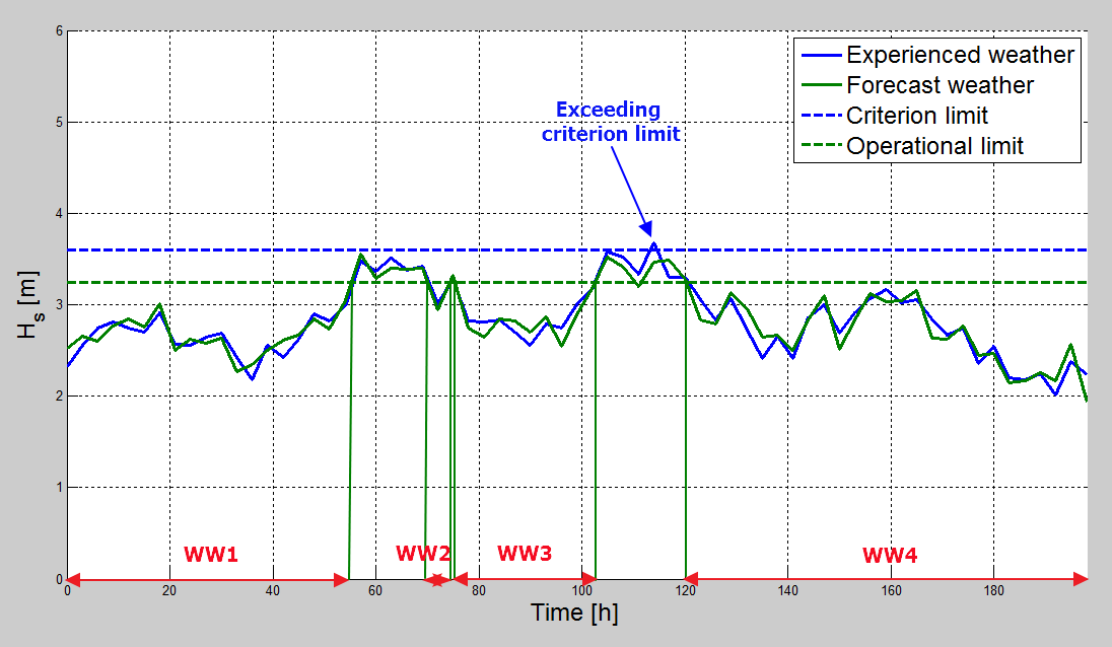

Figure 7.1: Operability assessment

Figure 7.1 illustrates some of the differences between the methodology adopted in

this thesis and the execution of subsea lifting operations. The blue lines represent the methodology in this thesis, with the experienced weather and criterion limit as the solid line and dotted line respectively. The experienced seastates only exceeds the criterion limit once, resulting in a large operability value in the results. The green lines represents the basis of which the decision is made to carry out the operation, with the forecast weather and the operational limit as the solid and dotted line respectively. Start-up is based upon the weather windows indicated by the red arrows. Depending on the required operational period, WW1-WW4 may not all be deemed safe for start-up. The operability is therefore considerably lower in this case.

Note that figure 7.1 is made for illustration without using actual weather data. The importance of this difference may therefore be exaggerated. It is not easy to determine the difference between the obtained operability values and the values obtained by applying a method which accounts for these differences. It is however certain that not taking weather windows and α-factor into account will overestimate the operability. The operational limit is proportional to the criterion limit, meaning that for comparison purposes, the methodology is valid.

7.3.2 Evaluating operability using global criteria

During the literature study on operational criteria in section 5.2.1, it was found that several studies have been performed that use global criteria for evaluating operability. Global criteria are criteria that affect the whole vessel globally, for instance a set limit of roll or pitch angle. Such criteria may be derived by local assessments of the operation, but the operational performance is measured on the ship as a whole.

To answer whether such criteria are equally good in terms of capturing the operational performance, a comparison is performed towards the vessels, criteria and method of total operability in this thesis.

- The North Sea is chosen as operational area.
- The smallest vessel is chosen as comparison vessel since operability changes faster at lower operability levels (ref. Fonseca and Soares 2002, discussed in section 5.2).
- Global roll and pitch motion is used as criteria. The limit is taken at the same operability level as the total operability for basecase vessel 1. The limits are found to be:
  - Roll 0.7 deg RMS
  - Pitch 1.4 deg RMS

The operability was calculated for all parametric variations. Graphs showing the computed differences in operability is shown in figure 7.2. The results show that the global roll criterion overestimates the change in operability for all parametric variations. The applied parametric variations is found to have little influence on the pitch criteria. This means that if vessel design towards optimal operability is performed using global criteria, the change in true operational performance is not captured. Local motion must be assessed in order to evaluate the effect of parametric variation accurately.

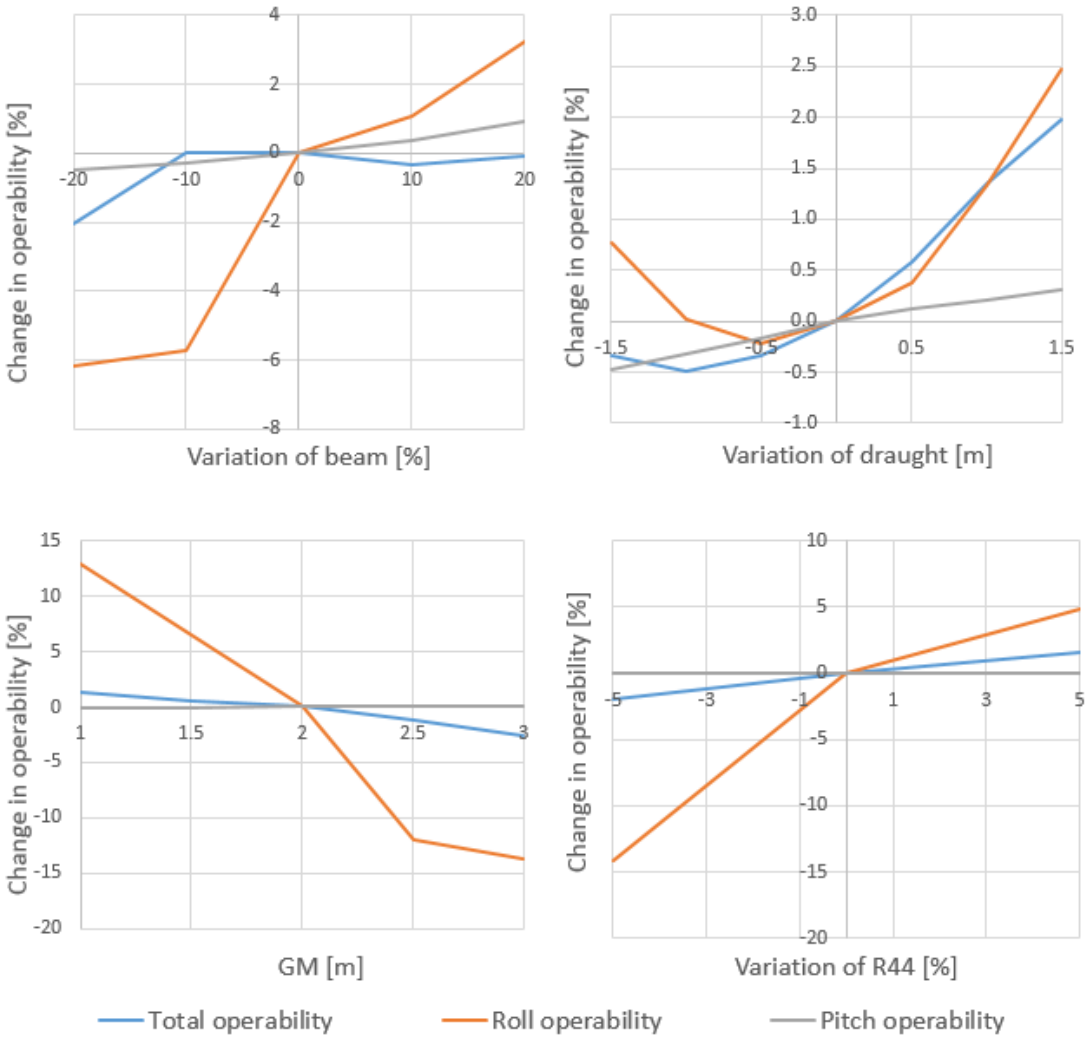

Figure 7.2: Operability assessment global and local criteria

7.3.3 Importance of linearization wave amplitude on operability

In section 3.2.4 and 4.3.2 the theory behind and choice of linearization wave amplitude for computing non-linear roll damping is described. The choice was made to apply a wave amplitude of 2.0 m for linearization of roll damping.

Since damping is linearised for a certain wave amplitude, the use of the resulting RAO is only applicable for that particular amplitude. These are the same limitations that occur for the RAO for heave motion of the submerged compressor damped by drag forces in section 5.3.3. However, the operability study in this thesis apply the same roll RAO calculated for the same linearization amplitude to calculate the short term statistics for all seastates in the scatter diagrams. This is done under the assumption that the operability levels will not vary significantly for different linearization wave amplitudes.

To check the validity of this assumption, a sensitivity study on the operability as a function of the linearization wave amplitude is performed. Vessel 3 is used in the analysis. The basecase vessel is limited by the vertical crane tip motion during lowering through the splash-zone. This criterion is therefore applied in the study. The North Sea is applied as operational area.

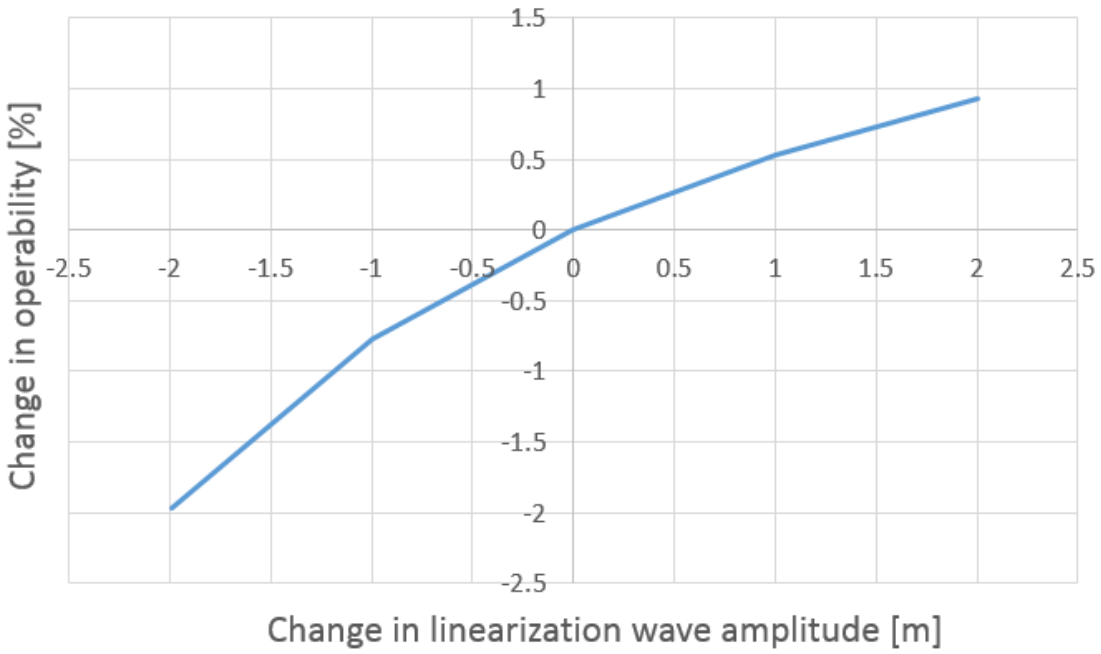

Figure 7.3: Change in operability for different roll damping linearization amplitudes

Figure 7.3 show the change in operability compared to the applied amplitude of 2.0 meters. The change in operability for amplitudes from 0-4 m is in the same order of magnitude as for the parametric variations. This means that the if the study aims to find the operability level, the choice of roll motion linearization amplitude is important, and analysis with several amplitudes should be performed to map the level of uncertainty. Since this is a comparative study, it is the operability difference that is of interest. The change in operability is found to be larger for lower operability levels. This means that the effect of measures to increase operability may be overestimated if the linearization amplitude is set too low, and underestimated if set too high. If we assume that the amplitude of 2.0 m is set with a maximum deviation of $\pm$ 1.0 m compared to the correct value, the change in operability in the North Sea is found to be 1.5 $\%$ in figure 7.3. For a total operability difference of 1.5 $\%$, the difference of changes in operability for parametric variations is negligible. This means that for a linearization wave amplitude between 1-3 m, the effect of parametric variations on operability is identical.

7.3.4 Assessing pendulum motion

Finding criteria for assessing the occurrence of pendulum motion was found to be difficult. As explained in section 5.3.1, the pendulum motion is a low damped dynamic system where the response is a function of both horizontal motion amplitude A and the excitation frequency. This means that the criterion to check for the occurrence of pendulum motion is a function of T_z.

Low damping result in unacceptable response at resonance for the linearized model of the dynamic system. To check the occurrence of resonance, the natural periods were assessed for the vessels.

Pendulum motion natural frequency

The natural frequency for the pendulum motion is a calculated as follows:

$$\omega_n = \sqrt{\frac{g}{L}} \tag{7.2}$$

A study of general arrangement drawings and crane curves for the vessels resulted in an estimate for L between 5 and 40 meters. The corresponding natural periods are shown in figure 7.4.

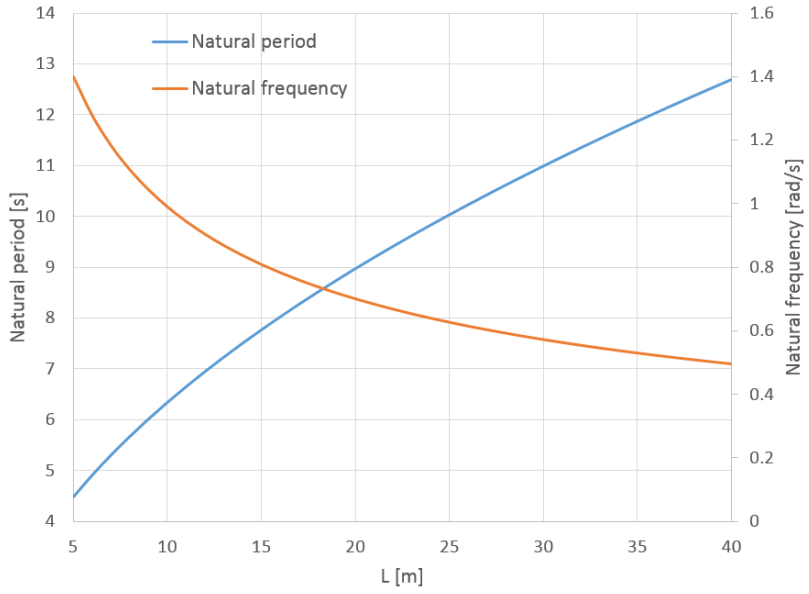

Figure 7.4: Pendulum motion natural periods

The natural period of the pendulum motion is found to vary between 4.5 - 13.7 seconds. This period range indicates that resonant pendulum motion is likely to be excited by first order wave loads. The analysis in section 5.3.1 indicate that operation during resonant pendulum motion require very low horizontal motion components. Results show that the only way to achieve this is by making vessels very long, wide and with a high natural roll period. This is found to be very expensive, and not economically feasible.

As an alternative approach, it is suggested to design the vessel and crane in a way that allow control of the natural period. By making it possible to vary the distance between the crane tip and COG of the lifted object L, resonance can be avoided and larger horizontal crane tip motions allowed. Operability will then be decided by the range of possible natural periods compared to the expected occurrence of T_z. Since subsea structures varies in height, the operability will vary depending on type of structure.

7.4 Choosing parameter configuration

This thesis aims to give advice for achieving ship design with optimal operability. Parameters influencing the dynamic characteristics of the vessels have been varied, and estimates of change in cost have been performed. Operability has been assessed for the North Sea and Norwegian Sea, which represent common areas of operation for Norwegian OSCVs.

Section 7.1 show that it is the roll motion that has the greatest influence on the total operability of the vertical motion components. Roll affects all assessed criteria except the surge motion criteria in phase 1. Finding a parameter configuration that limits the occurrence of resonant roll motion will therefore improve operability for several criteria critical for the execution of lifting operations. This require a statistical study of the planned area of operation, as the most frequent values of T_z vary. It is generally not feasible, nor advised due to stiff behaviour, to reduce the natural period for roll to below the most frequent T_z. Increasing the natural period is a better option. This may be done by reducing GM within acceptable limits with regards to stability, or increasing R_{44}, displacement or added mass. Chapter 6 show that the change of operability is different for the four assessed vessels. Whether the change of operability is positive or negative and the extent of the change is dependent on the vessel and operational area. The optimal parametric configuration including the change in building, machinery and fuel costs will therefore be vessel dependent.

Table 7.5: Operability and costs

Parameter	***ΔOperability***	***Fuel costs***	***Mach. costs***	***Hull steel costs***
Length (+20 m)	+6-8 %	+40-45 %	+25-30 %	+23-40 %
Beam $\pm$20 %	1.5-5 %	15-20 %	10-12 %	20-23 %
GM $\pm$1 m	1.5-6 %	-	-	-
Draught $\pm$1.5 m	1-4 %	30-40 %	15-25 %	20-30 %
R_{44} $\pm$5 %B	2-4 %	-	-	-

Table 7.5 show the change of operability and costs for parametric variations. The influence of length has been found by comparing the difference in operability and costs

for the basecase vessels, which increase in length by increments of 20 m. As mentioned above, the changes in operability and costs is unique to each vessel and operational area. The entries in table 7.5 are therefore given as ranges to reflect the magnitude and variation of the results.

Variation of length result in the highest change of operability and costs. This is therefore considered a good option for vessels where high operability is the most important criterion. This could for instance be the case if the vessel is build to handle particularly delicate lifting operations, or if the vessel is designed to do operations in harsh and remote areas.

The results in table 7.5 show that the increase of operability per cost is higher for beam than for draught variations. The increase of building costs is found to be relatively similar, but a larger increase in required power for increased draught result in higher costs for machinery and fuel. A combination where the beam is increased and fitted with tanks that has capacity to significantly change the draught is a possible option. That way the tanks can be filled during operation, and the benefit of increased operability for high beam and draught can be collected, while only the increase of power due to high beam is experienced during transit. This configuration can however be difficult to achieve due to the difficulty of keeping a low GM for high beam values, as discussed in section 7.2.1. The increase in operability is also found to be area and vessel dependent, meaning that a beneficial degree of increased operability is not certain in all cases.

Section 7.2.1 show how varying draught and beam present a challenge with respect to maintaining a constant GM without making radical changes to the general arrangement. Given that the GM may be decided by the designer, results show that an decrease of GM improves operability. This is due to reduction of roll stiffness, which increases the natural period for roll motion. Lowering GM should of course be done while staying within acceptable limits of stability. The increase of costs has not been assessed in this thesis since GM has no direct effect on hull geometry. The possible benefit of increased operability is found to similar in magnitude to increasing the beam.

Variation of the radius of gyration in roll gave similar results for the North Sea and Norwegian sea. Operability increased for both areas and all vessels when the radius of gyration was increased. The magnitude of the operability increase is found to be similar to as for draught variation. It is difficult to estimate the difficulty of increasing the radius of gyration compared to the other parametric variations. However, it will certainly require changes to the general arrangement, which in general require much work and skill from designers in order to result in good solutions. It may also be that the equipment onboard require a certain layout which is more important to the customer than optimizing the design with respect to operability. In cases where space and general arrangement proves a challenge, increasing the beam, draught or length may also be considered. It has been shown that such modifications often result in improved operability. The decision will as always come down to if the reward exceeds the increase of cost.

Chapter 8

Further work and conclusion

8.1 Further work

8.1.1 Operability assessment

During the initial stages of this thesis, the question arised as to how to assess operability. The chosen methodology was to use frequency domain calculations and scatter diagrams which resulted in the percentage of time of which the vessel is able to perform the operation.

However, as mentioned in section 7.3, this methodology does not capture all aspects of performing a marine operation. It may be that other statistical representations gives a better understanding of operational performance.

- Probability of waiting on weather
- Probability of having to abort the operation after start-up
- Expected number of weather windows during one season
- Expected overall duration of operation including waiting on weather

The key for assessing these performance indicators will be to include a model for the forecast weather, of which the decisions concerning the operation is based upon. A suggestion is to apply the model presented by Natskår, Moan, and Alvær discussed in sec-

tion 2.3.1 concerning the difference between forecast and experienced weather. Stochastic time domain simulations may use this model to generate realizations of operational cases with different limits of operation. Benchmarking of the mentioned performance indicators towards the one used in this thesis can then be performed to reveal potential benefits and drawbacks. It would also be interesting to do a case study of design of an OSCV using different operational performance indicators to see the differences in the obtained design.

8.2 Conclusion

This thesis show that parameters affecting the roll natural period have the largest effect on operability. Increasing vessel length is found to result in the largest, most consistent increase of operability for the studied vessels and areas. Vertical crane tip displacements during lowering through the splash-zone is found to limit operation for most vessels.

Vessel length is found to be the parameter with the largest influence on fuel, machinery and building costs. Increasing beam is more cost effective than draught for improving operability. Beam variations is found to require more changes in general arrangement than draught variations if a constant GM is required. Roll radius of gyration and GM should be set towards increasing the natural period of roll motion. The cost and complexity of varying these parameters have not been assessed.

The increase of operability for parametric variations is found to be dependent on the operability level of the original vessel. Low operability vessels obtain a larger increase of operability. Increase of operability is higher in the Norwegian Sea than the North Sea because harsh conditions result in lower operability on original vessels. The optimum choice of parameters is therefore dependent on vessel and operational area.

Applying global criteria is not recommended for design towards high operational performance. Establishing local criteria reflecting the limitations of all critical operational phases is necessary to capture the effect of parametric variations.

References

Aker Solutions ASA. 2012. *Aker Solutions Delivers Subsea Templates for Skuld Fast-Track Development*. Visited on 06/27/2016. http://subseaworldnews.com/2012/01/23/norway-aker-solutions-delivers-subsea-templates-for-skuld-fast-track-development/.

Bergen Engines AS. 2016. *Bergen Engines Products and Applications*. Tech. rep. Bergen, Norway: Rolls-Royce AS.

Boyd, Danny. 2015. *The Tubular Bells Tale*. Visited on 06/27/2016. http://www.aogr.com/magazine/editors-choice/hess-scores-major-success-with-tubular-bells-project-in-deepwater-miocene-p.

DNV. 2014. *DNV-OS-H205 Lifting Operations (VMO Standard - Part 2-5)*. Tech. rep. April.

— . 2007. *DNV-RP-C205 - Environmental Conditions and Environmental Loads*. Tech. rep. April. DNV.

— . 2011a. *OS-H101 - Marine Operations, General*. Tech. rep. October. DNV.

— . 2015. *OS-H202 - Sea Transport Operations*. Tech. rep. October. DNV.

— . 2003. *RP-H101 - Risk Management in Marine- and Subsea Operations*. Tech. rep. January. DNV.

— . 2011b. *RP-H103 - Modelling and Analysis of Marine Operations*. Tech. rep. April. DNV.

Faltinsen, O.M. 1990. *Sea Loads on Ships and Ocean Structures*. Cambridge University Press.

Fathi, D. 2014. *ShipX Vessel Responses (VERES) - Users's Manual*. Tech. rep. Trondheim: MARINTEK.

Fathi, Dariusz Eirik, and Jan Roger Hoff. 2014. *ShipX Vessel Responses (VERES) - Theory Manual*. Tech. rep. Trondheim: MARINTEK AS.

Fonseca, Nuno, and Carlos Guedes Soares. 2002. "Sensitivity of the Expected Ships Availability to Different Seakeeping Criteria". In *OMAE2002-28542*. Oslo, Norway.

H. Eriksen, Jan. 2000. *Common Procedures for Seakeeping in The Ship Design Process*. Tech. rep. NATO - Military Agency for Standardisation.

Himeno, Yoji. 1981. *Prediction of Ship Roll Damping - State of the Art*. Tech. rep. Department of Naval Architecture and Marine Engineering, University of Michigan.

Hogben, N, N M C Dacunha, and G F Olliver. 1986. *Global Wave Statistics*. Unwin Brothers Limited. ISBN: 0 946653 38 0.

Hultgreen, Liv Randi, et al. 2011. *TMR4105 - Marin Teknikk 1 - Kompendium*. 4th ed. Ed. by Geir Fuglerud and Eivind Magnussen. Trondheim: Marin Teknisk Senter, NTNU.

Ikeda, Yoshiho. 1978a. *On Eddy Making Component of Roll Damping Force on Naked Hull*. Tech. rep. Osaka: Department of Naval architecture Osaka University.

— . 1978b. *On Roll Damping Force of Ship - Effect of Friction of Hull and Normal Force of Bilge Keels*. Tech. rep. Osaka: Department of Naval architecture Osaka University.

— . 1979. *On Roll Damping Force of Ship - Effect of Hull Surface Pressure Created by Bilge Keels*. Tech. rep. Osaka: Department of Naval architecture Osaka University.

Kato, H. 1958. "On the Frictional Resistance to the Rolling of Ships". *Journal of Zosen Kiokai*.

Kjell Larsen. 2015. *TMR4225 - Marine Operations - Lecture 2*. Trondheim.

Larsen, Carl M. 2012. *TMR4182 - Marine Dynamics*. 5th ed. Institute of Marine Technology, NTNU.

MARINTEK AS. 2009. *Project - Offshore Vessels for the Next Generation*. Tech. rep., Rep. no. 530385 - Not Published. Trondheim.

Mata-Álvarez-Santullano, Francisco, and Antonio Souto-Iglesias. 2014. “Stability, safety and operability of small fishing vessels”. *Ocean Engineering* 79:81–91.

Myrhaug, Dag. 2007. *Irregular sea*. Akademika forlag.

Natskår, Asle, Torgeir Moan, and Per O. Alvær. 2015. “Uncertainty in forecasted environmental conditions for reliability analyses of marine operations”. *Ocean Engineering*.

Newland, D.E. 1993. *An introduction to random vibrations, spectral and wavelet analysis*. 3rd ed.

Nielsen, Finn Gunnar. 2007. *Lecture Notes in Marine Operations*. 4th ed. Trondheim/Bergen: Faculty of Marine Technology, NTNU.

Norsk Oljemuseum. 2016. *Ormen Lange*. Visited on 07/22/2016. `http://www.norskolje.museum.no/ormen-lange/`.

Olsen, Camilla Waldum. 2015. “Including the Effect of Shielding in Prediction of Weather Window for Offshore Lifting Operations”. Master Thesis, NTNU.

Palmqvist, M, and J Hua. 1995. *A Description of SMS - A Computer Code for Ship Motion Calculation*. Naval Architecture, Departement of Vehicle Engineering, KTH, Stockholm.

Salvesen, N, E.O Tuck, and O.M. Faltinsen. 1970. “Ship Motions and Sea Loads”. *SNAME*.

Schneekluth, H. 1987. *Ship design for efficiency and economy*. 1st ed. Butterworth & Co. Ltd. ISBN: 0-408-02790-8.

Selvåg, Anders. 2013. “Wave Impact Forces on complex structures during lowering through the splash zone”. Master Thesis, NTNU.

Shell Global. *Ormen Lange Overview*. Visited on 01/01/2016. `http://www.shell.com/about-us/major-projects/ormen-lange/ormen-lange-overview.html`.

SMSC. 2009. *Lifting operations*. Visited on 06/27/2016. `http://www.smsc.no/custom-simulations/lifting-operations`.

Statoil ASA. 2012. *Aker Solutions Delivers Subsea Templates for Skuld Fast-Track Development*. Visited on 06/27/2016. http://subseaworldnews.com/2012/01/23/norway-aker-solutions-delivers-subsea-templates-for-skuld-fast-track-development/.

— . 2015. *Starting subsea gas compression boosting Gullfaks recovery*. Visited on 06/27/2016. http://www.statoil.com/en/NewsAndMedia/News/2015/Pages/12Oct{_}Gullfaks{_}subsea{_}compression.aspx.

Subsea 7. 2015. *Seven Arctic Booklet Reference*. http://www.subsea7.com/content/dam/subsea7/documents/whatwedo/fleet/constructionvertical/SevenArticBooklet2015-Reference.pdf.

Tezdogan, Tahsin, Atilla Incecik, and Osman Turan. 2014. "Operability assessment of high speed passenger ships based on human comfort criteria". *Ocean Engineering* 89:32–52.

Torsethaugen, Knut, and Sverre Haver. 2004. "Simplified Double Peak Spectral Model for Ocean Waves". *Proceedings of 14th international offshore and polar engineering conference. ISOPE* 3. ISSN: 10986189.

Vard Group AS. *3 07*. Visited on 07/22/2016. http://www.vard.com/offshore/construction/Pages/OSCV-07.aspx.

Yan, Hongmei, et al. 2013. "Evaluation of Forces on Bilge Keels in Oscillating Flow using CFD". In *OMAE2013-10294*, 1–9. Nantes, France.

Zhang, Hui, and Tian-wei Ma. 2015. "Period-One Rotating Solutions of Horizontally Excited Pendulum Based on Iterative Harmonic Balance". *Advances in Pure Mathematics* 5 (June): 413–427.

Appendices

Appendix A

Scatter Diagrams

A.1 Barents Sea

AREA 1 ANNUAL		Tz										SUM	Cum. SUM
		3.5	4.5	5.5	6.5	7.5	8.5	9.5	10.5	11.5	12.5		
Hs	0.5	11	59	75	37	10	2	0	0	0	0	194	194
	1.5	2	38	116	111	50	14	3	0	0	0	334	528
	2.5	0	12	60	85	54	20	5	1	0	0	237	765
	3.5	0	4	23	43	34	15	5	1	0	0	125	890
	4.5	0	1	8	19	18	9	3	1	0	0	59	949
	5.5	0	0	3	8	9	5	2	1	0	0	28	977
	6.5	0	0	1	4	4	3	1	0	0	0	13	990
	7.5	0	0	1	2	2	1	1	0	0	0	7	997
	8.5	0	0	0	1	1	1	0	0	0	0	3	1000
	9.5	0	0	0	0	1	1	0	0	0	0	2	1002
	10.5	0	0	0	0	0	0	0	0	0	0	0	1002
	11.5	0	0	0	0	0	0	0	0	0	0	0	1002
	12.5	0	0	0	0	0	0	0	0	0	0	0	1002
	13.5	0	0	0	0	0	0	0	0	0	0	0	1002
	14.5	0	0	0	0	0	0	0	0	0	0	0	1002
SUM		13	114	287	310	183	71	20	4	0	0	1002	
Cum. SUM		13	127	414	724	907	978	998	1002	1002	1002		

Figure A.1: Annual scatter diagram Barents Sea

A.2 Norwegian Sea

AREA 4 ANNUAL		Tz										SUM	Cum. SUM
		3.5	4.5	5.5	6.5	7.5	8.5	9.5	10.5	11.5	12.5		
Hs	0.5	1	14	35	30	11	3	0	0	0	0	94	94
	1.5	0	6	52	102	78	31	8	2	0	0	279	373
	2.5	0	2	24	77	92	55	20	5	1	0	276	649
	3.5	0	0	8	36	58	45	21	7	2	0	177	826
	4.5	0	0	2	14	28	26	15	6	2	0	93	919
	5.5	0	0	1	5	12	13	9	4	1	0	45	964
	6.5	0	0	0	2	5	6	5	2	1	0	21	985
	7.5	0	0	0	1	2	3	2	1	1	0	10	995
	8.5	0	0	0	0	1	1	1	1	0	0	4	999
	9.5	0	0	0	0	0	1	1	0	0	0	2	1001
	10.5	0	0	0	0	0	0	0	0	0	0	0	1001
	11.5	0	0	0	0	0	0	0	0	0	0	0	1001
	12.5	0	0	0	0	0	0	0	0	0	0	0	1001
	13.5	0	0	0	0	0	0	0	0	0	0	0	1001
	14.5	0	0	0	0	0	0	0	0	0	0	0	1001
SUM		1	22	122	267	287	184	82	28	8	0	1001	
Cum. SUM		1	23	145	412	699	883	965	993	1001	1001		

Figure A.2: Annual scatter diagram Norwegian Sea

A.3 North Sea

AREA 11 ANNUAL		Tz										SUM	Cum. SUM
		3.5	4.5	5.5	6.5	7.5	8.5	9.5	10.5	11.5	12.5		
Hs	0.5	19	86	94	41	10	2	0	0	0	0	252	252
	1.5	3	49	121	99	40	10	2	0	0	0	324	576
	2.5	1	17	63	73	40	13	3	1	0	0	211	787
	3.5	0	6	27	39	26	10	3	1	0	0	112	899
	4.5	0	2	11	19	14	6	2	1	0	0	55	954
	5.5	0	1	4	9	7	4	1	0	0	0	26	980
	6.5	0	0	2	4	4	2	1	0	0	0	13	993
	7.5	0	0	1	2	2	1	1	0	0	0	7	1000
	8.5	0	0	0	1	1	1	0	0	0	0	3	1003
	9.5	0	0	0	1	1	0	0	0	0	0	2	1005
	10.5	0	0	0	0	0	0	0	0	0	0	0	1005
	11.5	0	0	0	0	0	0	0	0	0	0	0	1005
	12.5	0	0	0	0	0	0	0	0	0	0	0	1005
	13.5	0	0	0	0	0	0	0	0	0	0	0	1005
	14.5	0	0	0	0	0	0	0	0	0	0	0	1005
SUM		23	161	323	288	145	49	13	3	0	0	1005	
Cum. SUM		23	184	507	795	940	989	1002	1005	1005	1005		

Figure A.3: Annual scatter diagram North Sea